Catalytic Decomposition of Ammonia and Tar for Hot Gas Cleanup in Biomass Gasification Using Activated Carbon Supported Catalysts and Natural Limonite Ores

By

Jaclyn Donald

Supervisor:

Dr. C. Charles Xu (Lakehead University)

Co-supervisor:

Dr. Yasuo Ohtsuka (Tohoku University, Japan)

Environmental Engineering

Lakehead University

Thunder Bay, Ontario, Canada.

August, 2009

Abstract

Biomass gasification produces a gas (or syngas) containing primarily CO_2, H_2, CO, CH_4 and (C_2+C_3), as well as some contaminants such as tars, NH_3, H_2S and SO_2. In order to achieve better efficiencies of the syngas applications, these contaminants must be removed or converted before the syngas is used for internal combustion, gas engines, and in particular for fuel cells and methanol synthesis. Compared with conventional wet scrubbing technologies, catalytic decomposition of ammonia and tar is more advantageous with respect to energy efficiencies.

As Part-I of this thesis, activated carbons (ACs) were produced from a Canadian peat by chemical activation using either H_3PO_4 or $ZnCl_2$ as the activation agent, followed by carbonization at a relatively low carbonization temperature (400°C). $ZnCl_2$ was found to be an effective activation agent for developing microporous structures in the ACs, leading to greater surface areas, while H_3PO_4 is highly active in developing the mesopores, leading to much higher mesopore volumes and average pore sizes. The effects of intrinsic minerals in the precursor on the textural properties of the activated carbon products were examined by demineralization of the peat with HCl washing before the activation and carbonization. The demineralization of the precursor greatly promoted the development of micropores during the activation process, leading to significantly higher surface areas of the resulting ACs irrespective as to which activation agent was used, and the AC derived from the demineralised peat activated by $ZnCl_2$ attained the highest BET surface area of 888 m^2/g. The demineralization of the precursor could also significantly improve the mesoporous structure of the $ZnCl_2$-activated ACs.

In Part-II of this research, two novel carbon-based Ni/Fe catalysts were developed and tested for catalytic decomposition of ammonia into N_2 and H_2. These catalysts were prepared using a meso-porous activated carbon (AC) support derived from a Canadian peat by H_3PO_4 activation. The newly developed catalysts proved to be highly active for

ammonia decomposition. The conversion of 2000 ppm NH_3 diluted in helium over the Fe catalyst reached as high as 90% at 750°C and at the space velocity of 45000 h^{-1}, compared with only about 15% with the activated carbon alone without metal loading. In addition, the new Fe/Ni catalysts showed superior performance with respect to their resistance to catalyst deactivation. Both catalysts remained active as the reaction time increased up to 10 hours without showing a sign of deactivation. Fresh and spent catalysts were characterized by X-ray diffraction (XRD), X-ray photoelectron spectroscopy (XPS) and temperature programmed desorption (TPD). A cycle mechanism, involving both metal phosphides and metal nitrides, was proposed for the NH_3 decomposition reactions over these new Fe/Ni catalysts.

In Part-III of this work, the catalytic performance of the peat-derived activated carbon supported Fe/Ni catalysts as well as three natural limonite ores (from Australia, Brazil and Canada) towards hot gas NH_3 decomposition in a simulated gas (14.9% CO, 2.9% CH_4, 11.2% H_2, 11.2% CO_2) with and without 5-15% H_2O, was investigated at 750°C. The Fe/AC and Ni/AC catalysts and all natural limonite ores were very active for ammonia decomposition in the inert atmosphere. However, both AC-supported catalysts could be severely deactivated by the simulated gas, and the Fe/AC catalyst was also deactivated by the presence of H_2O in the gas. In the presence of the simulated gas and H_2O, the activities of these two catalysts dropped drastically to as low as <10%. The three limonite ores showed high activities towards ammonia conversion to N_2 (>90% at 750°C) in both inert atmosphere or in a simulated gas with 0-15% H_2O. The deactivation of the Ni/AC and Fe/AC by the simulated gas and H_2O vapor may be caused by the carbon deposition resulting from Boudouard reaction of CO or decomposition of CH_4, by the oxidation of metal phosphides and metallic metals into less or inactive phosphates in the presence of the simulated gas species CO and H_2O, or by the competing adsorption of CO_2 and H_2O with NH_3 on the catalyst surface.

In the Part-IV of this work, three types of natural limonite iron ores originated from

Canada (CL), Brazil (BL), and Australia (AL) were tested as the inexpensive catalysts for tar reforming/cracking experiments at 500-900°C using benzene as the model compound (1000-1400 ppm) in the co-existence of H_2O/helium a simulated gas mixture containing $H_2/CH_4/CO/CO_2$ with and without H_2O. The activities of these limonite catalysts of benzene decomposition follow the order of priority of BL > AL > CL. Canadian Limonite (CL) was inactive for steam reforming of benzene, probably resulting from the chemical deactivation of catalyst by the H_2O vapor to prevent formation of the active α-Fe species on the catalyst surface. However, in the presence of the simulated gas consisting without H_2O, the CL showed improved higher activity, of about 65% at 900°C, while its performance was deactivated slightly by the presence of H_2O in the gas. The Brazilian limonite (BL) showed the highest activities in benzene decomposition in the presence of the simulated gas with and without H_2O, owing to theist high Fe content with smaller crystalline sizes of active Fe-species in the fresh sample or during the benzene decomposition tests. The use of BL catalyst obtained almost complete conversion of benzene (>95%) at above 650°C in the simulated gas irrespective of whether or not 15 vol% H_2O was present in the reactant gas. The activity of the BL catalyst was unaffected by the addition of H_2O and the presence of H_2O was found to be beneficial to maintain the high activity of BL by preventing formation of carbon deposition. The activation energies were determined as E_a =130 kJ/mol and 120 kJ/mol for benzene decomposition over CL at 750-900°C in the simulated gas with and without 15vol.% H_2O, respectively. The obtained E_a values are much lower than the literature values for benzene decomposition reactions under similar conditions with other catalysts such as CaO.MgO and Ni/MgO, suggesting the limonite material can be a promising less expensive catalyst for hot gas cleaning of tar in the biomass gasification syngas.

Keywords: *Biomass gasification, Hot gas cleanup, Tar, Ammonia, Benzene, Catalysts, Activated Carbon, Peat, Ammonia decomposition, Ni/AC, Fe/AC, Metal phosphides, Metal nitrides, Simulated gas, Carbon-based catalysts, Limonite.*

Acknowledgements

I would first like to express my sincere appreciation and deepest gratitude to my supervisor Dr. C. Charles Xu, for his constant guidance, encouragement and continuous support in the Masters program. He was always there to talk about ideas, to proofread and revise my work, without his help I could not have finished this thesis. I would also like to thank Dr. Y. Ohtsuka for co-supervising, and allowing me to work with his research team. He was always gave me his expert advice and to ask me good questions to help me think through my problems. He showed me different ways to approach a research problem and the need to be persistent to accomplish any goals. He also took the time to arrange my living arrangements in Japan, taught me about Japanese culture, arranged excursions, and threw numerous lab parties, making my stay all the more interesting.

Besides my advisors, I would also like to thank Enkhsaruul Byambajav for all her help, in and outside the lab, helping me through analytical and computational problems as well as acting as a translator. She helped me through many situations, always going out of her way to make me feel more at home in Japan. It has been a great experience working with her. Also, I would like to give a special acknowledgment to Hiroyuki Hashimoto, Takemitsu Kikuchi, and Naoto Tsubouchi at Tohoku University for all their help in the lab, teaching me how to use my apparatus and all the required equipment needed to complete this project.

The present work was carried out as a part of the Atikokan Bioenergy Research Center (ABRC) Theme-1 Project, financially supported by Ontario Ministry of Energy and Ontario Centres of Excellence. This research was also supported by Natural Science and Engineering Research Council of Canada (NSERC) through the Discovery Grants awarded to Prof. Xu, also in part by a Grant-in-Aid for Scientific Research (B) from the Ministry of Education, Science, Sports, and Culture, Japan (No. 19310044)

I sincerely acknowledge all professors in the Department of Chemical Engineering and the Graduate Program in Environmental Engineering, especially, Professors: B. Liao,

B.H. Kjartanson and L. Catalan, A. Gilbert for their help in my courses study and helpful comments on my research. Besides, I am full of gratitude to my thesis Supervision Committee for their time and comments.

I am also thankful the fellow students in Dr. Xu's Green Energy Laboratory, as well as in Dr. Ohtsuka's laboratory for their generous assistance in my study and research towards this work. My special thanks are extended to Dr. Andrew Conly in Department of Geology at Lakehead University, for supplying me with limonite ore, and Mr. Garry Rathje for his great assistance on preparing peat samples and allowing me to use his laboratory and equipment for my sample preparation.

Last but not least, I thank my family, my parents, sisters and Spencer, for their unconditional support, love and encouragement to pursue my interests.

Table of Contents

List of Tables

List of Figures

CHAPTER 1

Introduction

1.1. Background on biomass gasification

Due to the increasing concerns about the release of greenhouse gasses (GHG), mercury and sulphur into the atmosphere, and the depletion of the fossil fuels, research into renewable energies such as hydro, wind, solar and biomass has attracted increasing interest in recent years. Coal-fired power plants are among the largest producers of anthropogenic mercury emissions in the world as well as SO_2, NO_x [1, 2]. In Ontario, coal-fired plants have been the largest sources of GHGs and smog-containing pollutants [3], and because of this, there are regulations in place to phase out the province's coal-based electricity by 2014, and to switch to other cleaner fuels such as renewable biomass by co-firing coal with biomass.

In addition to combustion or co-firing, biomass can be gasified using gasification agents such as air/oxygen and steam into medium Btu fuel gases. Substituting fossil fuels such as coal with biomass in gasification processes is one step that can be taken towards reducing GHG, sulphur and mercury emissions, as well as the reliance on imported fuels. The gases produced (e.g. H_2, CO, CO_2, CH_4 and C_{2+}) can be utilized directly as fuels for heat and electricity generation, or as feedstock for productions of methanol, ethanol, dimethyl ether, and Fischer-Tropsch oils, etc. [4]. Although there is great potential and extensive research for clean power and chemical production through the gasification of coal [5], the long-standing problem for coal gasification is that coal is non-renewable and the coal reserves will be eventually depleted. Alternatives to coal as a feedstock in gasification processes, biomass resources such as, forestry/agricultural residues, municipal solid wastes (MSW), domestic and industrial wastewater sludge, can be used to produce electricity. Annual world biomass production is 220 billion dry tonnes or 4,500 EJ [6], equivalent to 9 times of world energy consumption in 2006 (498 EJ).

Biomass feedstock can thus be an abundant source for energy, fuels, chemicals and materials.

1.2. Problems associated with biomass gasification

The producer gas from biomass gasification contains mainly CO, H_2, CO_2, CH_4, H_2O, and N_2 (if air is used as the gasification agent), but may also contain undesirable inorganics, such as H_2S, HCl, NH_3 and alkali metals, and organic tars and impurities and particulates [7]. The tars are the products of major concern in biomass gasification. Tar is a condensable fraction of the gas product and contains components which are largely aromatic hydrocarbons with molecular weights greater than that of benzene [8], and can cause plugging in pipes, filters, and downstream fuel lines etc. In order to use biomass in commercially advanced gasification technologies, it is necessary to remove, convert or deconstruct the tar contained in the gas product.

If the final application depends on the purity of the gas, complete elimination of tar and ammonia may be necessary, for example, polymer electrolyte membranes (PEM) fuel cells require pure H_2 as the fuel so the biomass-derived gas product requires conditioning by removing or converting the tar as well as ammonia [7]. Other applications such as integrated gasification combined cycles (IGCC) can be more efficient if ammonia is converted [9]. Gas turbine power generating plants utilize syngas from either coal or biomass gasification, and ammonia present in the stream can form nitrogen oxides (NOx) during combustion, which are significant contributors to acid rain, or may react with other pollutants such as sulphur dioxide and nitrous oxide forming smog. In order for biomass gasification to be feasible on an industrial scale, the concentrations of tar and ammonia contaminants need to be reduced to levels that comply with the environmental regulations as well as the final levels required by the end use applications [10]

Ammonia in biomass fuel is conventionally eliminated using scrubbers or selective catalytic reduction (SCR), in which the ammonia is reacted with NO_x to form N_2 and water. Tar removal can take place in the gasifier itself or downstream from the gasifier. Prevention within the gasifier may involve reactor design, parameter

optimization, or use of catalysts [11]. Downstream from the gasifier, tar may be removed through scrubbing and filtration or converted by thermal or catalytic cracking. Thermal cracking requires high temperatures (>1000°C) in order to obtain a high conversion. This can be achieved by adding oxygen to the process, but these high temperatures can lead to soot formation in the product stream [12].

Wet scrubbing is an effective gas conditioning method that can remove significant amounts of ammonia and tars from the producer gas, but requires that the gas be cooled, and if the final application requires that the gas remain at high temperatures then there is a cost of reheating the gas. In some cases tars in the form of aerosols are difficult to remove even at temperatures below the boiling points, and may remain in the vapour phase and NH_3 concentrations my not be low enough to comply with the environmental regulations [13,14]. Another disadvantage of this method is that the tar is only transferred from a vapour phase to a condensed phase, decreasing the energy content of the producer gas and more importantly producing a secondary waste stream that needs to be treated. By converting the tar to gas products through catalytic cracking, the heating value of the final gas product can be improved, and the gas does not need to be cooled and reheated for its final use. In addition, by converting the tar to desired gas components, the treatment of secondary waste streams is avoided [7].

1.3. NH_3 and tar decomposition with the use of catalysts

Catalysts can be used to lower the required reaction temperatures and increase the conversion of tar and ammonia to desirable gas products, and therefore eliminating waste streams, and increasing the fuel energy value. Catalytic tar cracking and NH_3 decomposition can be achieved by passing the raw gas produced from the biomass gasification process, over a catalyst bed (a fixed or fluidized bed) at elevated temperatures [15], converting tar to CO and H_2 or NH_3 to N_2 and H_2. There are several types of catalysts that have the potential for cracking tars and decomposing NH_3 generated by biomass gasification, and they are classified as primary or secondary catalysts. Primary catalysts are used within the gasifier to enhance biomass gasification reactions, and secondary catalysts are used in a separate fixed/fluidized bed reactor

located downstream from the gasifier to reduce these components in the gasification product gas.

1.4. Activated Carbon

Activated carbons (ACs) have been used extensively as adsorbents or catalytic supports in environmental remediation applications such as gas purification, separation processes, and effluent treatment to remove specific impurities. The high surface areas make it an ideal adsorbent, and their surface properties can be further enhanced through chemical treatment and made to adsorb specific impurities from gas streams. ACs can be produced from a variety of carbonaceous materials such as coal, wood, coconut shells, or peat. The use of an abundant resource such as peat or other low cost forestry/agricultural wastes would make the AC manufacture more economically feasible for large-sale industrial applications of ACs such as catalysts or a catalyst support [16, 17].

1.5. Motivation for the present study

There have been several studies on the decomposition of tar and NH_3 mainly focusing on Ni, Fe, and Ru based catalysts [7-9]. Activated carbon-based catalysts have been used mainly for the adsorption of noxious gases and removal of chemical warfare agents [10]. The research on ammonia and tar decomposition using metal loaded, or impregnated activated carbon (less expensive) is quite limited. Therefore the objective of this study is to investigate NH_3 and tar decomposition using the Canadian peat-derived AC-supported metals as the catalysts. Peat was chosen as the AC precursor mainly because it is present in abundance in Canada, and hence it's of low cost. In addition, another less expensive natural mineral resource, Canadian Limonite, abundant in Northwestern Ontario, was also investigated as a catalyst for the NH_3 and tar decomposition studies, in comparison to other limonite samples from Brazil and Australia.

1.6. Objectives

The ultimate goal of this study was to decompose ammonia and tar into desirable gas products, using benzene and toluene as model compounds in the studies, using less expensive catalysts including peat-derived activated carbon-supported metals, and limonite ores from Canada, Brazil and Australia. The possible reaction mechanisms governing the catalytic decomposition reactions of ammonia and tar on the surfaces of the catalysts are also investigated. The specific objectives of this study are:

1. To produce and characterize the activated carbons derived from Canadian peat and the activated carbon-supported metal catalysts
2. To investigate the effects of the AC-based catalysts on NH_3 decomposition in an inert and simulated gas
3. To investigate the effects of Canadian Limonite on NH_3 decomposition in an inert and simulated gas
4. To investigate the effects of Limonite from Canada, Brazil and Australia, on tar decomposition in an inert and simulated gas
5. To characterize the spent catalysts and to determine possible reaction mechanisms that may govern the NH_3 and tar decomposition reactions.

1.7. Organization of the Thesis

This thesis is composed of seven chapters.

Chapter 1 – Introduction. It provides a general introduction and a brief literature review on the related fields of the present research work, describing the research background, state-of-the-art of the research and objectives of the present work.

Chapter 2 – Literature Review. It provides a detailed literature review on the related fields of the present research work, i.e, Biomass gasification, catalysts used for hot gas

removal of ammonia and tar, including dolomite, iron-based, nickel and other metal supported catalysts.

Chapter 3 – Production and Characterization of Activated Carbons form a Canadian Peat. It provides the methods used in producing the activated carbons and compares the effects of using different activating agents.

Chapter 4 – Novel Carbon-based Ni/Fe Catalysts Derived from Peat for Hot Gas Ammonia Decomposition. It provides a method used for producing novel Ni and Fe loaded activated carbon catalysts and their activity towards ammonia decomposition in inert atmosphere.

Chapter 5 Hot Gas Decomposition of NH_3 in Simulated Gas over Carbon-based Ni/Fe Catalysts and Natural Limonite Ores. It provides the results on the performance of the Ni and Fe loaded activated carbon catalysts, as well as Natural limonite ores in ammonia decomposition in simulated gas atmospheres.

Chapter 6 – Catalytic Decomposition of Model Tar Compound using Natural Limonite Ores for Hot Gas Cleanup of Biomass Gasification Gas. It provides the performance of Brazilian, Canadian and Australian limonite ores in hot gas decomposition of benzene in simulated gas with and without H_2O.

Chapter 7 – Conclusions. It presents the overall conclusions and recommendations for future work.

Reference

[1]. S. Ito, T. Yokoyama, K. Asakura. Emissions of mercury and other trace elements from coal-fired power plants in Japan. *Science of the Total Environment* 368 (2006) 397– 402

[2]. D. Pudasainee , J.H. Kim, S.H. Lee, J.M. Park, H.N. Jang, G.J. Song, Y.C. Seo. Hazardous air pollutants emission from coal and oil-fired power plants. *Asia-Pacific Journal of Chemical Engineering.* 2009; DOI:10.1002/apj.268

[3]. Ontario Ministry of Energy and Infrastructure. McGuinty Government Coal Replacement Strategy Queen's Printer for Ontario, 2008 http://www.energy.gov.on.ca/index.cfm?fuseaction=english.news&back=yes&news_id=100&backgrounder_id=75

[4]. P. McKendry, Energy production from biomass (part 3): gasification technologies. *Bioresource Technology* 83 (2002) 55-63.

[5]. A.J. Minchener, "Coal gasification for advanced power generation" *Fuel* 2005; 84: 2222-2235.

[6]. Klass DL, Biomass for renewable energy, fuels and chemicals (Ed.), Academic Press, San Diego, 1998

[7]. D. Dayton "A Review of the Literature on Catalytic Biomass Tar Destruction. National Renewable Energy Laboratory. NREL/TP-510-32815 (2002)

[8]. T. Nordgreen, T. Liliedahl, K. Sjostrom. Metallic iron as a tar breakdown catalyst related to atmospheric, fluidised bed gasification of biomass. Department of Chemical Engineering and Technology, *Fuel.* 2006;85:689-694

[9]. N. Tsubouchi, H. Hashimoto, Y. Ohtsuka. Catalytic Performance of Limonite in the Decomposition of Ammonia in the Coexistence of Typical Fuel Gas Components Produced in an Air-Blown Coal Gasification Process. *Energy & Fuels* 2007; 21: 3063-3069

[10]. J. Colls, Air Pollution – An Introduction, E & FN Spon, TJ International Ltd,Padstow, Cornwall, UK, 1997.

[11]. Lopamudra Devi, K.J. Ptasinski, F. J. J. G. Janssen. A review of the primary measures for tar elimination in biomass gasification processes. *Biomass and Bioenergy* 2003; 24: 125-140

[12]. E. Kurkela,. Air Gasification of Peat, Wood and Brown Coal in a Pressurized Fluidized-Bed Reactor. I. Carbon Conversion, Gas Yields and Tar Formation. *Fuel Processing Technology* 1992; 31: 1-21.

[13]. T. Wang, J. Chang, P. Lv. Novel Catalyst for Cracking of Biomass Tar. *Energy & Fuels* 2005; 19: 22-27

[14]. L.P. Harris, R.P. Shah. Energy conversion alternatives study (ICAS), General Electric Phase II Final Report: Vol. II, Advanced Energy conversion systems-conceptual designs. Part 3. Open cycle gas turbine and open cycle. MHD; General Electric Report No. SRD-76-064-2, NASA Report No. NASA CR-123929; National Aeronautics and Space Administration, Washington, DC, 1976.

[15]. J. Gil, J. Corella, et al.,. Biomass Gasification in Atmospheric and Bubbling Fluidized Bed: Effect of the Type of Gasifying Agent on the Product Distribution. *Biomass and Bioenergy*. 1999;17: 389-403.

[16]. L.R. Radovic and F. Rodriguez-Reinoso. Carbon Materials in Catalysis Chemistry and Physics of Carbon. P.A. Thrower (Ed.), Vol. 25, pp. 243–358, Marcel Dekker, New York,1997.

[17] F. Rodríguez-Reinoso. The role of carbon materials in heterogeneous catalysis. *Carbon* 1998; 36:159-175

CHAPTER 2

Recent Advances in Catalysts for Hot Gas Removal of Tar and NH_3 from Biomass Gasification

Biomass gasification produces a low to medium BTU product gas (or syngas) containing primarily CO_2, H_2, CO, CH_4 and (C_2+C_3), as well as some contaminants such as tars, NH_3, H_2S and SO_2, etc. In order to achieve better efficiencies of the syngas applications, these contaminants must be removed before the syngas is used for internal combustion, gas engines, and in particular for fuel cells and methanol synthesis. Compared with the wet scrubbing technology, hot gas clean-up technology to remove tar, ammonia and other contaminants at the "hot" state is more advantageous with respect to energy efficiencies. This paper provides an overview on recent advances in catalysts for hot gas removal of tar and ammonia from biomass gasification. The review focuses on the recent development and applications of dolomite catalysts, iron-based catalysts, nickel and other metal supported catalysts, and the novel carbon based catalysts on hot gas tar removal and ammonia decomposition.

Keywords: Biomass gasification, Hot gas cleanup, Tar, Ammonia, Catalysts

2.1 Introduction

In biomass gasification, the biomass fuel is partially oxidized/gasified in a oxidizing atmosphere of air, oxygen and/or steam to form a low to medium-BTU product gas (also called producer gas or syngas) containing primarily CO_2, H_2, CO, CH_4 and (C_2+C_3), which can be used for heat and electricity generation, or for synthesis of liquid fuels and methanol [1-5], The overall reaction of biomass gasification may be described by the following generalized reaction:

$$Biomass + O_2 \text{ or } H_2O \rightarrow CO + CO_2 + H_2O + H_2 + CH_4 + other\ HCs \rightarrow tar + char + ash \quad (1)$$

$$\rightarrow HCN + NH_3 + HCl + H_2S + other\ sulfur\ gases(SO_2, COS, etc.)$$

Temperature, pressure, residence time, gasifying agent and feedstock, have significant effects on the compositions and heating values of the resulting gas. For example, in an air-blown gasification study it was found that increasing the gasification temperature led to a higher concentration of CO_2 accompanied with a decreased H_2 concentration in the gas product [2]. Gil et al. [6] examined the effects of gasifying agents (air, steam and mixed steam/oxygen) on the product gas composition and found that when air was used, the H_2 to CO mol ratio was close to 1, but the N_2 content in the product gas was high as expected. Using steam as the gasifying agent minimized the N_2 content, and increased the H_2 and CO contents, but the tar yield was increased. Different gasifying agents will favour different intermediate reactions, leading to a variation in the gas composition, and therefore affecting the calorific value of the gas product. In oxygen- or steam-blown gasifiers, lower heating values (LHV) of 10-14 MJ/Nm^3 can be attained for the product gas, compared with only 4-7 MJ/Nm^3 in a typical air-blown process [6,7], as shown in Table 2-1.

Table 2-1: Typical gas composition and yields from gasification of pine wood chips in a bubbling fluidized bed with different gasifying agents (summarized from Gil et al. [6])

Gasifying agent	T(°C)	Gas Composition (vol%, db[a])							Yields	
		H_2	CO	CO_2	CH_4	C_2H_n	N_2	H_2O[b]	Tars (g/kg)	LHV (MJ/Nm^3)
Air	780-830	5-16	10-22	9-19	2-6	0-3	42-62	11-34	4-62	4-8
Steam	750-780	38-56	17-32	13-17	7-12	2	0	52-60	60-95	12-14
Steam+ O_2	785-830	14-32	43-52	14 -36	6-8	3-4	0	38-61	2-46	10-14

[a] On a dry basis; [b] Moisture content in the producer gas.

Biomass gasification also produces some contaminants in the product gas, such as tars, NH_3, H_2S and SO_2, etc. [1-5]. These contaminants must be removed before the syngas is used for internal combustion, gas engines, and in particular for fuel cells and methanol synthesis, in order to achieve better efficiencies of the syngas applications. Tar,

representing all organics with a molecular weight greater than that of benzene [8], is highly undesirable because of the detrimental problems associated with condensation of tar in the process equipment, pipe lines as well as in end use applications such as engines and turbines. The allowable limits for tar in the producer gas depend on the process and end use applications. Milne and Evans [9] reported tar tolerance limits for various end use devices: for example, less than 50-500 mg/ Nm^3, 50-100 mg/Nm^3 and 5 mg/Nm^3 is recommended for compressors, internal combustion systems, and direct-fired industrial gas turbines, respectively. For methanol synthesis, the contents of tar and ammonia are required to be <0.1 mg/Nm^3, and <10 ppm, respectively [2. 4, 5]. The content of NH_3 in the product gas, typically of 1000-5000 ppm [10], is dependant on the type of biomass used, as well as the gasifier parameters and operating conditions. Most of the nitrogen that is contained within biomass ends up mainly as NH_3, N_2, and some HCN, HNCO, and NO_x [11-17]. As much as 60-80% of the nitrogen in biomass would convert to NH_3 during the gasification process [18], and as much as 50-90% of the NH_3 would form NO in gas turbines when the gas is combusted to produce power [19]. A large number of studies were reported on the formation of tar and ammonia during gasification. It has been generally shown that increasing the air to fuel ratio decreased the ammonia and tar in the product gas [6, 20, 21], a high temperature decreased the formation of tar but a longer residence time could increase ammonia formation [22, 23].

The tar, ammonia and other contaminants in the product gas can be cleaned by wet scrubbing technologies, widely adopted in the existing biomass gasification processes. Compared with the wet scrubbing technology, hot gas clean-up technology, employing catalysts to remove these contaminants at the "hot" state, is more advantageous with respect to energy efficiencies as it eliminates the need for cooling the product gas and re-heating again for the syngas applications (internal combustion, gas engines, fuel cells and methanol synthesis, etc.). The light hydrocarbons and tars formed during the gasification process could be removed through steam/dry reforming or cracking/hydro-cracking reactions as shown below [24]:

Steam reforming: $$C_nH_m + nH_2O \leftrightarrow nCO + (n+\frac{m}{2})H_2 \qquad (2)$$

Dry reforming: $$C_nH_m + nCO_2 \leftrightarrow 2nCO + (\frac{m}{2})H_2 \quad (3)$$

Cracking: $$C_nH_m \leftrightarrow nC + (\frac{m}{2})H_2 \quad (4)$$

Hydro-cracking: $$C_nH_m + (\frac{4n-m}{2})H_2 \leftrightarrow nCH_4 \quad (5)$$

Without the use of catalyst, steam reforming of tars occurs appreciably at >900°C (due to the endothermic nature of these reactions and a high activation energy >250-350 kJ/mol). Steam and dry reforming reactions with the use catalysts have shown to be a promising way to remove the tar components from the gasification gas at a lower temperature [25]. Dolomite and VIII metals such as Ni, Fe, Co, etc. were the most common catalysts for the tar removing reactions [26]. For instance, the use of dolomite and $NiMo/Al_2O_3$ could significantly reduce the activation energy of the steam reforming reaction of toluene to 123 kJ/mol and 56 kJ/mol, respectively, at 650-850°C [27]. The decomposition of benzene at 900°C through steam reforming without catalyst led to only 2% conversion, while the addition of a dolomite catalyst increased the conversion significantly, reaching 40% at 950°C and 80% at 1000°C [28]. In addition, dolomite catalysts were found to be active for tar cracking.

The ammonia in the producer gas can be reduced by hot gas cleanup either through catalytic decomposition or selective oxidation, as shown in the following reactions (eqs. 6 and 7) [29]. For some applications such as hydrogen fuel cells, complete decomposition of ammonia into H_2 and N_2 is desirable. In catalytic decomposition of ammonia, dehydrogenation occurs forming some reaction intermediate or N and H on the surface of a catalyst, which subsequently form N_2 and H_2 through surface reaction on the catalyst. Other gas components (CO, CO_2, H_2, etc.) present in the bio-syngas may have a negative effect on the decomposition of ammonia, as they would compete for the adsorption and reactive sites on the catalyst, and they could also react with NH_3 to form HCN [29].

$$2NH_3 \rightarrow 3H_2 + N_2 \quad (6)$$

$$4NH_3 + 3O_2 \rightarrow 2N_2 + 6H_2O \quad (7)$$

The ammonia decomposition reaction (to form N_2 and H_2) over iron-based catalyst was found to be first-order with respect to the partial pressure of ammonia whose rate expression was shown as follows [30]:

$$r = k_0 \exp(Ea/R/T)p_{NH3} \quad (8)$$

where E_a is the activation energy of ammonia decomposition. The value of E_a was found to be 96 kJ/mol for the Fe-catalyst with potassium as a promoter, and 87 kJ/mol for the catalyst without potassium. Chellappa et al. [31] investigated ammonia decomposition using Ni-Pt/Al_2O_3 catalyst, and the reaction proved to be first order reaction too, with the activation energy of about 200 kJ/mol.

From the above discussion, it is clear that development of effective and stable catalysts are extremely critical for the development of viable hot gas cleanup technologies. This is because the reactions for steam/dry reforming or cracking/hydro-cracking of tars and ammonia decomposition are highly endothermic and require high activation energies in the absence of a suitable catalyst. As such, this review focuses on the recent development and applications of catalysts for hot gas removal of tar and ammonia from biomass gasification.

2.2 Catalysts for Hot Gas Tar Removal

The biomass-derived tars consist of a wide range of condensable hydrocarbon and oxygen containing hydrocarbons compounds, which are mostly aromatics and complex poly-aromatic hydrocarbons (PAHs) [24]. The complex composition of biomass tars makes it difficult to understand the reaction mechanisms. Therefore, most studies used model tar compounds such as benzene, toluene, phenol, and naphthalene in the research. The properties of these model compounds are shown in Table 2. It was observed that in the fluidized-bed air-blown gasification of peat, the major component is benzene, representing 50-75% of the total tar, followed by toluene and naphthalene [32]. Naphthalene is a popular model tar compound for most research on tar decomposition,

since it is likely the most stable and difficult to decompose among all the compounds in the biomass-derived tars.

Table 2-2 Characteristics of the common model tar compounds [9, 27]

Compound	Characteristics
Benzene	A stable aromatic structure in tars formed with high-temperature processes
Toluene	A stable aromatic structure apparent in tars formed with high-temperature processes. With toluene, catalyst deactivation due to charring can be less severe and the hydrocarbon conversion to gases is much higher in comparison with real tar.
Phenol	The major tar compound from process at temperatures lower than 800°C.
Naphthalene	The major single compound in tars. The thermal reactivity follows the order of toluene > naphthalene > benzene.

There has been extensive research on catalysts that have the potential for decomposing tars generated in biomass gasification. Alkali metal catalysts have been studied as primary catalysts to enhance the gasification reactions in the gasifier, but have been found to be less active for carbon conversion and hard to recover. Materials such as dolomite, calcium-magnesium carbonates and Ni-based catalysts have been used widely as the secondary catalysts to minimize tar in gasification product gas [33].

2.2.1 Dolomite Catalysts

Several studies using calcined dolomites (MgO-CaO), formed by the decomposition of dolomite $CaMg(CO_3)_2$ at high temperatures from 800 to 900°C, as the secondary catalysts have shown great success for minimizing tar in the product gas [33]. The increased surface area and oxides contents on the surface make it more active than the un-calcined dolomite for tar decomposition [34, 35]. Corella et al. [36] studied calcined dolomites as both primary and secondary catalysts, and they observed that calcined dolomites can be equally effective as either a primary or secondary catalyst. Simell et al. [37, 38] studied tar removal using secondary catalysts containing CaO and

MgO, and found that the catalytic activities were ranked in the following sequence: CaO > CaO-MgO > MgO > NiMo/γ–Al_2O_3, suggesting that the presence of CaO in dolomite might be responsible for its activity in tar conversion. Using calcined dolomites as the secondary catalysts could increase the H_2 content and the H_2/CO ratio in the product gas owing to cracking and reforming of the tars [28,39]. Hu et al. [40] compared a calcined dolomite (by calcination at 900°C) with the un-calcined dolomite as well as a calcined olivine and the raw olivine (a mineral containing magnesium, iron and silicon) as the secondary catalysts for apricot stone gasification [40], where it was found that among all the catalysts tested the calcined dolomite was the most effective catalyst for increasing the H_2 content in the gas.

For tar conversion, however, it was demonstrated that the activity of dolomite increased with increasing Fe_2O_3 content in the material and its pore diameter [41]. In another study, powdered dolomite was modified by mixing with Fe_2O_3 powders to increase its Fe_2O_3 content, and it was observed that the addition of Fe_2O_3 powders led to a slight increase in tar conversion at 850°C [42]. .

Although calcinated dolomite catalysts have shown to be very active for decomposition of phenols and oxygenated compounds, typically formed in steam gasifiers, the dolomite catalysts were less effective for removal of PAHs, formed in air-blown gasification [43, 44]. Another problem with using calcined dolomite is that it can be easily eroded as it is a soft and fragile material, limiting its use in some types of reactors such as a fluidized bed reactor [24]. .

2.2.2 Iron-based Catalysts

Olivine is a natural mineral containing magnesium, iron and silicon in the form of either Fe_2SiO_4 or Mg_2SiO_4. In a study by Kuhn et al [45], olivine catalysts of different origins were comparatively tested for tar decomposition using naphthalene and toluene as tar models. With a simulated gas of 400 ppm $C_{10}H_8$ diluted in 16%H_2- 8%CO-12% CO_2 - 16% H_2O-4% CH_4 - N_2 (balance), an Austrian olivine showed the greatest activity of 100% tar conversion at 900°C at GHSV = 1166 h^{-1}. Calcination of olivine (at 1600°C) could deactivate the catalyst: the tar conversion at 800°C with the calcinated Austrian olivine decreased from 90% to 32%. In another study by Devi et al [24], however, it was

found that calcined olivine was more active than un-calcined olivine [24]. The calcinations were carried out at 900°C in the presence of air, and with various lengths of time ranging from 1 to 10 hours. They found that increasing the calcinations time from 1 h to 10 h increased the activity for naphthalene decomposition from 62% to 81%, respectively, compared with a naphthalene conversion of only 47% with the un-calcined olivine. Using the X-ray photoelectron spectroscopy (XPS) technique, it was found that the content of Fe (III) on the surface of the catalysts increased with increasing calcinations times. In the study by Hu et al [38], discussed earlier, it was also found that calcined olivine increased the gas yield from 37% to 47%, and therefore was more active for tar cracking than the un-calcined olivine. The above contradictory results on the effects of calcinations observed from different studies might be due to the different calcinations conditions. For example, the calcination temperature in the study by Kuhn et al [45] was very high (1600°C), compared with the temperature (900°C) used by Devi et al [24] and Hu et al [40]. Hence, it might be concluded that a too high temperature for calcination of olivine is not desirable for tar decomposition.

Limonite is a naturally occurring iron ore with a high iron content that has been used in tar decomposition studies. Limonite is an attractive alternative to the commercial Ni catalysts, as it is less expensive and abundant in resource and the spent limonite catalyst waste can be used directly for iron and steelmaking [46]. In a study by Li et al [46], Indonesian limonite was used for the decomposition of coal volatiles from a coal carbonization process. The limonite ore was composed mainly of goethite (FeOOH) with an iron content of 41.4%. They studied the effects of reduction temperatures on the catalyst and found that at temperatures above 400°C, FeOOH was reduced to Fe_3O_4, and metallic iron was dominant at temperatures above 600°C. For the tar decomposition experiments, the samples were reduced at temperatures above 650°C to obtain samples with mainly metallic iron. The tests were carried out in a two stage reactor with hydropyrolysis of coal occurring in the first stage and the catalyst bed in the second stage using a 50 vol% H_2 gas and a temperature of 750°C. The Indonesian limonite showed a high conversion of tar resulting in only 0.3 wt% of the carbon remaining in the tar and the liquid fractions after the catalytic reactor [46]. The effects of the catalyst bed temperature on the decomposition of coal-derived volatile were also investigated. Without catalyst

placed in the second-stage reactor, the yields of CH_4 and C_2-C_4 gases increased with increasing temperature as expected, while in the presence of limonite the yield of CH_4 decreased with increasing temperature, accompanied with an increase in CO yield. This result might imply that limonite catalyzed the steam reforming reactions in the second-stage reactor [46]. Matsumura et al. [47] tested a slurry catalyst containing 30 wt% Yandi Yellow Australian limonite with a Fe content of 57 wt % for the decomposition of asphaltene from a vacuum residue, compared with a conventional NiO–MoO_2/Al_2O_3 (NiMo) catalyst. The asphaltene conversions obtained with the limonite slurry were slightly higher than with the NiMo catalyst. At a LHSV of 0.5 h^{-1}, the use of the Australian limonite led to asphaltene conversion of 83% at 460°C, which was higher than that with the NiMo catalyst being about 77% at the same temperature [47]. In another study by the same authors, Brazilian limonite, with an iron content of 46 wt%, was examined for asphaltene decomposition, and its activity was also higher than the NiMo catalyst, while the activity was lower than that of the Australian limonite [48].

Besides olivine and limonite, other iron containing catalysts that have been studied for tar reduction include iron oxides (FeO, Fe_2O_4, Fe_3O_4, Fe_2O_3), ankerite ($CaFe(CO_3)_2$ as a ferrous dolomite), sintered iron ore, and pelletized iron ore. Nordgreen et al [49] gasified Sweedish birch in a fluidized bed, where pre-reduced hematite (Fe_2O_3) was used in a downstream reactor and almost 100% tar decomposition was achieved at 900°C. In contrast, other iron oxides, e.g., FeO, Fe_2O_4, and Fe_3O_4 had very little catalytic activity towards tar decomposition. Leppalahti et al [50] compared the effects of ferrous dolomite and a sintered iron ore, and found that the sintered iron ore had a very low activity for tar conversion, although the sintered iron ore had a larger content of Fe (59.2 wt%) than the Fe-dolomite (4.6 wt%). In this study, the Fe-dolomite was calcined at 900°C. A possible reason why the Fe-dolomite showed a higher activity than the sintered iron ore could be that the dolomite had a higher calcium content of 19.2 wt% compared with 5.4wt% for the sintered iron ore, while CaO in dolomite was believed to be a highly active component in tar conversion [37, 38].

2.2.3 Nickel and Other Metal Supported Catalysts

Nickel-based catalysts, used extensively in the petrochemical industry, have shown high activities for tar reforming/decomposition in coal and biomass gasification. When used as the secondary catalysts, the supported nickel catalysts could attain nearly complete decomposition of both tar and ammonia decomposition [51, 52]. As the primary catalysts, however, Ni catalysts were less effective for tar conversion due to the severe coke formation and leading to deactivation of the catalysts [33].

Simell and Bredenberg [53] studied the effectiveness of 11 wt% Ni/Al_2O_3 and several other catalysts including dolomite, activated alumina, silica-alumina, and silica carbide for tar decomposition. It was found the Ni/Al_2O_3 almost completely decomposed the tar and light hydrocarbons at 900°C. Sutton et al. [54] compared several Ni-supported catalysts, prepared either by wet-impregnation or co-precipitation, for tar reduction from peat pyrolysis. A variety of supports including Al_2O_3, ZrO_2, TiO_2, SiO_2 were used with a nickel loading of 5 wt%. For the co-precipitated catalysts, a nickel to aluminium ratio of approximately 1:6 and 1:3 were used. Among all the wet-impregnated catalysts, the Ni/TiO_2 catalyst was the most active catalyst, attaining a tar conversion of 98.1% at 800°C, followed by Ni/ZrO_2 with a 95.2% conversion. Under the same reaction conditions, the co-precipitated catalysts were slightly less effective, obtaining about 92 % tar conversion. In another study by the same authors [55], the supports were tested without the addition of Ni, and the tar conversion over the supports alone were significantly lower than with the addition of Ni, for example the TiO_2 and ZrO_2 alone obtained a conversion of only 79.5% and 78.4%, respectively at 800°C [55].

The addition of nickel to dolomite and olivine has been found to significantly improve the activity towards tar conversion [45, 56, 57]. The olivine alone showed almost no activity for steam reforming of toluene at 750°C whereas the Ni/olivine had a toluene conversion of approximately ~85%. In addition, the Ni/olivine showed good selectivity to H_2, CO, and CO_2 [54[. For conversion of naphthalene, the addition of Ni to calcinated olivine remarkably enhanced the conversion, almost double that of the olivine alone [24], 58, 59]. The addition of Ni to dolomite drastically increased the tar conversion at 650°C from 43% to 84% [42].

Dou et al. [52] studied tar cracking catalysts including alumina-supported NiMo, Y-zeolite, Alumina, Lime and Silica, using 1-methylnaphthalene as the tar model component, and found that the $NiMo/Al_2O_3$ (4% NiO, 14.3% MoO_3, 82.7% Al_2O_3) and Y-zeolite (34.1% Al_2O_3, 44.5% SiO_2, 14.5% CaO, 6.9% Na_2O) were the most effective catalysts, removing almost 100% tar at temperatures above 500°C. The use of the alumina-supported NiMo catalyst initially led to a high conversion of nearly 100% but it dropped to less than 80% after 9 hours on-stream, due to catalyst deactivation. Silica showed much less activity for tar reduction compared to the other catalysts. The long-term durability of alumina-supported catalysts remains the biggest challenge in application of this type of catalysts.

2.2.4 Carbon-based Catalysts

Abu El-Rub et al. [60] compared the activity of a biomass char to other catalysts that are commonly used for tar decomposition, including calcined dolomite (21 wt% MgO, 30 wt% CaO, 0.2 wt% Fe_2O_3), olivine (50 wt% MgO, 42 wt% SiO_2, and 7 wt% Fe_2O_3), and a nickel catalyst (70 wt% NiO, 12 wt% Al_2O_3 and 7 wt% SiO_2). The biomass char was produced by pyrolysis of pinewood at 500°C. Phenol (8-13 g/Nm^3) and naphthalene (40 or 90 g/Nm^3) were used as tar models and the tests were carried out with the presence of CO_2 (6 vol%), H_2O (10 vol%) and N_2 (balance) at 700 and 900°C. At 900°C all the catalysts showed high activities, and phenol was completely converted. At 700°C the Ni catalyst had the highest phenol conversion, and the biomass char was less active, but still more effective than the olivine. The naphthalene conversion tests were carried out at a temperature of 900°C. The biomass char achieved nearly complete conversion of $90g/Nm^3$ naphthalene, whereas the dolomite obtained only 55 wt% conversion of $40g/Nm^3$ naphthalene. Being slightly inferior to the Ni catalyst, the biomass char was found to be more active for naphthalene conversions than the other catalysts tested (olivine and dolomite) [60].

AC derived from coconut shells was used in a study by Lu et al. [61] for toluene decomposition. The AC was used as a support for three copper precursors, i.e., copper nitrate, copper acetate and copper sulphate, and the effects of Cu loadings and reaction temperatures were examined. The tests were carried out using 200 ppm toluene in a N_2

gas containing 10% O_2, and at a space velocity of 40000 h^{-1}. The copper nitrate precursor produced a catalyst with the highest toluene conversion at lower temperatures. The effect of the Cu loading on the toluene decomposition was investigated using the AC the copper nitrate and copper acetate precursors at 270°C and a space velocity of 158,720 h^{-1}. The copper loadings were varied from 1 to 5 wt%. A increase in Cu loadings for the Cu (nitrate)/AC led to an increase in its activity, approaching to 73% at 5 wt% Cu loading, but for the Cu (acetate)/AC catalysts, its activity peaked at copper loading of 3%. A higher loading of Cu on the AC-supported catalysts might cause agglomeration of the copper particles, leading to large particles on the surface of the AC, therefore decreasing its activity. In another study using activated carbon derived from coconut shells by Takaoka et al [62], H_2O_2 and HNO_3 were used as an oxidizing agent to modify the AC for decomposition of pentachlorobenzene. The catalysts were prepared by mixing the AC with oxidizing agents for either 3 or 24 hours, It was observed that by oxidizing the AC, a greater number of pores were formed with larger pore diameters. In the tar decomposition tests, the temperatures varied from 300 to 400°C, and GHSV maintained at 400 h^{-1} for 30 minutes. The HNO_3-treated AC samples (for 24 h) had high conversions of pentachlorobenzene at 98% in air and 86% in N_2 at 300°C. At 400°C all catalyst samples including the untreated AC showed 100% conversion of pentachlorobenzene.

2.3 Catalysts for Hot Gas Ammonia Decomposition

The activation energy required for ammonia decomposition is high, and the typical temperatures in fluidized bed gasifiers, ranging from 800-900°C, is not effective for ammonia decomposition without the presence of a suitable catalyst [14,32]. A catalyst is required to reduce and even eliminate ammonia completely from the product gas at a relatively low temperature, and secondary catalytic processes are most commonly used. Many of the same catalysts used for tar decomposition, such as dolomite catalysts [28] have also been used to minimize the ammonia in the syngas by decomposing it into N_2 and H_2. The most common catalysts used in NH_3 decomposition studies are metals of Fe [30, 63], Ni [63, 64-66] and Ru [63, 64, 67,68].

2.3.1 Dolomite Catalysts

It was found that ammonia could partially decompose on CaO, MgO and on dolomites at temperatures of about 800°C in inert gas atmospheres, but the presence of other gas species such as CO, CO_2, N_2 and H_2 would interfere with the reaction [28]. it was also found that calcined dolomite was more active than CaO or MgO alone in inert helium gas, but with the presence of other gases the decomposition of NH_3 was hindered [14, 32, 69]. Compared to other catalysts (e.g., ferrous materials and nickel catalysts), dolomite was less effective for ammonia decomposition. When being used as a primary catalyst in biomass gasification, dolomite, as well as limestone, actually increased the ammonia content of the gas product at temperatures below 1000°C. Corella et al. [44] also observed that the addition of dolomite as a primary catalyst to the gasifier, for the purpose of tar decomposition, increased the amount of ammonia of the product gas. It was suggested that this might be because dolomite has a high activity for tar cracking, thus releasing the tar-bound nitrogen to ammonia. Therefore, although ammonia can decompose over dolomite, the presence of other competing components, such as tar, will actually decrease its activity towards ammonia decomposition [44].

2.3.2 Iron-based Catalysts

Very few studies have been done using olivine for the purpose of ammonia decomposition, as olivine was found to be less active. In contrast, high conversions of NH_3 to N_2 were achieved using an Australian limonite with a high content of α-FeOOH in a study by Tsubouchi et al [70]. In a gas stream of NH_3 diluted with high purity helium, almost complete conversion of ammonia (≥99%) was obtained at a temperature of 500°C and a space velocity of 45,000 h^{-1} with an Australian limonite. The limonite catalyst was reduced with H_2 at 500°C prior to the ammonia decomposition experiments. In a later study by the same authors [71], the efficiency of the Australian limonite was tested for ammonia decomposition in an inert gas and a simulated gas typical of an air-blown gasification process, containing CO, H_2, CO_2, and H_2O. In the presence of fuel gas (20%CO/10%H_2) the ammonia conversion was found to decrease significantly at lower temperatures, accompanied with a higher conversion to HCN. At higher temperatures (>750°C), however, there was no deactivation of the limonite by the presence of CO and

H_2. Also, it was found that the addition of 10%CO_2 or 3% H_2O, helped to restore the ammonia conversion to approximately 90% at 750°C, and by increasing the temperature further the conversion could approach to 100% [71]. Limonite also showed a higher activity than other reference Fe oxides (Hematite (α- Fe_2O_3) and magnetite (Fe_3O_4)) for ammonia conversion [68].

Leppälahti et al [50], studied several inexpensive catalysts including iron sinter, iron pellet, ferrous dolomite, dolomite and limestone, and inert silicon carbide and a commercial nickel catalyst as the reference, for decomposition of ammonia in the gas product from peat gasification. The research demonstrated that the ferrous materials and the commercial nickel were more effective than dolomite and limestone for decomposing ammonia. Ohtsuka et al [72] were able to obtain complete conversion of 2000 ppm NH_3 by using Fe and Ca supported on brown coal chars at 650°C at a space velocity of 45,000h^{-1}. They found that the 2-6 wt% Fe catalysts were actually more effective than using an 8% Fe catalyst loaded on commercial activated carbon, owing to the high dispersion of the iron particles on the coal char catalysts. Cycle mechanisms involving the formation of N-containing intermediate species and the subsequent decomposition to N_2 were proposed for the Fe and Ca catalysts in NH_3 decomposition [72].

2.3.3 Nickel and Other Metal Supported Catalysts

Mojtahedi and Abbasian [73] studied the activity of Ni/Al_2O_3 catalysts with different nickel loadings of 2, 7.5 and 15 wt% in a gas mixture containing CO, CO_2, CH_4, H_2, H_2O, N_2 and varying NH_3. The ammonia conversion was found to be strongly dependent on the Ni content of the catalyst, and the largest ammonia conversion was obtained with the 15 wt% Ni/Al_2O_3. Nassos et al. [74] studied the effect of Ni loading on various supports with varying space velocities. Ni loadings of 5 and 10 wt% were used on the supports $Ce_{0.9}La_{0.1}O_2$, $Ce_{0.9}Zr_{0.1}O_2$, and Al_2O_3. For the Ni supported on $Ce_{0.9}La_{0.1}O_2$, and $Ce_{0.9}Zr_{0.1}O_2$, they found that the ammonia decomposition efficiency was directly related to the Ni loading, increasing with increased Ni content. It was also found that the catalytic activities differed greatly with Ni loadings at lower temperatures of 500-600°C, while this difference was minimized at higher temperatures. More interestingly, there was remarkable effect of catalyst support on the catalyst's activity for ammonia

decomposition. For instance, the 10 wt% Ni loaded on the $Ce_{0.9}La_{0.1}O_2$ and $Ce_{0.9}Zr_{0.1}O_2$ supports achieved ammonia conversion of 97% and 94%, respectively at 750°C, compared with only 32% conversion with the Al_2O_3-supported 10% Ni at the same temperature. Simell et al. [37] were able to convert 80% of ammonia using a nickel monolith catalyst (NiMo/γ–Al_2O_3) and completely decompose tar at temperatures greater than 900°C. In a study by Wang et al [75], nickel catalysts were used to reduce both tar and ammonia in the product gas from a pilot-scale fluidized-bed gasifier, where 95% of the ammonia removal was obtained with the Ni catalysts at 874°C at a GHSV of 1200 h^{-1}. In addition, some commercial Ni-based catalysts, such as G43-A (United Catalyst), 2800 Raney Nickel (Grace Davison), 146 (Johnson Matthey) were tested for pure ammonia decomposition for the PEM fuel cell applicaiton, and they showed good activities (ammonia conversions of >80%) at temperature above 600-700°C, but they were less effective (ammonia conversion <30%) at <600°C [76]. However, a Ni-Pt/Al_2O_3 catalyst exhibited a very high activity for pure ammonia decomposition, leading to almost compete conversion of NH_3 (97.4%) at 560°C (at 28.44 g cat. h/ g mol NH_3) [76].

In the same study by Mojtahedi and Abbasian [73], comparison was made between Ru/Al_2O_3 and Ni/Al_2O_3 catalysts. The Ru/Al_2O_3 catalyst was demonstrated much more effective than the Ni catalysts. For example, the Ru/Al_2O_3 catalyst obtained ammonia conversions of 95.3%, compared with 90.4% for the Ni catalysts at 850°C. When toluene was added to the gas feed, the Ni and Ru catalysts were slightly deactivated towards ammonia decomposition. In another study by Li et al [64], 10 wt% Ru supported on SiO_2 was also found to be much more effective than the 10 wt% Ni/SiO_2 catalyst. In a 50 ml/min flow of pure ammonia at a GHSV of 30000 h^{-1}, the Ru/SiO_2 catalyst achieved ammonia conversion of 64%, compared to only 10% conversion with the Ni/SiO_2 catalyst. Ru catalysts at a loading of 3-10 wt% supported on Al_2O_3 [77], SiO_2[77], TiO_2 [78] and MgO [79] have been widely tested for pure ammonia decompositions for fuel cell applications, and these Ru catalysts attained 30-40% conversions at a low temperature (400°C). Moreover, Al_2O_3 supported Ru or Ru-Ni catalysts (6-9 wt% total metal loading) have shown to be effective for decomposition of ammonia 1000 ppm in a simulated coal-derived syngas (10 vol% H_2, 28 vol% CO, 54 vol% N_2, 3.6 vol% CO2 and

3 vol% H_2O), leading to ~90% ammonia conversion at 900°C and a GHSV of 20000 h^{-1} [80].

However, the major problem for these Al_2O_3-supported Ni or Ru catalysts for hot gas removal of ammonia or tar is associated with the deactivation by fouling of the catalyst due to the carbon deposition and by H_2S [81,82]. The problem would be serious for tarry fuel gases from gasification and pyrolysis of coal or biomass solid fuels, containing contaminants of tar, CO, CH_4 and H_2S. To prevent the carbon deposition and hence the catalyst deactivation, effective strategies include introduction of steam in the product gas so as to gasify the accumulated coke/carbon [83], and using non-alumina (MgO or CeO_2) as catalyst supports or promoters [84]. It was reported that, an $Rh/CeO_2/SiO_2$ catalyst was able to maintain its activity for tar decomposition even in the presence of a high concentration of H_2S (180 ppmv) in the gas stream [85].

2.3.4 Carbon-based Catalysts

Activated carbons (ACs), produced physically and chemically from various carbonaceous materials, have larger surface areas and higher porosities, which make them good materials as adsorbents for removal of some specific contaminants from gas/liquid streams. Commercial ACs have been found to be much less active towards NH_3 decomposition compared to other catalysts such as dolomite, olivine, iron-based and Ni-based catalysts, as well as chars derived from coals [86,87]. In a study by Fortier et al [88], commercial ACs derived from coconut shells with and without impregnation of $ZnCl_2$ were tested to adsorb a variety of vapours including ammonia, cyclohexane, nitrogen and water. The research showed that the AC alone had a very low adsorption capacity for ammonia, 0.011+/- 0.002 mmol NH_3/g AC, and the capacity was improved by impregnation of $ZnCl_2$ up to a loading of 3.5 mmol $ZnCl_2$/g AC. The low ammonia adsorption capacity of the commercial AC towards ammonia might be a key factor responsible for its low activity for hot gas ammonia decomposition. Although AC and AC supported catalysts are less active for ammonia and tar decomposition than those supported on other materials such as Al_2O_3, SiO_2, TiO_2, MgO, CNTs, etc., further research into the development of effective AC supported catalysts is worth the effort because activated carbon materials have high surface areas and relatively low costs. In

the current thesis, novel less expensive activated carbon-supported (Fe, Ni) catalysts derived from peat have been developed for hot gas decomposition of ammonia (under patenting) and are discussed in Chapter 4 of this work. The proprietary AC-supported catalysts obtained > 90% ammonia conversion at 750°C with 2000 ppm/helium and at a GHSV of 45000 h^{-1}.

In a study by Xu et al [86], pyrolysis chars from low rank coals (brown and sub-bituminous coals) were tested as catalysts for the conversion of NH_3 to N_2. It was found that the inherently present Fe and Ca minerals in the coal chars were responsible for their activities towards ammonia decomposition. Studies using simulated gases containing CO, CO_2 and H_2 were also conducted [86], and the chars initially showed a lower activity for NH_3 conversion, but after an induction period on stream, they attained high conversions (~80% at 750°C) as in the inert atmosphere experiments. In another study by the same group [87], decomposition of ammonia with Fe and Ca catalysts supported on coal chars was investigated using 2000 ppm NH_3 diluted in helium in a fixed bed. The coal-char-supported Fe and Ca catalysts were found to be very effective for ammonia decomposition. An iron content of 6 wt% on an Australian brown coal char attained a conversion of nearly 100% at 750°C and a GHSV of 45000 h^{-1}.

Yin et al. [88,89] demonstrated that the use of carbon nanotubes (CNTs) as a catalyst support for Ru for ammonia decomposition. The catalytic performance of Ru catalysts was strongly dependent on support materials: under similar reaction conditions, NH_3 conversion decreased in the order of Ru/CNTs > Ru/MgO > $Ru/TiO_2 \cong Ru/Al_2O_3 \cong Ru/ZrO_2$ > Ru/AC. The excellent catalytic performance of Ru/CNTs was believed to be related to the high dispersion of Ru on the CNTs. Moreover, Yin et al. [63, 89] proposed that the conductivity of the support might also be an important factor for catalytic activity. A conductive support is beneficial for the transfer of electrons from promoter and/or support to Ru, which would facilitate desorption of surface N atoms to form N_2. It was further demonstrated by Yin et al. [63, 89] that a support of high acidity is unsuitable for NH_3 decomposition. Accordingly, CNTs (of high conductivity due to the graphitization of carbon atoms) combined with a basic support (MgO) may lead to an enhanced activities for supported Ru catalysts. As a matter of fact, this has been evidenced by

another study by Yin et al. [90], where the Ru/MgO–CNTs catalyst with an equal weight of MgO and CNTs exhibited a catalytic activity higher than that of Ru/MgO or Ru/CNTs.

2.4 Conclusions

(1) Biomass gasification produces a low to medium-BTU product gas (or syngas) containing primarily CO_2, H_2, CO, CH_4 and (C_2+C_3), as well as some contaminants such as tars, NH_3, H_2S and SO_2, etc. In order to achieve better efficiencies of the syngas applications, these contaminants must be removed before the syngas is used for heat and electricity generation, or in particular for synthesis of liquid fuels and methanol.

(2) The contaminants of tars and ammonia from the gasification processes could be removed by hot gas clean-up technology through catalytic steam/dry reforming or catalytic cracking/hydro-cracking reactions of tar, and through catalytic decomposition of ammonia to form N_2 and H_2.

(3) Calcined dolomites can be equally effective as either the primary or secondary catalysts for minimizing tar in the product gas. The presence of CaO in dolomite might be responsible for its activity in tar conversion. Compared to other catalysts (e.g., ferrous materials and nickel catalysts), dolomite is less effective for ammonia decomposition. The major problem with using calcined dolomite is that it is a soft and fragile material, which would limit its use in some types of reactors such as a fluidized bed reactor.

(4) Fe-based natural mineral catalysts, including olivine (Fe_2SiO_4 or Mg_2SiO_4), limonite (composed mainly of goethite, FeOOH), hematite (Fe_2O_3), ankerite (as a ferrous dolomite), are active for tar decomposition. Olivine is less active for ammonia decomposition, but an Australian limonite with a high content of α-FeOOH was found to be very effective for ammonia decomposition. Cycle mechanisms involving the formation of N-containing intermediate Fe species were proposed for the Fe catalysts in NH_3 decomposition.

(5) Nickel-based supported catalysts, used extensively in the petrochemical industry, have shown high activities for tar reforming/decomposition and ammonia

decomposition in coal and biomass gasification. When used as the secondary catalysts, the supported nickel catalysts could attain nearly complete decomposition of both tar and ammonia at > 800°C. The addition of nickel to dolomite and olivine could significantly improve the activity towards tar conversion. The Al_2O_3 or SiO_2-supported Ru catalyst was showed to be much more effective than the Ni catalysts. However, the major problem for these Al_2O_3-supported Ni or Ru catalysts for hot gas removal of ammonia or tar is associated with the deactivation by fouling of the catalyst due to the carbon deposition or by H_2S. The strategies to prevent the carbon deposition and hence the catalyst deactivation include introduction of steam in the product gas so as to gasify the accumulated coke/carbon, and using non-alumina (MgO or CeO_2) catalyst supports or promoters.

(7) Commercial Activated carbons (ACs) have been found to be much less active towards NH_3 decomposition compared to other catalysts such as dolomite, olivine, iron-based and Ni-based catalysts, as well as chars derived from coals. Pyrolysis chars of low rank coals (brown and sub-bituminous coals) and coal-char-supported Fe and Ca catalysts showed high activities towards ammonia decomposition. More noticeably, carbon nanotubes supported Ru catalysts exhibited excellent catalytic performance in ammonia decomposition, owing to the high dispersion of metal particles on the support and the conductivity of the support itself.

References

[1] X.T. Li, J.R. Grace, C.J. Lim, A.P. Watkinson, H.P. Chen, J.R. Kim. Biomass gasification in a circulating fluidized bed. *Biomass and Bioenergy* 2004; 26:171 – 193.

[2] P.L. Spath, D.C. Dayton. Preliminary Screening—Technical and Economic Assessment of Synthesis Gas to Fuels and Chemicals with Emphasis on the Potential for Biomass-Derived Syngas; National Renewable Energy Laboratory: Golden, CO., 2003. http://www.nrel.gov/docs/fy04osti/34929.pdf.

[3] M.P. Aznar, M.A. Caballero, J. Corella, G. Molina, and J.M. Toledo. Hydrogen production by biomass gasification with steam-O_2 mixtures followed by a catalytic steam reformer and a CO-shift system. *Energ. Fuel* 2006; 20: 1305–1309.

[4] T. Bui, R. Loofand, S.C. Bhattacharya, Multi-stage reactor for thermal gasification of wood. *Energy* 1994; 19:397–404.

[5] L.K. Mudge, E.G. Baker, D.H. Mitchell, M.D. Brown. Catalytic steam gasification of biomass for methanol and methane production. *J. Solar Energ. Eng.*, 1985;107 (1): 88–92.

[6] J. Gil, J. Corella, M. P. Aznar, M. A. Caballero. Biomass Gasification in Atmospheric and Bubbling Fluidized Bed: Effect of the Type of Gasifying Agent on the Product Distribution. *Biomass and Bioenergy* 1999; 17: 389-403.

[7] G. Schuster, G. LoVer, K. Weigl, H. Hofnauer. Biomass steam gasification—an extensive parametric modeling study. *Bioresource Technology* 2001;77:71–9.

[8] J.P.A. Neeft, H.A.M. Knoef, P. Onaji. Behaviour of tar in biomass gasification systems. Tar related problems and their solutions. *Energy from Waste and Biomass* (EWAB), Novem Report No. 9919. The Netherlands, 1999.

[9] T.A. Milne, R.J. Evans. Biomass gasification "tars": their nature, formation and conversion. NREL, Golden, CO, USA, Report no. NREL/TP-570-25357, 1998.

[10]. J. Zhou, S.M. Masutani, D.M. Ishimura, S.Q. Turn, C.M. Kinoshita, Release of fuel-bound nitrogen during biomass gasification. Ind. Eng. Chem. Res. 39 (2000): 626–634.

[11] P.F. Nelson, A.N. Buckley, M.D. Kelly. 24th Symp (Intl) Combust, The Combustion Institute, Pittsburgh, PA, 1992. p. 1259–67.

[12] J.E. Varey, C.J. Hindmarsh and K.M. Thomas. The detection of reactive intermediates in the combustion and pyrolysis of coals, chars and macerals *Fuel* 1996; 75: 164.

[13] S. Kambara, T. Takarada, Y. Yamamoto and K. Kato. Relation between functional forms of coal nitrogen and formation of nitrogen oxide (NOx) precursors during rapid pyrolysis. *Energy and Fuels* 1993; 7: 1013.

[14] J. Leppälahti. Formation of NH_3 and HCN in slow-heating-rate inert pyrolysis of peat, coal and bark. *Fuel* 1995; 74: 1363.

[15] R. Bassilakis, Y. Zhao, P.R. Solomon and M.A. Serio. Sulfur and nitrogen evolution in the Argonne coals. Experiment and modeling. *Energy and Fuels* 1993; 7:710-720.

[16] J. Leppälahti and T. Koljonen. Nitrogen evolution from coal, peat and wood during gasification: Literature review. *Fuel Process Technol* 1995; 43, p. 1-45.

[17] P.F. Nelson, C.-Z. Li and E. Ledesma. Formation of HNCO from the Rapid Pyrolysis of Coals. *Energy and Fuels* 1996; 10: 264-265

[18] W. Mojtahedi, M. Ylitalo, T. Maunulab, J. Abbasian. Catalytic decomposition of ammonia in fuel gas produced in pilot-scale pressurized fluidized-bed gasifier. *Fuel Processing Technology* 1995; 45: 221-236

[19] J. A.Miller, M. D. Smooke, R. M Green, R. J. Kee. Kinetic Modelling of the Oxidation of Ammonia in Flames. *Combustion Science Technology* 1983; 34:149–176.

[20] I. Narvaez, A. Orio, M. P. Aznar, J Corella. Biomass Gasification with Air in an Atmospheric Bubbling Fluidized Bed. Effect of Six Operational Variables on the Quality of the Produced Raw Gas. *Industrial & engineering chemistry research* 1996; 35: 2110-2120.

[21] E. Kurkela,. Air Gasification of Peat, Wood and Brown Coal in a Pressurized Fluidized-Bed Reactor. I. Carbon Conversion, Gas Yields and Tar Formation. *Fuel Processing Technology* 1992; 31: 1-21.

[22] J. Zhou, S.M. Masutani, D.M. Ishimura, S.Q. Turn, C. M. Kinoshita. Release of Fuel-Bound Nitrogen during Biomass Gasification. *Industrial & engineering chemistry research* 2000; 39: 626-634.

[23] J. Leppalahti, T. Koljonen. Nitrogen Evolution from Coal, Peat and Wood During Gasification: Literature Review. *Fuel Processing Technology* 1995; 43: 1-45

[24] L. Devi, K.J. Ptasinski, F. J. Janssen .Pretreated olivine as tar removal catalyst for biomass gasifiers: investigation using naphthalene as model biomass tar. *Fuel Processing Technology* 2005; 86: 6: 707-730

[25] R. Coll, J. Salvado, X. Farriol, D. Montane. Steam reforming model compounds of biomass gasification tars: conversion at different operating conditions and tendancy towards coke formation. *Fuel Processing Technology* 2001; 74: 19-31

[26] P. A. Simell; J.O. Hepola; A. Krause. Effects of gasification gas components on tar and ammonia decomposition over hot gas cleanup catalysts. *Fuel* 1997; 76: 1117-1127

[27] G. Taralas, M.G. Kontominas, Kinetic modelling of VOC catalytic steam pyrolysis for tar abatement phenomena in gasification/pyrolysis technologies. Fuel, 83(2004): 1235–1245.

[28] P. Simell, E. Hirvensalo, V. Smolander. Steam Reforming of Gasification Gas Tar over Dolomite with Benzene as a Model Compound. Industrial *& Engineering Chemistry Research* 1999; 38: 1250-1257

[29] W. Torres et al. W. Torres; S.S. Pansare , J. G. Jr. Goodwin. Removal of Tars, Ammonia, and Hydrogen Sulfide from Biomass Gasificaiton Gas. *Catalysis Reviews* 2007; 49:4, 407 -456

[30] W. Arabczyk, J. Zamłynny, Study of the ammonia decomposition over iron catalysts. Catalysis Letters 60 (1999) 167-171.

[31] A.S. Chellappa, C.M. Fischer, W.J. Thomson, Applied Catalysis A: General 227 (2002) 231.

[32] J. Leppalahti, E. Kurkela. Behaviour of nitrogen compounds and tars in fluidized bed air gasification of peat. *Fuel* 1991; 70: 491-497.

[33] D. Dayton. A Review of the Literature on Catalytic Biomass Tar Destruction. National Renewable Energy Laboratory. NREL/TP-510-32815 (2002)

[34] Donnot, A., Reningovolo, P., Magne. P. and Deglise. X. *J.* Flash pyrolysis of tar from the pyrolysis of pine bark. *Journal of analytical and applied pyrolysis* 1985; 8:401–414

[35] A. Donnot, P. Magne, X. Deglise. Experimental approach to the catalyzed cracking reaction of tar from wood pyrolysis *Journal of analytical and applied pyrolysis* 1991; 21: 265-280

[36] J.Corella, M.P. Aznar, J. Gill, M.A. Caballero. Biomass Gasification in Fluidized Bed: Where To Locate the Dolomite To Improve Gasification. *Energy Fuels* 1999; 13: (6) 1122-1127

[37] P. Simell, E. Kurkela, P. Ståhlberg, J. Hepola. Catalytic hot gas cleaning of gasification gas. *Catalysis Today* 1996; 27:55-62

[38] P.Simell, E.Kurkela, P. Ståhlberg; J. P. Hepola. Development of catalytic gas cleaning in biomass gasification. *VTT symp* 1996;164:133–140

[39] S. Rapagnà, N. Jand, P. U. Foscolo. Catalytic gasification of biomass to produce hydrogen rich gas. *International Journal of Hydrogen Energy* 1998; 23 (7): 551-557

[40] G. Hu, S. Xu, S. Li, C. Xiao, S. Liu. Steam gasification of apricot stones with olivine and dolomite as downstream catalysts. *Fuel Processing Technology* 2006; 87: 375-382.

[41] A. Orı´o; J. Corella, I. Narvaez. Performance of Different Dolomites on Hot Raw Gas Cleaning from Biomass Gasification with Air. *Industrial & Engineering Chemistry Research* 1997; 36: 3800-3808

[42 T.J. Wang, J. Chang, P.M. Lv. Novel Catalyst for Cracking of Biomass Tar. *Energy & Fuels* 2005; 19:22-27.

[43] P. Perez, P M Aznar, M. A . Ccaballero, J. Gil, J.A. Martin, J. Corella. Hot gas cleaning and upgrading with a calcined dolomite located downstream a biomass fluidised bed gasifier operating with steam-oxygen mixtures. *Energy Fuel* 1997; 11, 1194-203

[44] J. Corella. A. Orío, J. M. Toledo. Biomass gasification with air in a fluidizedbed: exhaustive tar elimination with commercial steam reforming catalysts. *Energy Fuels* 1999; 13: 702–709

[45] J.N. Kuhn, Z. Zhao, L. G. Felix, R. B. Slimane, C. W. Choi, U. S. Ozkan. Olivine catalysts for methane and tar steam reforming. *Applied Catalysis B: Environmental* 2008; 81:12-26.

[46] L. Li, K. Morishita, T. Takarada. Light fuel gas production from nascent coal volatiles using a natural limonite ore. *Fuel* 2007; 86:1570-1576

[47] A. Matsumura, S. Sato, T. Kondo, I. Saito, W. Ferraz de Souza. Hydrocracking Marlim vacuum residue with natural limonite. Part 2: experimental cracking in a slurry-type continuous reactor. *Fuel* 2005; 84: 17-421

[48] A. Matsumura, T. Kondo, S. Sato, I. Saito, W. Ferraz de Souza. Hydrocracking Brazilian Marlim vacuum residue with natural limonite. Part 1: catalytic activity of natural limonite. *Fuel* 2005; 84:411–416

[49] T Nordgreen, T. Liliedahl, K. Sjostrom. Metallic iron as a tar breakdown catalyst related to atmospheric, fluidised bed gasification of biomass. *Fuel* 2006; 85: 689-694

[50] J. K. Leppälahti, P. A. Simell, E. A. Kurkela. Catalytic conversion of nitrogen compounds in gasification gas. *Fuel Processing Technology* 1991; 29: 43-56

[51] J. Han, H Kim.The reduction and control technology of tar during biomass gasification/pyrolysis: An overview. *Renewable and Sustainable Energy Reviews* 2008; 12: 397–416.

[52] B. Dou, J. Gao, X. Sha, S. Wook Baek. Catalytic cracking of tar component from high temperature fuel gas. *Applied Thermal Engineering* 2003; 23: 2229-2239

[53] P. A. Simell, J.B.-son Bredenberg. Catalytic purification of tarry fuel gas. *Fuel*, 1990; 69: 1219-1225

[54] D. Sutton, B. Kelleher, A. Doyle, J. R. H Ross. Investigastion of nickel supported catalysts for the upgrading of brown peat derived gasification products. *Bioresource Technology 2001*; 80: 111-116.

[55] D. Sutton, B. Kelleher, J. R. H Ross. Catalytic conditioning of organic volatile products produced by peat pyrolysis. *Biomass and Bioenergy* 2002; 23: 209-216.

[56] D. Swierczynski, S. Libs, C. Courson, A. Kiennemann. Steam reforming of tar from a biomass gasification process over Ni/olivine catalyst using toluene as a model compound. *Applied Catalysis B: Environmental* 2007;74: 211–222

[57] J. Kuhn, Z. Zhao, A. Senefeld-Naber, L. G. Felix, R. B. Slimane, C. W. Choi, U. S. Ozkan. Ni-olivine catalysts prepared by thermal impregnation: Structure, steam reforming activity, and stability. *Applied Catalysis A: General* 2008; 341: 43–49

[58] L. Devi, K. J. Ptasinski, F. J. J. G. Janssen. A review of the primary measures for tar elimination in biomass gasification processes. *Biomass and Bioenergy* 2003; 24: 125-140

[59] L. Devi, M. Craje, P. Thüne, K. J. Ptasinski, F.J.J.G. Janssen. Olivine as tar removal catalyst for biomass gasifiers: Catalyst characterization. *Applied Catalysis A: General* 2005: 294: 68-79

[60] Z. Abu El-Rub,E.A. Bramer, G. Brem. Experimental comparison of biomass chars with other catalysts for tar reduction. *Fuel* 2008; 87: 2243–2252

[61] C.Y. Lu, M.-Y. Wey, Y.-H. Fu. The size, shape, and dispersion of active sites on AC-supported copper nanocatalysts with polyol process: The effect of precursors. *Applied Catalysis A: General* 2008; 344: 36–44

[62] M. Takaoka, H. Yokokawa, N. Takeda. The effect of treatment of activated carbon by H_2O_2 or HNO_3 on the decomposition of pentachlorobenze. *Applied Catalysis B: Environmental* 2007; 74: 179-186

[63] S.F. Yin, Q.H. Zhang, B.Q. Xu, W.X. Zhu, C.F. Ng, C.T. Au, Investigation on catalysis of COx-free hydrogen generation from ammonia. J. Catal. 224 (2004) 384-396.

[64] X.-K. Li, W.-J. Ji, J. Zhao, S.-J. Wang, C.-T. Au. Ammonia decomposition over Ru and Ni catalysts supported on fumed SiO_2, MCM-41, and SBA-15. *Journal of Catalysis* 2005; 236: 181.

[65] W. Zheng, J. Zhang, Q. Ge, H. Xu, W. Li. Effects of CeO_2 addition on Ni/Al_2O_3 catalysts for the reaction of ammonia decomposition to hydrogen. *Applied Catalysis B: Environmental* 2008; 80:98.

[66] M.E.E. Abashar, Y.S. Al-Sughair, I.S. Al-Mutaz, Investigation of low temperature decomposition of ammonia using spatially patterned catalytic membrane reactors. *Applied Catalysis A: General.* 2002; 236:35-53.

[67] M.C.J. Bradford, P.E. Fanning, M.A. Vannice. Kinetics of NH_3 Decomposition Over Well Dispersed Ru. J. Catal. 172 (1997) 479-484.

[68] K. Hashimoto, N. Toukai, J. Mol. Decomposition of Ammonia over a Catalyst Consisting of Ruthenium Metal and Cerium Oxides Supported on Y-Form Zeolite *Catal. A: Chem.* 2000; 161:171.

[69] E. Bjoirkman, K Sjostrom Decomposition of ammonia over dolomite and related compounds. *Energy Fuel* 1991, 5: 753–760.

[70] N. Tsubouchi, H. Hashimoto, Y. Ohtsuka, High catalytic performance of fine particles of metallic iron formed from limonite in the decomposition of a low concentration of ammonia. *Catalysis Letters* 2005; 105: 203-208.

[71] N. Tsubouchi, H. Hashimoto, Y. Ohtsuka. Catalytic Performance of Limonite in the Decomposition of Ammonia in the Coexistence of Typical Fuel Gas Components Produced in an Air-Blown Coal Gasification Process. *Energy & Fuels* 2007;*21*: 3063–3069

[72] Y. Ohtsuka, C. Xu, D. Kong, T.Naoto Decomposition of ammonia with iron and calcium catalysts supported on coal chars. *Fuel* 2004; 83: 685-692

[73] W Mojtahedi, J. Abbasian. Catalytic decomposition of ammonia in a fuel gas at high temperature and pressure. *Fuel* 1995; 74:1698-1703

[74] S. Nassos, E. Elm Svensson, M. Boutonnet, S.G. Jaras. The influence of Ni load and support material on catalysts for the selective catalytic oxidation of ammonia in gasified biomass. *Applied Catalysis B: Environmental* 2007;74:92–102

[75] W. Wang, N. Padban, Z. Ye, G. Olofsson, A. Andersson, I. Bjerle. Catalytic Hot Gas Cleaning of Fuel Gas from an Air-Blown Pressurized Fluidized-Bed Gasifier. *Ind. Eng. Chem. Res.* 2000; 39: 4075 -4081,

[76] A. Chellappa, S. Fischer, W. Thomson. Ammonia decomposition kinetics over Ni-Pt/Al2O3 for PEM fuel cell applications. *Applied Catalysis A: General* 2002;227:231–240

[77] T.V. Choudhary,C. Sivadinarayana, D. W. Goodman. Production of CO_x-free hydrogen for fuel cells via step-wise hydrocarbon reforming and catalytic dehydrogenation of ammonia. *Chemical Engineering Journal,* 2003;93: 69-80

[78] S.F. Yin, B.Q. Xu, X.P. Zhou, C.T. Au. A mini-review on ammonia decomposition catalysts for on-site generation of hydrogen for fuel cell applications. *Applied Catalysis A: General*, 2004; 277:1-9

[79] J. Zhang et AL. H. XU, Q. GE, W. LI. Highly efficient Ru/MgO catalysts for NH3 decomposition:Synthesis, characterization and promoter effect. *Catalysis Communications* 2006;7: 148–152

[80] Y. Ozawa et al. Catalytic decomposition of ammonia in simulated coal-derived gas. Chemical Engineering Science 62 (2007) 5364 – 5367

[81] G.N. Krishnan, W.J. Wood, G.T. Tong, J.G. McCarty, Study of Ammonia Removal in Coal Gasification Processes; Report DOE/MC/23087-2667; SRI International: Menlo Park, CA, 1988.

[82] H. Depner, A. Jess, Kinetics of nickel-catalyzed purification of tarry fuel gases from gasification and pyrolysis of solid fuels. Fuel, 78 (1999) 1369-1377.

[83] R. Coll, J. Salvado, X. Farriol, D. Montane, Steam reforming model compounds of biomass gasification tars: Conversion at different operating conditions and tendency towards coke formation. Fuel Process. Technol., 74 (2001):19–31.

[84] M. Asadullah, S. Ito, K. Kunimori, M. Yamada, K. Tomishige, Biomass gasification to hydrogen and syngas at low temperature: Novel catalytic system using fluidized-bed reactor. J. Catal., 208 (2002): 255–259.

[85] K. Tomishige, T. Miyazawa, T. Kimura, K. Kunimori, N. Koizumi, M. Yamada, Resistance to sulfur poisoning of hot gas cleaning catalysts for the removal of tar from the pyrolysis of cedar wood. Appl. Catal., B, 60 (2005): 299–307.

[86] C. Xu, N. Tsubouchi, H. Hashimoto, Y. Ohtsuka Catalytic decomposition of ammonia gas with metal cations present naturally in low rank coals. *Fuel* 2005:84:1957–1967

[87] Y. Ohtsuka, C. Xu, D. Kong, N. Tsubouchi. Decomposition of ammonia with iron and calcium catalysts supported on coal chars. *Fuel* 2004; 83: 685–692

[88] H. Fortier, P. Westreich, S. Selig, C. Zelenietz, J.R. Dahn. Ammonia, cyclohexane, nitrogen and water adsorption capacities of an activated carbon impregnated with increasing amounts of $ZnCl_2$, and designed to chemisorb gaseous NH_3 from an air stream. *Journal of Colloid and Interface Science* 2008;320:423–435

[89] S.F. Yin, B.Q. Xu, C.F. Ng, C.T. Au, Nano Ru/CNTs: A highly active and stable catalyst for the generation of COx-free hydrogen in ammonia decomposition. Appl. Catal. B: Environ. 48 (2004) 237.

[90] S.F. Yin, B.Q. Xu, S.J.Wang, C.F. Ng, C.T. Au, Magnesia–Carbon Nanotubes (MgO–CNTs) Nanocomposite: Novel Support of Ru catalyst for the Generation of CO_x-Free Hydrogen from Ammonia. Catal. Lett. 96 (2004) 113-116.

CHAPTER 3

Production and Characterization of Activated Carbons from a Canadian Peat

ABSTRACT

In this study, activated carbons (ACs) with surface areas of 675-888 m^2/g and total pore volumes of 0.36-0.51 cm^3/g were produced from a Canadian peat by chemical activation using either H_3PO_4 or $ZnCl_2$ as the activation agent, followed by carbonization at a relatively low carbonization temperature (450°C). $ZnCl_2$ was found to be an effective activation agent for developing microporous structures in the ACs, leading to greater surface areas, while H_3PO_4 is highly active in developing the mesopores, leading to much higher mesopore volumes and average pore sizes. The effects of intrinsic minerals in the precursor were examined by demineralization of the peat with HCl washing before the activation and carbonization. The demineralization of the precursor greatly promoted the development of micropores during the activation process, leading to markedly improved the surface areas of the resulting ACs irrespective as to which activation agent was used, and the AC derived from the demineralised peat activated by $ZnCl_2$ attained the highest BET surface area of 888 m^2/g. The demineralization of the precursor could also significantly improve the mesoporous structure of the $ZnCl_2$-activated ACs.

Keywords: *Activated Carbon, Peat, H_3PO_4 Activation, $ZnCl_2$ activation, Demineralization.*

3.1. Introduction

Activated Carbons (ACs) have been widely used as adsorbents or catalytic supports because of their high surface areas (ranging from 250-3000 m^2/g) and porosity (as high as 0.6 cm^3/g), pore distribution and several oxygenated surface functional groups which provide a means of adsorption [1, 2]. Activated carbon is a non-graphitic, microcrystalline form of carbon. Its structure is more disordered than that of graphite, and contains crystallites only a few layers thick and less than 10 nm wide [3]. ACs have pore structures ranging from micropores (< 2nm), to mesopores (2-50 nm) and to macropores (> 50nm), as illustrated in Figure 1. Depending on the types of application, there are different requirements on the pore structures of ACs. For liquid-phase applications higher pore volume in the macropore range is required for disusing liquids into the mesopore and micropore regions, whereas in gas-phase applications, a higher pore volume in the meso- and micro-pore region is more desirable [5].

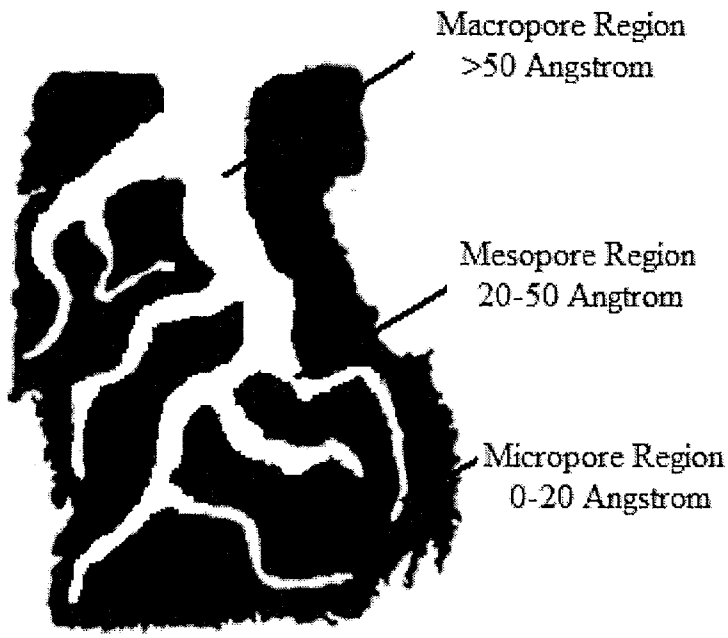

Figure 3-1 Textural structure of activated carbon [4]

Activated carbons can be produced through physical or chemical activation from any carbonaceous material such as wood, coal, lignite and peat [6]. In physical activation processes, the precursor is carbonized at high temperatures (>800°C) followed by activation with steam or

carbon dioxide. Compared with chemical activation methods, normally the physical methods are inferior with respects to carbon yields and surface areas of the final products. In chemical activation the precursor is soaked in a chemical agent such as H_2SO_4, $ZnCl_2$, KOH, or H_3PO_4 [7] and carbonized at relatively low temperatures (<800°C). The use of potassium (K) during chemical activation has been found to increase microporosity as well as surface area, and calcium (Ca) has been found to promote development of mesopores [8,9].

Different methods used for activation can result in different surface characteristics such as the BET surface area, porosity, number of active sites, and functional groups. For example, in the study by Macia-Agullo et al. [10], coal tar pitch was activated both physically and chemically to compare the effects of the activation methods on the surface characteristics. Physical activation was carried out at temperatures ranging from 820-900°C, with a CO_2 gas flow of 100ml/min and activation times ranging from 2.5 to 26 hours. The chemical activations were carried out using varying ratios of either KOH or NaOH at 750°C, followed by washing with 5M HCl and drying in air. It was found that the coal char chemically activated with NaOH at in a NaOH-to-char ratio of 8:1 (w/w), produced the greatest BET surface area of 3033 m^2/g. The physically activated coal char also attained a large BET surface area of 2487m^2/g at 890°C and an activation time of 22.5 hrs, but had the lowest yield of only 6%. The samples prepared by physical activation had wider pore size distributions.

Girgis et al. [7] used both physical and chemical activation methods to activate peanut hulls. As a physical activation method, pyrolysis for 2 hours at 600°C generated an AC with a surface area of 253m^2/g. In the chemical activation methods, the peanut hulls were impregnated with one of the following chemicals, 50% $ZnCl_2$, 1:1 KOH and 85% or 41% H_3PO_4 and with varying ratios [7]. The sample prepared with 85wt% H_3PO_4 with an acid/precursor ratio of 1, and heat treated for 3 hours at 500°C resulted in the highest BET surface area (1177 m^2/g) at a yield of about 22%. This study found that samples impregnated with KOH was not effective for activating the peanut hulls under the test conditions, although it was successful in the study by Macia-Agullo et al. [10], this may be due to the KOH clogging the pores.

Metal compounds such as KOH are used for activation of coal precursors or chars, while H_3PO_4 and $ZnCl_2$ are widely used for the activation of lignocellulosic materials such as in the studies discussed above [7, 10]. When compared to $ZnCl_2$, phosphoric acid is a more preferred activation agent due to the environmental disadvantage associated with zinc chloride. In addition, the ACs produced using $ZnCl_2$ are not accepted in pharmaceutical and food industries as it may

contaminate the product. Phosphoric acid activation has been widely applied on a wide variety of cellulosic precursors such as peanut hull [7], coconut shell [11, 12], sugar cane bagasse [13], and wood sawdust [14]. The H_3PO_4 activation processes can be either as single-stage or two-stage activation process carried out either in an inert or oxidizing atmosphere.

Peat is accumulation of partially decayed vegetation matter formed in wetlands. Over the past 50 years, the use of peat fuel in industry and for large-scale power generation has been very common in Europe, in particular in Finland, Ireland, Russia, Belarus and Sweden [15, 16]. Peat can also be used as a raw material for the production bio-oil and bio-char [15]. Peatlands cover an estimated 400 million hectares (about 3%) of the Earth's land surface and Canada contains some 40% of the world's peatlands – about 170 million hectares [16]. Therefore, peat can be an immense resource for the production of both fuel and carbon materials. The main objectives of this study is to produce and characterize inexpensive activated carbons from Canadian peat by chemical activation using phosphoric acid and $ZnCl_2$, and to examine the effects of demineralization of the raw peat by HCl pretreatment on the product characteristics (surface areas and pore structures).

3.2. Experimental Materials and Methods

3.2.1 Peat

The peat sample used was obtained from an Eastern Canadian company, Peat Resources Ltd. Prior to use, the peat was dried for 24 hrs at 105°C, and then ground with a Wiley mill and screened to particles smaller than 40 mesh (~0.4 mm). Elemental analysis of the raw peat was carried out using a CEC (SCP) 240-XA Elemental Analyzer. The proximate analysis results were determined by thermogravimetric analyzer (TGA). The analysis results of the raw material of peat are given in Table 3-1.

Table 3-1 Proximate and ultimate analyses of the peat sample.

Proximate analysis, wt% (d.b.[1])			Ultimate analysis, wt% (d.a.f.[2])				
VM[3]	FC[4]	Ash	C	H	N	S	O[5]
65.6	29.0	5.4	54.7	5.5	2.1	0.2	32.1

[1] On a dry basis; [2] On a dry-and-ash-free basis; [3]volatile matter; [4]fixed carbon content; [5] By difference

3.2.2 Production of Activated Carbons using H_3PO_4 or $ZnCl_2$

The activated carbon was prepared by a chemical activation method using either H_3PO_4, or $ZnCl_2$ and the overall synthesis process is shown in Figure 3-2. The AC samples were prepared by mixing 40 grams of the dried raw peat powder with 100 ml of 60wt% H_3PO_4 or 60wt% $ZnCl_2$. The mixture was stirred thoroughly to form uniform slurry, and allowed to soak overnight at room temperature. The sample was then thermally treated in a muffle furnace pre-set at 200°C for 15 min in air, followed by carbonization at 450°C for 45 min in air. After the sample was cooled down to room temperature, it was washed with distilled water repeatedly until a neutral pH was obtained. The washed sample was dried overnight at 105°C in air before being crushed and sieved into particles sized of 300-850 μm. The yields of the resulting ACs, determined in terms of the weights, were 55-60% and 60-62% for the H_3PO_4 and $ZnCl_2$ process, respectively. The obtained AC samples are designated H_3PO_4 AC-raw or $ZnCl_2$ AC-raw in this study.

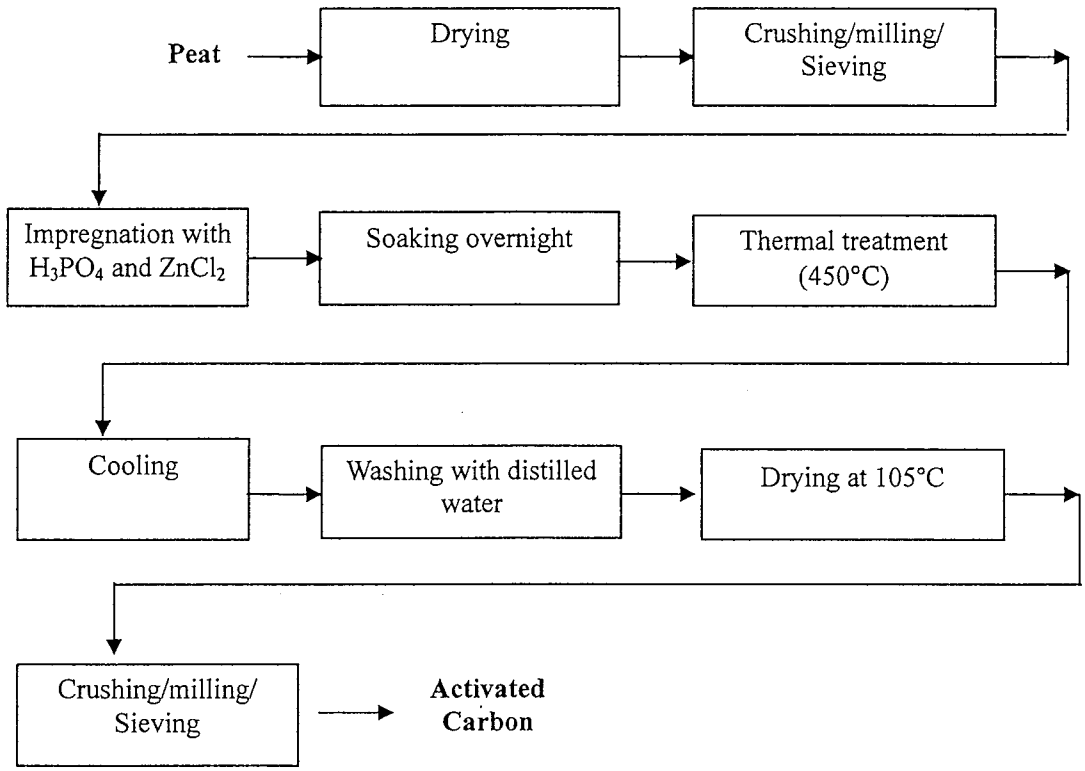

Figure 3-2 Process flow diagram of production of activated carbon from peat.

In order to determine the effects of ash and intrinsic minerals, the peat was de-mineralized with HCl pre-treatment before the activation and carbonization. The peat powder was demineralized by adding 400 ml of 18% hydrochloric acid (HCl) solution to 40 grams of dried peat. This was then treated under a magnetic stirrer for 16 hours at 60°C in a water bath. After treatment with HCl, the peat slurry was cooled down to room temperature, filtrated and washed with distilled water repeatedly until a neutral pH was obtained. The demineralized peat sample was subject to analysis of ash content and mineral compositions. The results are comparatively given in Table 3-2. The demineralized peat was then used to produce activated carbon chemically activated with H_3PO_4 or $ZnCl_2$ using the same method as described in the previous section. The yields of the resulting ACs were determined at about 64% for both processes employing either H_3PO_4 or $ZnCl_2$. To distinguish the obtained ACs from those derived from raw peat, the prepared ACs are denoted as H_3PO_4 AC-dem or $ZnCl_2$ AC-dem, wherein the "dem" designates the "demineralized peat".

Table 3-2 Ash content and concentrations of major inorganic elements in the precursor for AC synthesis

Precursor	Ash	Major inorganic elements, (wt%, d.b.)[1,2]								
	(wt%, d.b.)	Na	K	Mg	Ca	P	Fe	S	Al	Si
Raw peat	5.4	0.1	0.4	2.3	15.6	1.0	11.1	1.1	4.6	1.0
De-mineralized peat	4.4	0.01	0.01	>0.01	0.02	n.d.	0.03	0.1	0.05	0.06

[1] On a dry basis; [2]Determined by ICP-AES

3.2.3 Characterization of ACs

The obtained AC samples were analyzed by N2 isothermal adsorption (77K) for its surface area and textural structures. N_2 isothermal adsorption (77 K) was conducted with a bench-top high speed gas sorption analyzer "NOVA 1200e/TO", manufactured by Quantachrome Instruments, USA. The Brunauer-Emmett-Teller (BET) equation was used to determine the surface area of the samples and the Barrett, Joyner and Halenda (BJH) method for evaluating the nitrogen adsorption isotherms was used to determine the area and volumes of the pores as well as their distributions. Prior to N_2 adsorption, the solids were outgassed for 2 hours at 200°C to ensure the removal of any gases present on the surface of the solids.

3.3. Results and Discussion

3.3.1 Adsorption-Desorption Isotherms

Figure 3-3 shows the N_2 adsorption/desorption isotherms of the H_3PO_4 AC-raw and H_3PO_4 AC-dem. It can be easily seen that the AC derived from demineralized sample shows a slightly higher N_2 adsorption capacity than that from raw peat sample, suggesting greater surface area and porosity in the H_3PO_4 AC-dem sample. Both ACs shows isotherm curves similar to a type between types I and II (as well as IV), indicating the presence of both micropores and mesopores [17]. Both isotherms also show a hysteresis loop between types of H_3 and H_4, indicative of slit-shaped pores and also microporosity [18]. Both samples show a high increasing slope at higher pressures (P/P_0) suggesting a wide distribution of pore sizes and higher mesoporosity and macroporosity [19].

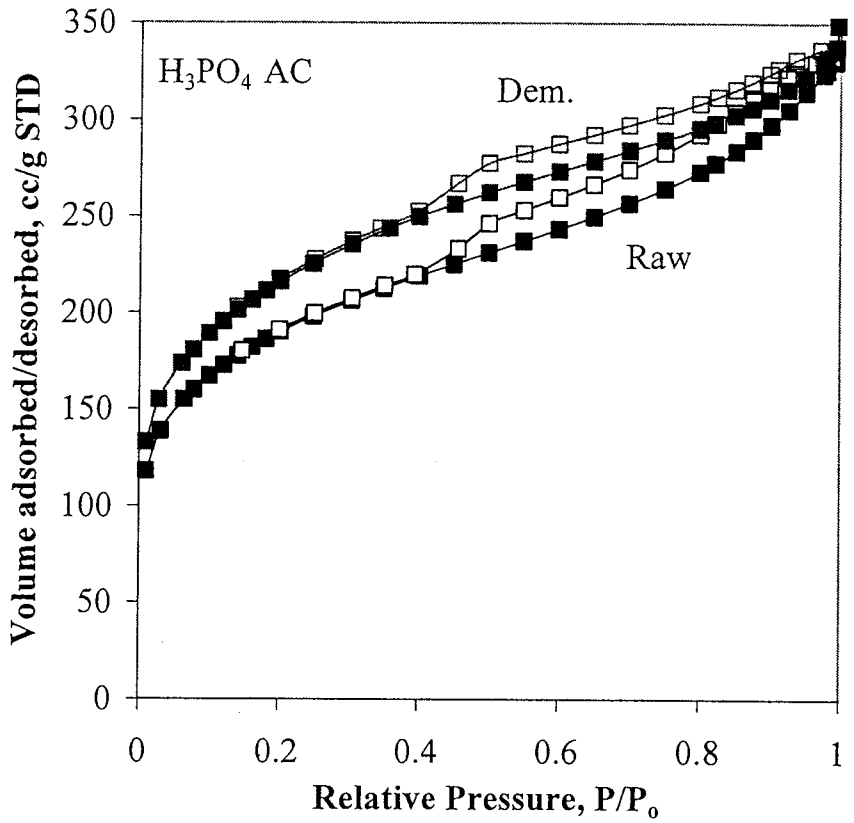

Figure 3-3 N_2 adsorption/desorption isotherms of H_3PO_4 AC-raw and H_3PO_4 AC-dem samples, the solid and hollow squares represented by adsorption and desorption respectively

Figure 3-4 presents the N_2 adsorption/desorption isotherms of $ZnCl_2$ AC-raw and $ZnCl_2$ AC-dem samples. Different from Figure 3-3 discussed above for the H_3PO_4 ACs, this figure clearly shows that the isotherms for the $ZnCl_2$ ACs derived either from raw or demineralised peat are typical of type II isotherm and H4 hysteresis loop. This suggests that the $ZnCl_2$ ACs are typical of microporous materials. Similarly as observed for the H_3PO_4 ACs (Figure 3-3), the AC derived from the demineralized peat had a greater N_2 adsorption capacity, suggesting an increased surface area and porosity.

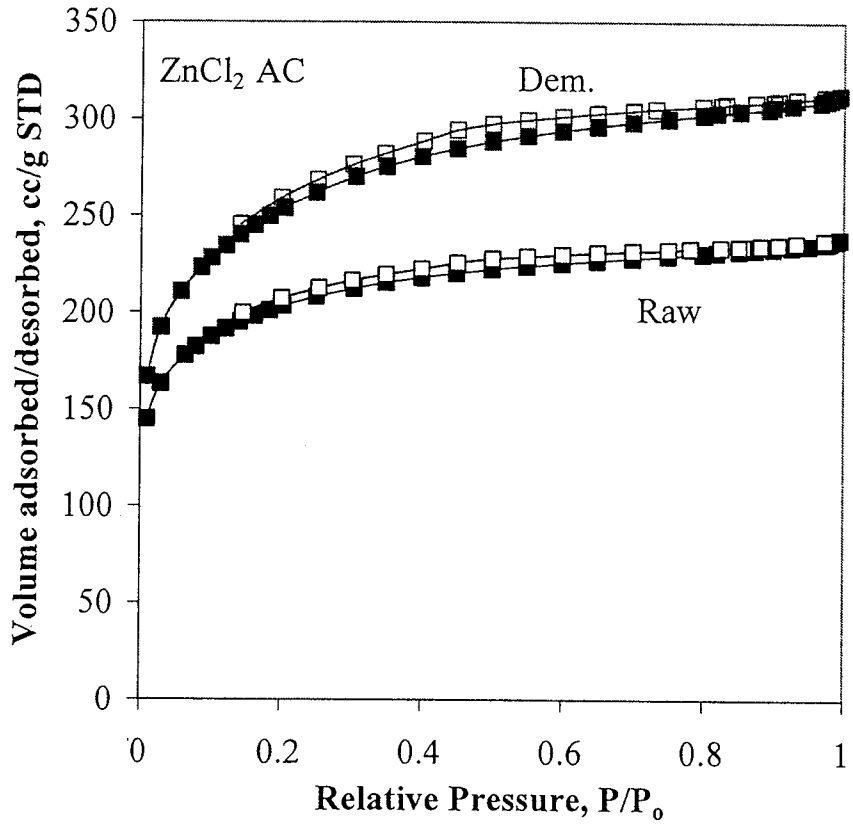

Figure 3-4 N_2 adsorption/desorption isotherms of $ZnCl_2$ AC-raw and $ZnCl_2$ AC-dem samples

3.3.2 Surface Areas and Textural Properties

The Multi-point BET surface areas, BJH desorption surface areas, the total pore (less than 163.33 nm) volumes, BJH desorption pore volumes, and average pore diameters for all the ACs prepared using either H_3PO_4 or $ZnCl_2$ as the activation agent are presented in Table 3-3. It is clearly seen that, $ZnCl_2$ is more effective than H_3PO_4 to produce ACs with a higher BET surface area for both the raw and demineralized peat precursors. For example, $ZnCl_2$-AC-raw has a BET surface area of 703 m^2/g compared with 675 m^2/g for the H_3PO_4-AC-raw. Whereas, there was an opposite trend observed for total pore volume. The use of $ZnCl_2$ resulted in ACs with a lower total pore volume compared with that of H_3PO_4. As shown in the table, the total volume is 0.36 cm^3/g and 0.50 cm^3/g for the $ZnCl_2$-AC-raw and H_3PO_4-AC-raw, respectively. The above mentioned difference in the trends between BET surface area and total pore volume may be explained by the different performance of these two activation agents in developing the pore structures in the ACs. As shown in the table, the BJH desorption surface areas (mainly for mesopore area) and the BJH desorption mesopore volumes and the average pore diameters are all

larger in the H_3PO_4 AC samples than those in the $ZnCl_2$ AC samples, irrespective as to whether the peat precursor was demineralized or not. The performance of H_3PO_4 and $ZnCl_2$ in developing the pore structures in the ACs can be more clearly shown in Figures 3-5, and 3-6, illustrating the BJH desorption pore size distributions of H_3PO_4 ACs and $ZnCl_2$ ACs, respectively. Figure 3-5 shows that both H_3PO_4 ACs from raw or demineralized peat have a major peak in the mesopore range, (3.6 and 4.4 nm), while the $ZnCl_2$ ACs (from Figure 3-6) show very strong adsorption in the micropore range (<2 nm) and much weaker peaks in the mesopore range (3-4 nm). As such, it can thus be concluded that $ZnCl_2$ is an effective activation agent for developing microporous structures in the ACs, leading to greater surface areas, while H_3PO_4 is highly active in developing the mesopores, leading to much higher average pore diameters, as clearly shown in Table 3-3. The H_3PO_4 ACs with improved mesopore structures would make them excellent catalyst supports for some reactions such as hydroprocessing of tar/heavy residues/asphaltene, as the mesopores in catalyst supports play crucial roles in the activity and in restricting the carbon/coke deposition [20-22]

The effects of demineralization of the peat precursor on surface areas and textural properties of the resulting ACs are also shown in Table 3-3 and Figures 3-5 and 3-6. Similar as the observations from the isotherms shown in Figures 3-3 and 3-4, the analytical data in Table 3-3 indicate that the demineralization resulted in significant increases in BET surface areas and porosity of the ACs, irrespective of the activation agent. Specifically, the BET surface area increased from 675 m^2/g for the H_3PO_4 AC-raw to 768 m^2/g for the H_3PO_4 AC-dem. When $ZnCl_2$ was used as the activation agent, the demineralization yielded a marked increase (185 m^2/g) in BET surface area for the resulting ACs. As shown in Table 3-3, the $ZnCl_2$ AC-dem attained the highest BET surface area of 888 m^2/g. The demineralization also resulted in increased total pore volumes of the resulting ACs, in particular when the $ZnCl_2$ was used as the activation agent, e.g., $ZnCl_2$ AC-dem had a total pore volume of 0.48 cm^3/g, compared with 0.36 cm^3/g for the $ZnCl_2$ AC-raw. From Figures 3-5, and 3-6, it can be seen that the demineralization could greatly enhance the development of the micropores in the ACs, regardless which activation agent was used. The effects of demineralization in promoting micropore formation were more evident when $ZnCl_2$ was used in the activation process, leading to remarkably increases in BET surface areas and the micropore volumes in the $ZnCl_2$ AC-dem samples. With the $ZnCl_2$, the demineralization also caused significantly improved mesoporous structure (as shown in Figure 3-6), and a great increase in the BJH desorption pore (mesopore) volume, doubling from 0.13 cm^3/g in $ZnCl_2$ AC-

raw to 0.24 cm^3/g in $ZnCl_2$ AC-dem. Therefore, it is clear that demineralization of the precursor before the chemical activation could greatly promote the development of the micropores in the resulting ACs, and it could significantly improve the mesoporous structure when $ZnCl_2$ was used as the activation agent. The above results may be explained by the improved accessibility of the demineralized precursor to the activation agent (H_3PO_4 or $ZnCl_2$) due to the removal of some intrinsic metals (minerals) in the precursor.

Table 3-3 Surface areas and textural properties of the resulting ACs from peat

ACs		BET[(1)] (m^2/g)	BJH cumulative desorption surface area (m^2/g)	Total pore volume[(2)] (cm^3/g)	BJH cumulative desorption pore volume (cm^3/g)	Average pore size (nm)
Raw peat	$ZnCl_2$	703	183	0.36	0.13	2.08
	H_3PO_4	675	375	0.50	0.42	2.97
Deminerlized peat	$ZnCl_2$	888	339	0.48	0.24	2.16
	H_3PO_4	768	429	0.51	0.38	2.66

[1]Multi-point BET; [2]Total pore volume (less than 163.33 nm).

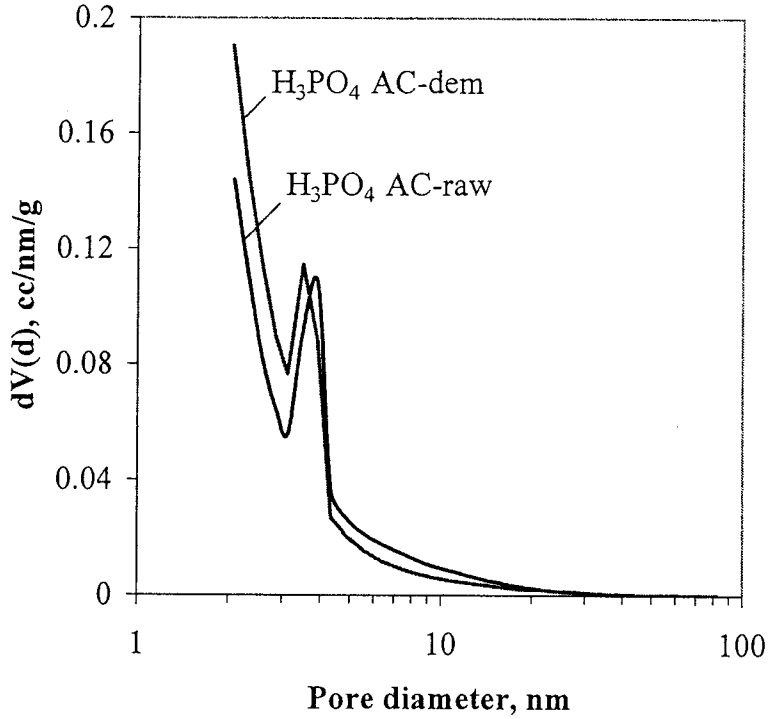

Figure 3-5, BJH desorption pore size distribution of the H_3PO_4 ACs derived from raw and demineralised peat

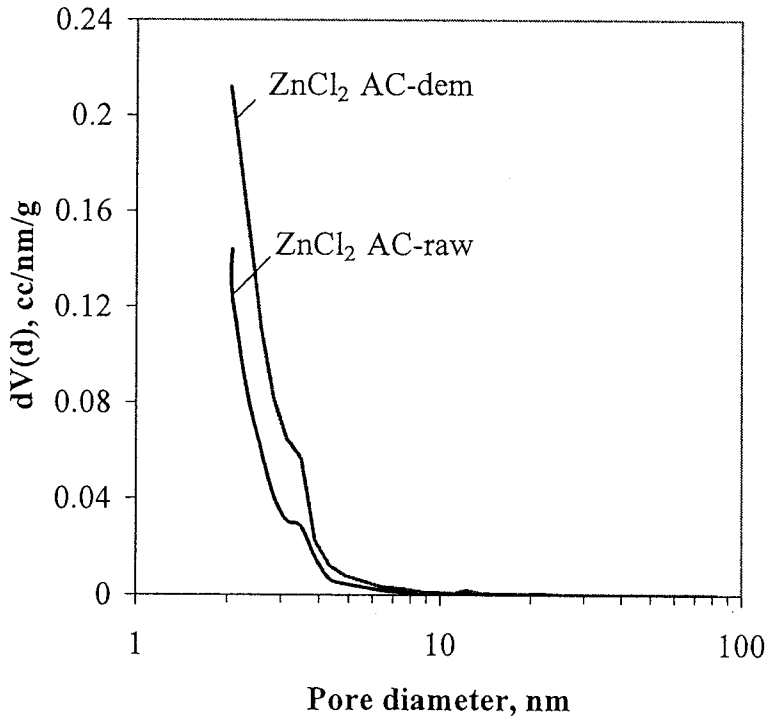

Figure 3-6, BJH desorption pore size distribution of the $ZnCl_2$ ACs derived from raw and demineralised peat

3.4. Conclusions

(1) Activated carbons (ACs) with surface areas of 675-888 m^2/g and total pore volumes of 0.36-0.51 $cm^{3/}g$ were produced from a Canadian peat by chemical activation using either H_3PO_4 or $ZnCl_2$ as the activation agent, followed by carbonization at 450°C.

(2) $ZnCl_2$ proved to be very effective for developing microporous structures in the ACs, leading to greater surface areas, while H_3PO_4 is highly active in developing the mesopores, leading to much higher mesopore volumes and average pore size.

(3) Demineralization of the peat precursor before the chemical activation greatly improved the surface area and pore structure of the resulting ACs. The demineralization greatly promoted the development of the micropores during the activation process irrespective of which activation agent was used, and it could also significantly improve the mesoporous structure when $ZnCl_2$ was used.

(4) The AC derived from the demineralised peat activated by $ZnCl_2$ attained the highest BET surface area of 888 m^2/g.

References

[1] A. Pigamo, M. Besson, B. Blanc, P. Gallezot, A. Blackburn, O. Kozynchenko, S. Tennison, E. Crezee, F. Kapteijn. Effect of oxygen functional groups on synthetic carbons on liquid phase oxidation of cyclohexanone. Carbon 2002;40:1267-1278.

[2] C.Y. Lu, M.Y. Wey, Y.H. Fu, The size, shape and dispersion of active site on AC-supported copper nanocatalyst with polyol process: the effect of precursors. Applied Catalysis A: General 2008;344:36-44.

[3] M. Smisek, S. Cerny. Active Carbon Manufacture, Properties and Aplications, Elsevier Pub., Comp., New York. (1970)

[4] X.-K. Li, W.-J. Ji, J. Zhao, S.-J. Wang, C.-T. Au. Ammonia decomposition over Ru and Ni catalysts supported on fumed SiO2, MCM-41, and SBA-15. Journal of Catalysis 2005; 236: 181.

[5] B. D. Zdravkov, J.J. Cermak, M. Sefara, J. Janku. Pore classification in the characterization of porous materials: A perspective. CEJC 2007; 5(2):385–395

[6] S.J.T. Pollard, G.D. Fowler, C.J. Sollars and R. Perry. Low-cost adsorbents for waste and wastewater treatment: a review, Sci Total Environ 1992;116: 31–52.

[7] B. Grigis, S. Yunis, A. Soliman.Characteristics of activated carbon from peanut hulls in

relation to conditions of preparation. Materials Letters 2002;57: 164-172

[8] T. Wigmans, A. Hoogland, P. Tromp and J.A. Moulijn. The influence of potassium carbonate on surface area development and reactivity during gasification of activated carbon by carbon dioxide, Carbon 1983;21:13–22.

[9] D. Cazorla-Amoros, D. Ribes-Perez, M.C. Roman-Martinez and A. Linares-Solano. Selective porosity development by calcium-catalyzed carbon gasification. Carbon 1996;34:869–878.

[10] J. Macia-Agullo, B. C. Moore, D. Cazorla-Amorós, A. Linares-Solano, Activation of coal tar pitch carbon fibres: Physical activation vs. chemical activation. Carbon 2004;42:1367-1370

[11] J. Laine, A. Calafat, M. Labady. Preparation and characterization of activated carbons from coconut shell impregnated with phosphoric acid. Carbon 1989; 27: 191–195.

[12] J. Laine, S. Yunes. Effect of the preparation method on pore size distribution of activated carbon from coconut shell. Carbon 1992; 30(4):601–604.

[13] M. Ahmedna, W.E. Marshall, R.M. Rao. Production of granular activated carbons from select agricultural by-products and evaluation of their physical, chemical and adsorption properties. Bioresource Technology 2000; 71:113–23.

[14] C. Srinivasakannan, M.Z. Abu Bakar. Production of activated carbon from rubber wood sawdust. Biomass and Bioenergy 2004; 27:89-96.

[15] C. Xu, J. Donald. Upgrading peat to gas and liquid fuels in supercritical water with catalysts Fuel, 2008: doi:10.1016/j.fuel.2008.04.042

[16] M. Strack (ed.) Peatlands and Climate Change, International Peat Society, Saarijärven Offset Oy, Saarijärvi, Finland, 223 pp.

[17] K. S. W. Sing. Reporting physisorption data for gas/solid systems with special reference to the determination of surface area and porosity. Pure & Appl. Chem. 1982;54:2201-2218.

[18] A. L. Myers, G. Belfort. Fundamentals of adsorption: proceedings of the Engineering Foundation conference held at Schloss Elmau, Bavaria, West Germany, May 6-11, 1983. The Foundation, 1984

[19] F. Rouquerol, J. Rouquerol, K.S.W. Sing. Adsorption by powders and porous solids. Principles, methods and applica tions, San Diego, CA: Academic Press, 1999

[20] H. Fukuyama, S. Terai, M. Uchida, J.L. Cano, J. Ancheyta. Activated carbon catalyst for heavy oil upgrading. Catalysis Today 2004; 98: 207-215.

[21] E. Byambajav, Y. Ohtsuka. Hydrocracking of asphaltene with metal catalysts supported on

BA-15. Applied Catal. A: Gen. 2003; 252: 193–204.

[22] S. Inoue, T. Takatsuka, Y. Wada, S. Nakata and T. Ono. A new concept for catalysts of asphaltene conversion. Catal. Today 1998; 43: 225-232.

CHAPTER 4

Novel Carbon-based Ni/Fe Catalysts Derived from Peat for Hot Gas Ammonia Decomposition

ABSTRACT

Two novel carbon-based Ni/Fe catalysts were developed and tested for catalytic decomposition of ammonia into N_2 and H_2. These catalysts were prepared using a meso-porous activated carbon (AC) support derived from a Canadian peat by H_3PO_4 activation. The newly developed catalysts proved to be highly active for ammonia decomposition. The conversion of 2000 ppm NH_3 diluted in helium over the Fe catalyst reached as high as 90% at 750°C and at the space velocity of 45000 h^{-1}, compared with only about 15% with the activated carbon alone without metal loading. In addition, the new Fe/Ni catalysts showed superior performance with respect to their resistance to catalyst deactivation. Both catalysts remained active as the reaction time increased up to 10 hours without showing a sign of deactivation. Fresh and spent catalysts were characterized by XRD, XPS and TPD. A cycle mechanism, involving both metal phosphides and metal nitrides, was proposed for the NH_3 decomposition reactions over these new Fe/Ni catalysts.

Keywords: Ammonia decomposition, Mesoporous carbon, Peat, Ni/AC, Fe/AC, Metal phosphides, Metal nitrides.

4.1 Introduction

Biomass gasification produces a low to medium BTU (5-14 MJ/Nm^3) product gas (or syngas) containing primarily CO_2, H_2, CO, CH_4 and (C_2+C_3), as well as some contaminants such as tars, NH_3, H_2S and SO_2, etc. In order to achieve better efficiencies of the syngas applications, these contaminants must be removed before the syngas is used for internal combustion, gas engines, and in particular for fuel cells and methanol synthesis. The content of NH_3 in the product gas, typically of 1000-5000 ppm [1], is dependant on the type of biomass used, as well as the gasifier parameters and operating conditions. As much as 50-90% of the NH_3 would form NO in gas turbines when the gas is combusted to produce power [2]

The ammonia in the producer gas can be efficiently reduced by hot gas catalytic decomposition. For ammonia decomposition, the most common catalysts tested include metals or alloys of Ni [3-6], Fe [5,7], Pt [5], Ru [3, 5, 8, 9], Pd and Rh [5], Ni-Pt [10] and Ni-Ru [11]. Most of the catalyst metals were supported on solid acids such as Al_2O_3 and SiO_2. Choudhary and coworkers [12] found that the catalytic activity of NH_3 decomposition decreased in the order of Ru > Ir > Ni when pure NH_3 was employed as the reactant. Yin et al. [5] conducted a systematic investigation on the effects of carbon-nano-tubes (CNTs)-supported metals (Ru, Rh, Pt, Pd, Ni, Fe) on the reaction, and found that, under the same reaction conditions, the NH_3 conversion over Ru was much higher than those over the other metals, and the reaction rates in terms of turn-over frequencies (TOF) decreased in the order of Ru > Rh ≅ Ni > Pt ≅ Pd > Fe. It has been widely accepted that the roles of the metal catalysts in ammonia decomposition involve formation and decomposition of active metal-nitrogen compounds, i.e., metal nitrides, while these active nitrides can be deactivated by the presence of a small amount of O_2 or H_2O due to the competing adsorption and the formation of some less effective oxidized species [13,14]. It should however be noted that noble metals of Ru, Ir, and Rh are very expensive compared with Fe and Ni-based catalysts. As far as the cost is concerned, Ni and Fe metals could be an attractive alternative.

A good support for catalysts can not only enhance the dispersion and surface area of the active components, but greatly affect the activities of the catalysts. For instance, the Al_2O_3-supported Ru or Ir catalysts showed lower activities for ammonia decomposition than those supported on SiO_2, and the activity of Ni/HZSM-5 was much lower than that of Ni/SiO_2 [12]. Yin et al. [5, 15] demonstrated that the catalytic performance of Ru catalyst was strongly dependent on support materials: under similar reaction conditions, NH_3 conversion decreased in

the order of Ru/CNTs > Ru/MgO > Ru/TiO2 ≅ Ru/Al2O3 ≅ Ru/ZrO2 > Ru/AC. The excellent catalytic performance of Ru/CNTs was believed to be related to the high dispersion of Ru on the CNTs. Moreover, it was proposed that the conductivity of the support might also be an important factor for catalytic activity. A conductive support is beneficial for the transfer of electrons from promoter and/or support to Ru, which would facilitate desorption of surface N atoms to form N_2. It was further demonstrated by the same authors [5,15] that a support of high acidity is unsuitable for NH_3 decomposition. Accordingly, CNTs (of high conductivity due to the graphitization of carbon atoms) combined with a basic support (MgO) may lead to enhanced activities for supported Ru catalysts, as evidenced by another study by Yin et al. [16].

Compared with the abovementioned expensive Ru catalysts, less expensive and readily available carbon-based catalysts are of interest. Xu et al. [17] reported the use of pyrolysis chars of low rank coals as catalysts for ammonia decomposition, being more active than a commercial activated carbon. Ohtsuka et al. [18] investigated the decomposition of NH_3 with Fe catalysts supported on brown coal chars. The catalyst was prepared by pyrolyzing a brown coal with Fe ion added. In the decomposition of 2000 ppm NH_3 diluted with helium at 750°C and at a space velocity of 45,000 h^{-1}, the coal-char supported 6 wt% Fe catalyst led to about 95% ammonia conversion, compared with less than 30% conversion for the 8 wt% Fe catalyst loaded on a commercial activated carbon (AC). Although AC and AC supported catalysts were found to be much less active for ammonia decomposition than those supported on other materials such as CNTs, MgO, TiO_2, Al_2O_3, SiO_2, coal char, etc. [1, 17, 18], it is worth to develop effective AC supported catalysts for NH_3 decomposition by properly designing its chemical and textural structures and properties. This is mainly because activated carbon materials have high surface areas and relatively low costs. Chemical and textural structures and properties of the activated carbon materials could be altered by the activation process (activation reagent and conditions) and the precursor materials (coal, biomass or peat).

Peat is the accumulation of partially decayed vegetation matter formed in wetlands. Over the past 50 years, the use of peat fuel in industry and for large-scale power generation has been very common in Europe, in particular in Finland, Ireland, Russia, Belarus and Sweden [19, 20]. Peat can also be used as a raw material for the production bio-oil and bio-char [19]. Peatlands cover an estimated 400 million hectares (about 3%) of the Earth's land surface and Canada contains some 40% of the world's peatlands – about 170 million hectares [20]. Therefore, peat can be an immense resource for the production of both fuel and carbon materials.

The main objective of this study is to prepare and test novel, less expensive carbon-based catalysts (Fe, Ni) derived from a Canadian peat for catalytic decomposition of ammonia diluted in inert atmosphere (helium). Fresh and spent catalysts were thoroughly characterized by XRD, XPS and TPD, in order to investigate possible catalytic mechanisms governing the ammonia decomposition reactions over the new carbon-based catalysts.

4.2 Experimental Materials, Apparatus and Methods

4.2.1 Peat

The peat sample used as the activated carbon precursor was obtained from Eastern Canada. Prior to use, the peat was dried for 24 hrs at 105°C, and then ground with a Wiley mill and screened to particles smaller than 40 mesh (~0.4 mm). The proximate and ultimate analyses, as well as the compositions of inorganic maters in the raw peat sample are given in Table 4-1.

Table 4-1 Proximate and ultimate analyses of the peat sample and concentrations of major inorganic elements in the raw peat.

Proximate analysis, wt% (d.b.[1])			Ultimate analysis, wt% (d.a.f.[2])				
VM	FC	Ash	C	H	N	S	O[3]
65.6	29.0	5.4	54.7	5.5	2.1	0.2	32.1

Major inorganic elements, wt% (d.b.)[4]								
Na	K	Mg	Ca	P	Fe	S	Al	Si
<0.1	<0.1	0.1	0.8	0.1	0.6	0.1	0.3	0.1

[1] On a dry basis; [2] On a dry-and-ash-free basis; [3] By difference; [4]Determined by ICP-AES

4.2.2 Production of Activated Carbon from Peat and the Activated Carbon Supported Fe/Ni Catalysts

The activated carbon (AC) was prepared from raw peat by a chemical activation method using H_3PO_4, discussed previously in Chapter 3. Briefly, 40 grams of the dried raw peat powder was mixed with 100 ml of 60wt% H_3PO_4. The mixture was allowed to soak overnight at room temperature. The sample was then thermally treated in a muffle furnace pre-set at 200°C for 15 min in air, followed by carbonization for 45 min at 450°C in air. After the sample was cooled down to room temperature, and then washed with distilled water repeatedly until a neutral pH was obtained. The washed sample was dried overnight at 105°C in air before being crushed and sieved into particles sized of 300-850 μm.

The Fe and Ni loaded catalysts were prepared using the above prepared AC by the wet impregnation method using $Fe(NO_3)_3 \cdot 9H_2O$ or $Ni(NO_3)_2 \cdot 6H_2O$ as the metal sources. To prepare 13 wt% Fe or 13 wt% Ni supported on AC, 10 grams of the activated carbon support was mixed with 9.38 g of $Fe(NO_3)_3 \cdot 9H_2O$ or 6.41 g of $Ni(NO_3)_2 \cdot 6H_2O$ in 200 ml 50 wt% methanol/H_2O solution. The mixture was sonicated for 40 min to form a uniform slurry, and the CH_3OH and H_2O were then evaporated under reduced pressure at 40°C and 85°C, respectively. The samples were further dried in air at 105°C for 4 hr and then calcinated in a flow of 200ml/min of N_2 heated at a heating rate of 5°C/min from room temperature up to 500°C for 4 hrs in a tubular reactor. The as-prepared AC-supported Fe or Ni catalysts in this study were denoted as Fe/AC and Ni/AC for short.

4.2.3 Catalytic Tests of the Catalysts in Ammonia Decomposition

NH_3 decomposition experiments were carried out with a flow-type, vertical quartz reactor placed in an electric furnace. The catalyst bed within the reactor measured approximately 8 mm in height, and was held in place with fine grade quartz wool. Prior to NH_3 decomposition, the samples were heated to 500°C at a heating rate of 15°C/min in a helium flow of 180 ml/min, and then subjected to reduction using 200 ml/min of H_2 for 2 h. After H_2 reduction, the reactor was heated to 750°C with a heating rate of 15°C/min in a He flow of 180 ml/min. As the temperature reached 750°C, the helium flow was replaced with 2000 ppm NH_3 diluted with high purity He under the space velocity of 45000 h^{-1}. A high speed micro GC-TCD (gas chromatograph-thermal conductivity detector) and a photo acoustic multi-gas monitor were used to determine N_2 formed and the un-reacted NH_3, respectively.

4.2.4 Characterization of the Catalysts

The as-prepared AC sample and the AC-supported Ni/Fe catalysts were analyzed by N_2 isothermal adsorption (77K) for its surface area and textural structures, using NOVA 1200e/TO (Quantachrome Instruments). X-ray diffraction (XRD) with Cu Kα and Fe Kα radiation (Shimadzu XRD-6000, 30 mA and 40 kV) was used to characterize the crystalline structures of the catalysts before and after the ammonia decomposition tests. The average crystalline size of the particles was calculated using the Debye-Scherrer equation. X-ray photoelectron spectroscopy (XPS) was employed to characterize the chemical composition on the surfaces of the catalysts before and after ammonia decomposition experiments. The XPS experiments were

performed on a ULVAC PHI 5600 spectrometer with an Al anode for K_α X-ray source operating at 200W. Charging effects were corrected by adjusting the binding energy of C_{1s} peak of carbon contamination to 284.6 eV. In addition, temperature-programmed desorption (TPD) measurements were carried out by heating the catalyst sample in high-purity helium up to 800°C or 900°C and held at this temperature for 30 minutes, when the desorbed N_2 was detected by a GC-TCD.

4.3 Results

4.3.1 Performance of the Catalysts in NH_3 Decomposition

The activities of the new Fe/AC, Ni/AC catalysts towards NH_3 decomposition were investigated at 750°C for various lengths of time ranging from 4 to 10 hours. The ammonia decomposition efficiencies or ammonia conversions to N_2 and H_2 of these two new catalysts are compared with the peat-derived activated carbon (AC) without any metal loading in Figure 4-1. Conversion of NH_3 into N_2 and H_2 over the Ni catalyst attained approximately of 75%, and the Fe catalyst was found to have the greatest activity for ammonia decomposition reaching as high as 90%, while the conversion with AC alone was only about 15%. Our new catalyst of Fe/AC is thus much more active than the Fe catalyst supported on a commercial AC as reported in a previous work by Ohtsuka et al. [18], where the commercial AC-supported Fe catalyst led to ammonia conversion of only 30% under the same reaction conditions (750°C, 2000 ppm NH_3/He, and SV of 45000 h^{-1}). Compared with other patented carbon-based Fe catalysts [21], our new Fe/AC and Ni/AC catalysts showed superior performance with respect to their stable activity.

As also shown in Figure 4-1, the activities of both Ni and Fe catalysts remained stable as the reaction time increased up to 10 hours without showing a sign of deactivation, while the activity of the previously patented carbon based Fe catalysts declined significantly after about 3 hours on the stream [18,21]. The ammonia decomposition catalyzed by the Ni/AC or Fe/AC mainly yielded N_2 and H_2 as the dominant products, although very small amount of HCN was formed as a by-product (at a small selectivity generally <5%) from NH_3.

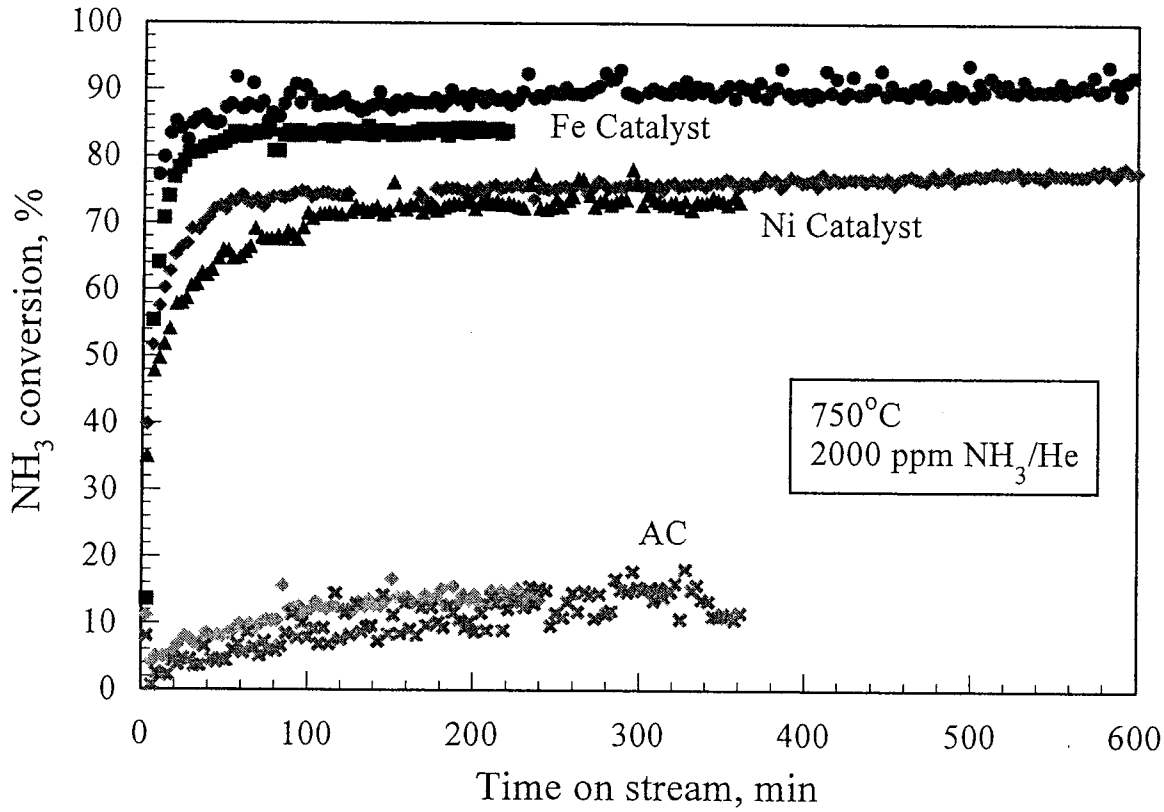

Figure 4-1 NH_3 conversions vs. time on stream at 750°C with catalysts of Fe/AC, Ni/AC as well as AC (space velocity of 45000 h^{-1}).

4.3.2 Characterization of the Fresh and Spent Catalysts

4.3.2.1 Surface Area and Textural Properties

The fresh as-prepared AC, Fe/AC and Ni/AC catalysts and the spent catalyst after ammonia decomposition experiments were analyzed using N_2 isothermal adsorption (77K) for their surface areas and textural structures, and the results are summarized in Table 4-2, and Figure 4-2 for pore size distributions. The as-synthesized AC has a BET surface area of 675 m^2/g, much greater than either the fresh Fe/AC (205 m^2/g) or the fresh Ni/AC (393 m^2/g), owing to the deposition of the metal ions (Fe or Ni) in the pores, as evidenced by the remarkably reduced total pore volumes (Table 4-2). The AC had a total pore (< 163 nm) volume of 0.50 cm^3/g, which dropped with the addition of the metals to 0.25cm^3/g for Ni/AC and 0.14cm^3/g for Fe/AC. The average pore diameters also decreased with the addition of the metals, possibly due to the

formation of micropores, or blocking of the mesopores by the metal ions. Table 4-2 also shows BJH cumulative desorption surface areas, pore volumes and pore diameters (or mesopore surface areas, pore volumes and pore diameters). The AC has a larger mesopore development (with a mesopore area of 375 m^2/g, mesopore volume of 0.42 cm3/g and mesopore diameter of 4.4 nm), and as expected the Ni/AC and Fe/AC catalysts have greatly decreased mesopore areas (of 11 and 41 m^2/g, respectively), mesopore volumes (of 0.02 and 0.06 cm^3/g, respectively) and mesopore diameters (of both 3.7 nm).

After NH_3 decomposition for 4-6 hours, the BET surface area, total pore volume and average pore diameter for the AC catalyst remained almost of no change, but the mesopore area and mesopore volume decreased, as shown in Table 4-2. For Ni/AC catalyst, its BET surface decreased slightly from 393 m^2/g to 327 m^2/g after 4 hours on stream for NH_3 decomposition, while it climbed to 346 m^2/g after 10 hours on stream for NH_3 decomposition, accompanied by a slight increase in total pore volume and average pore diameter, as shown in Table 4-2. The Fe/AC catalyst had similar trends as those observed for Ni/AC with respects to the changes in the BET surface area, total pore volume and average pore diameter with the increasing time on stream (Table 4-2). The BET surface area of the Fe/AC catalyst increased consistently during the ammonia decomposition. For instance, its BET surface area increased from 205 m^2/g (fresh) to 209 m^2/g (4h) and 236 m^2/g (10h). The total pore volume and mesopore volume of the Fe/AC catalyst also increased consistently with time on stream as shown in Table 4-2.

Very interestingly, however, both Ni/AC and Fe/AC catalysts showed remarkable increase in the mesopore areas and mesopore volumes after 4 and 10 hours on stream for NH_3 decomposition. As shown in Table 4-2, the mesopore area and mesopore volume of Ni/AC increased to 110 m^2/g and 0.31 cm^3/g after 10 hours on stream, compared to only 41 m^2/g and 0.06 cm^3/g for the fresh catalyst. This sharp increases in mosopore surface area and pre volume for these two metal catalysts can be clearly seen in Figure 4-2, where a sharp increase in the volume of mesopores (with a diameter of 3.7 nm) in the spent Ni/AC and Fe/AC catalyst is shown.

Table 4-2 Surface areas and textural properties of the as-synthesized AC and the AC-supported Fe and Ni catalysts, and the spent catalysts after the ammonia decomposition experiments.

Catalyst	Multi-point BET (m^2/g)	Total pore volume (< 163 nm) (cm^3/g)	Average pore diameter (nm)	Mesopore surface area (m^2/g)	Mesopore volume (cm^3/g)	BJH desorption average pore diameter (nm)
AC-fresh	**675**	0.50	3.0	**375**	0.42	4.4
AC-4h	678	0.54	3.2	179	0.26	3.7
AC-6h	655	0.51	3.1	164	0.24	3.7
Fe/AC-fresh	**205**	0.14	2.7	**11**	0.02	3.7
Fe/AC-4h	209	0.16	3.1	34	0.16	3.7
Fe/AC-10h	236	0.18	3.1	49	0.18	3.7
Ni/AC-fresh	**393**	0.25	2.7	**41**	0.06	3.7
Ni/AC-4h	327	0.24	2.9	65	0.24	3.7
Ni/AC-10h	346	0.31	3.5	110	0.31	3.7

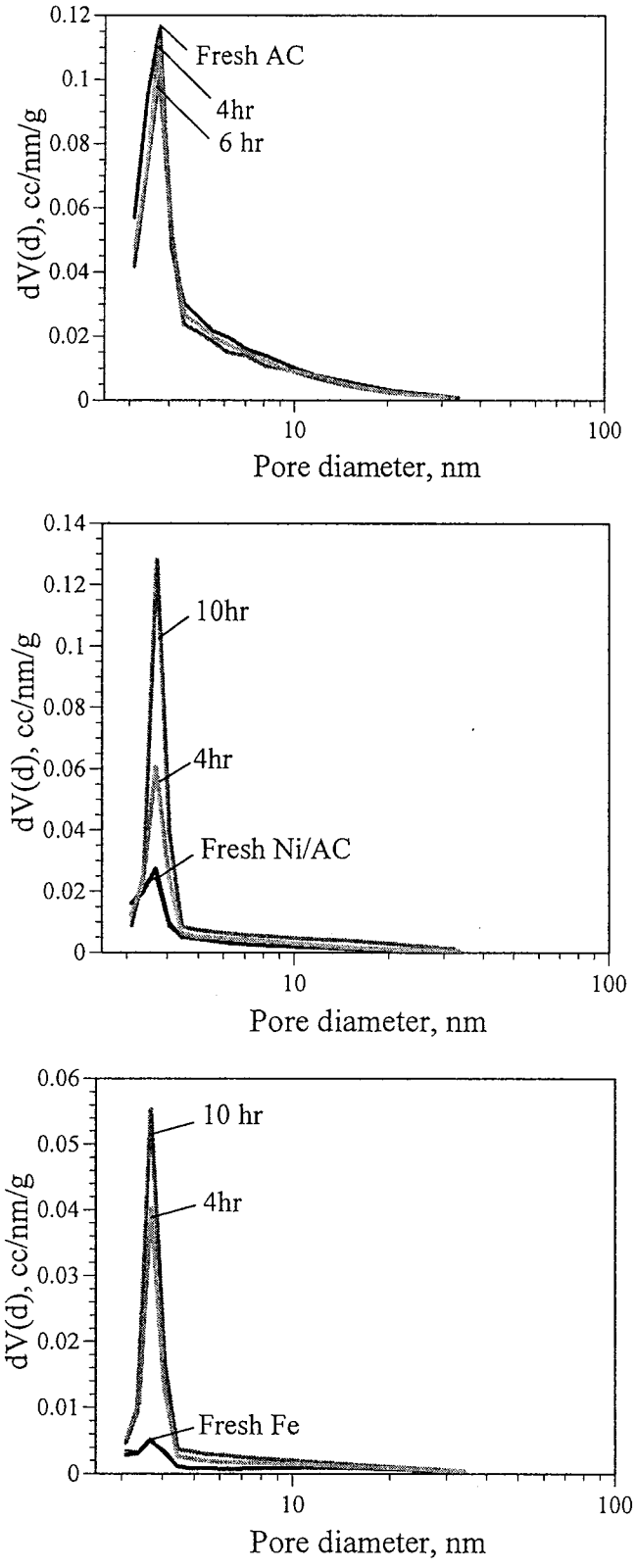

Figure 4-2 Pore size distributions for the fresh AC, Ni/AC and Fe/AC catalysts, and the spent catalysts after NH_3 decomposition

4.3.2.2 Crystalline Structures

Figure 4-3 shows the XRD (Cu-Kα) profiles for the Ni/AC catalyst before and after H_2 reduction at 500°C, and after the NH_3 decomposition at 750°C for 4 hours and 10 hours. In the fresh catalyst (Figure 4-3d), diffraction lines of metallic Ni were observed, existing as nanoparticles with an average crystalline size L_c = 14 nm, calculated using the Debye-Scherrer Equation. After H_2 reduction at 500°C (Figure 4-3c), the formation of $Ni_{12}P_5$ and Ni_3P were observed, accompanied by decreased intensities of the metallic Ni signals (L_c = 23 nm). After the subsequent NH_3 decomposition at 750°C for 4 hours (Figure 4-3b), the diffraction lines of $Ni_{12}P_5$ increased in intensities, compared with those after H_2 reduction at 500°C. Interestingly, the signals of Ni_3P were replaced by relatively strong signals of Ni_2P (L_c = 30 nm). When the time on stream (of NH_3) increased further to 10 hours, the signals of $Ni_{12}P_5$ weakened but the Ni_2P (L_c = 45 nm) became the dominate signals in the sample.

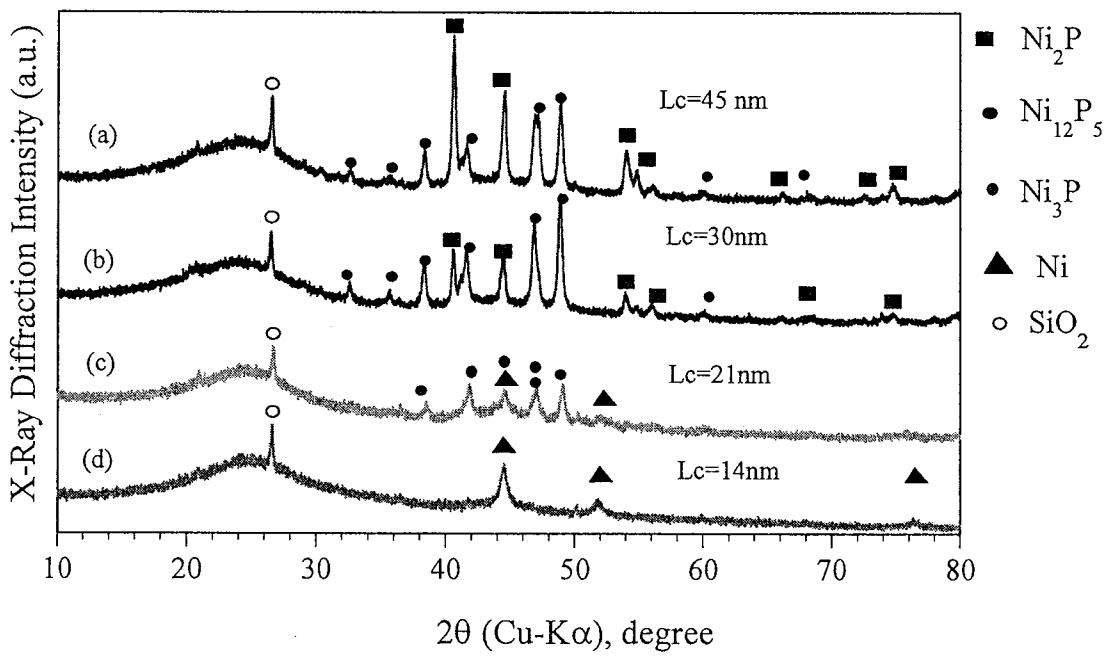

Figure 4-3 XRD profiles of the Ni/AC catalyst after the NH_3 decomposition experiment at 750°C for 10 h (a) and for 4 h (b), the Ni/AC catalyst after 2 h H_2 reduction at 500°C (c) and the fresh Ni/AC catalyst (d).

Figure 4-4 shows the XRD (Cu-Kα) profiles for the Fe/AC catalyst before and after H_2 reduction at 500°C, and after the NH_3 decomposition at 750°C for 4 hours and 10 hours. Using the XRD Cu-Kα filter, no diffraction lines of any Fe species could be detected, so when switched to a Fe-Kα, a very weak XRD peak probably due to α-Fe was detectable at 2θ (Fe-Kα) of about

57 degree after 2 h H_2 reduction at 500°C, as shown in Figure 4-4b. These observations strongly suggest that Fe particles before the NH_3 decomposition are finely dispersed on the AC support. When the Fe catalyst was subjected to the 4 h and 10 h decomposition at 750 °C, as seen in Figure 4- 4(a and b), the distinct XRD signals of Fe_2P appeared, and they were present as highly dispersed nanoparticles with an average crystalline size L_c =22 nm and L_c = 26 nm calculated by the Debye-Scherrer Equation.

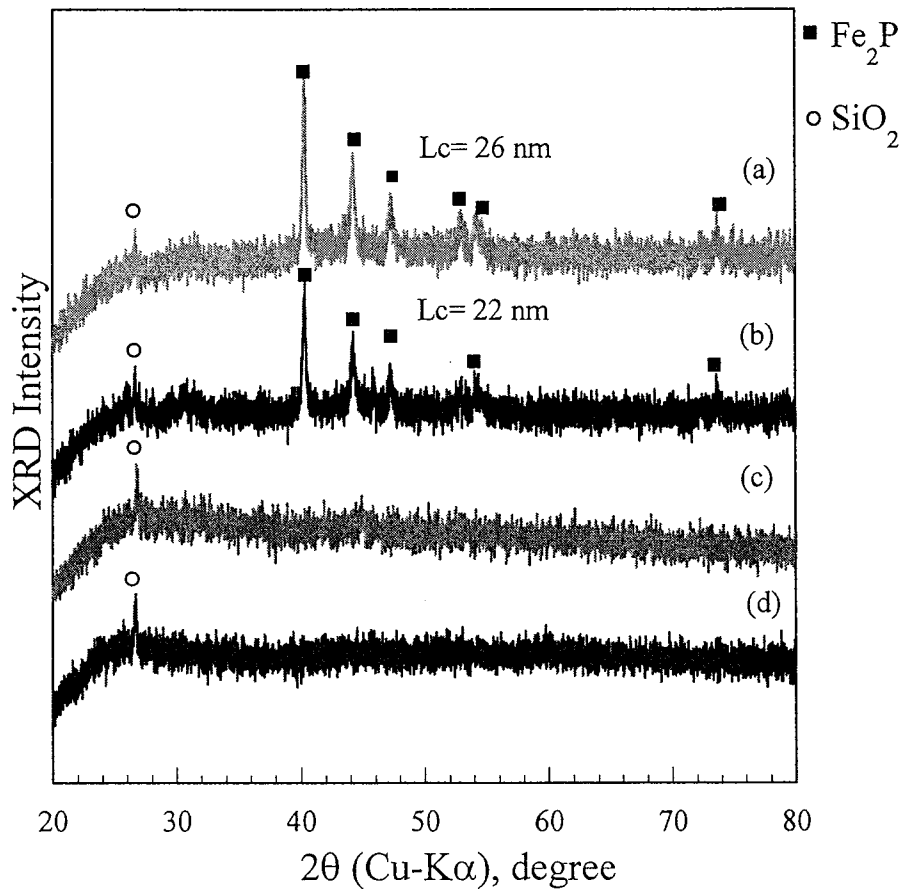

Figure 4-4 XRD profiles of the Fe/AC catalyst after the NH_3 decomposition experiment at 750°C for 10 h (a) and for 4 h (b), the Fe/AC catalyst after 2 h H_2 reduction at 500°C (c) and the fresh Fe/AC catalyst (d).

The detection of nickel/iron phosphides ($Ni_{12}P_5$, Ni_3P, and Ni_2P, Fe_2P) in the AC-supported catalysts after the hydrogen reduction and/or after the ammonia decomposition reveals the reaction of the Ni/Fe metal with P species remaining in the AC at elevated temperatures. There is no doubt, the presence of P in the AC support was due to the use of H_3PO_4 as the chemical activation agent in the AC production process. The presence of P in both Ni an Fe AC-supported catalysts was also evidenced by XPS analyses, which will be discussed in the subsequent section

of this paper. Interestingly, no metal nitride such as Ni_xN and Fe_xN was detectable by XRD in the spent catalysts after ammonia decomposition, while in some previous work with limonite Fe catalysts and brown coal chars supported Fe catalysts, Fe_xN species were detected after NH_3 decomposition, and these metal nitrides were considered as the active intermediates that were involved in the catalytic mechanism for NH_3 decomposition [23,18]. Furthermore, it has been demonstrated in the previous work with brown coal chars supported Fe catalysts that Fe carbide was formed during the ammonia decomposition process at 750°C [18]. It was also reported that the formation of iron carbide led to of the deactivation of the Fe catalyst [18]. For our two new catalysts (Ni/AC and Fe/AC), Fe carbides were not detected in the spent catalysts even after the ammonia decomposition for 10 hours as shown above in Figures 4-3 and 4-4, which might account for the high on-stream stability of these catalysts as shown in Figure 4-1.

4.3.2.3 Bulk Chemical Compositions

The Elemental (C, H,N) analysis of the catalysts before and after NH_3 decomposition studies is given in Table 4-3. The CHN analysis of the samples revealed that the activated carbon catalysts comprise 55-60% C, 2-3% H, and 1-2% N. With the addition of the Ni and Fe metals to the AC, there were no significant changes in the carbon contents compared with the AC support, although the addition of Fe to the AC led to a small decrease in the carbon content. The nitrogen content the AC-supported Ni or Fe catalyst was 1.6 wt% (d.b.), slightly higher than that of the AC support (1.4 wt%), most likely owing to the metal nitrate solutions used in the wet-impregnation process: $Fe(NO_3)_3 \cdot 9H_2O$ or $Ni(NO_3)_2 \cdot 6H_2O$. After H_2 reduction at 500°C, the carbon contents of the metal catalysts increased whereas the hydrogen and nitrogen remained approximately constant. After 4h or 10 h NH_3 decomposition reactions, the nitrogen contents of all the samples increased significantly, likely due to the adsorption of ammonia or other N-containing species or the formation of Fe and Ni nitrides species during the reactions.

Table 4-3, CHN analysis of the catalysts before and after NH_3 decomposition

	Sample	C%	H%	N%
AC	**Fresh**	59.5	3.1	1.4
	After 4 h	70.1	1.8	4.6
Ni/AC	**Fresh**	59.6	2.1	1.6
	After H_2 reduction	64.5	2.1	1.6

	After 10 h	64.8	1.3	**2.4**
	Fresh	55.9	2.0	1.6
Fe/AC	After H_2 reduction	57.0	2.0	1.5
	After 10 h	60.6	1.1	**2.2**

4.4 Discussion

4.4.1 Roles of Pore Structures in the Catalytic Reactions

The significantly increased mesopore surface areas and volumes for the Ni/AC and Fe/AC catalysts during the ammonia decomposition, as shown previously in Table 4-2 and Figure 4-2, might contribute to the high activities and stability of these catalysts in ammonia decomposition (Figure 4-1). The remarkable increases in mesoporous surface area and pore volume may be also clearly shown from the N_2 adsorption/desorption isotherms of these catalysts, as illustrated in Figure 4-5. The isotherms in the figure suggest the significant formation of mesopores during the reactions with the Ni/AC and Fe/AC catalysts, because the isotherm curves for these two catalysts resemble Type II isotherms after the NH_3 decompostion. In contrast, the fresh samples of these metal catalysts show a Type I isotherm, more typical of a microporous material. For the Ni/AC and Fe/AC catalysts, an increase in the hysteresis elbow was observed as the time on stream increased from 4 h to 10 h, suggesting widened mesopores and the possibility of deeper pore formations. The Fe/AC showed hysteresis extending to low relative pressures which might be related to complex micropore structures incorporating throats and cavities, or the sorbate-induced swelling of the microporous material [22]. Even though the surface area of the Fe catalyst was the lowest, it shows high microporosity based on the adsorption-desorption isotherms. As illustrated in Figure 4-5, The isotherm for AC alone, shows that there is not really any change of the pore structures after the reactions.

The remarkable increases in mesoporous surface area and pore volume might be explained by the release of the carbon element from the support material in the forms of CO and CH_4 (by hydro-pyrolysis or gasification) at an elevated temperature, generating more micro/meso-pores in the support. The release of carbon elements from the support materials could be catalyzed by the presence of nanoparticles of metals (Ni or Fe) in the catalysts, which may be evidenced by the measurements of the CO_2, CH_4 and CO evolved during the ammonia decomposition, as illustrated in Figure 4-6. As clearly shown in the figure, the total amount of

($CO+CH_4$) evolved from the ammonia decomposition reactions over the AC-supported Ni or Fe catalyst for 10h was about 6-10 times that from the reactions over AC only for 6h.

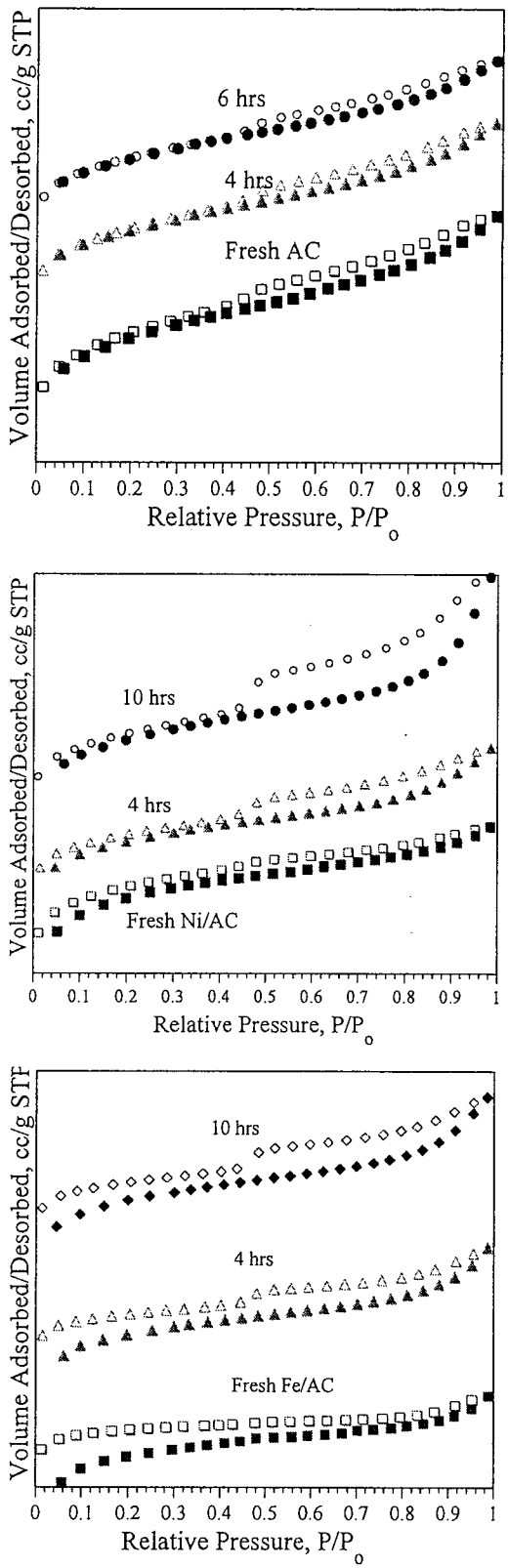

Figure 4-5 Adsorption/desorption isotherms for the fresh AC, Ni/AC and Fe/AC catalysts, and the spent catalysts after NH_3 decomposition.

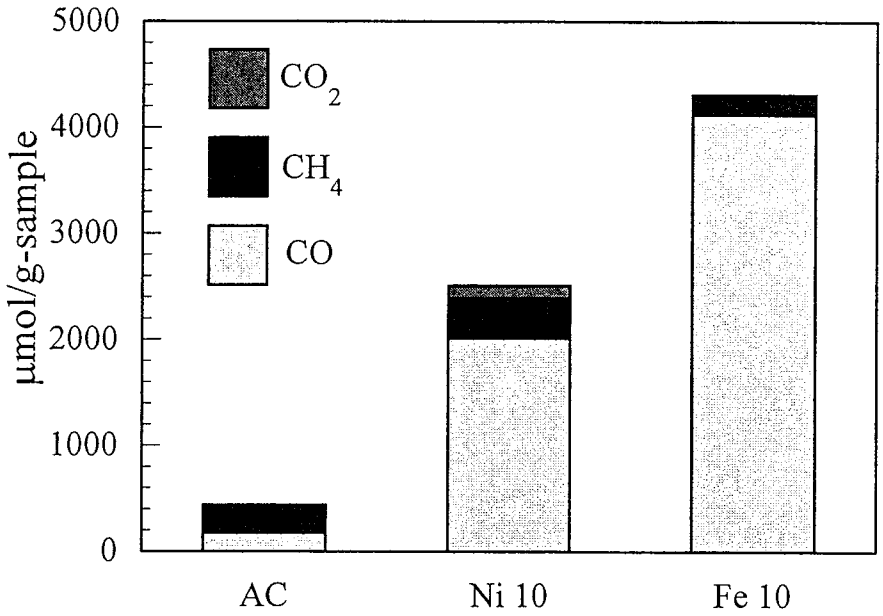

Figure 4-6 Total CO_2, CH_4 and CO evolved during decomposition of 2000 ppm NH_3/He over AC for 6 h, Ni/AC for 10 h and Fe/AC for 10 h.

4.4.2 Roles of Surface Chemical Structures in the Catalytic Reactions

As is well known, in a heterogeneous reaction system, a catalyst's surface chemical structures are more important than its bulk composition for the catalytic activities. The chemical states and compositions over the catalyst surfaces for the fresh and spent catalysts of Ni/AC and Fe/AC (after the ammonia decomposition experiments at 750°C for 4h and 10h) were analyzed by XPS. Figure 4-7 illustrates the XPS spectra of Ni 2p and P 2p for the fresh and spent catalysts of Ni/AC. Ni exists primarily in the forms of Ni^{3+} or Ni^{2+} (Ni 2p3/2 peak at around 856.8 eV) resulting from Ni_2O_3 and NiO formed by air oxidation of sample prior to or during the XPS measurements. Another Ni 2p peak observed at around 853.8 ± 0.1 eV in the spent catalysts after the ammonia decomposition experiments for 4h and 10h may be ascribable to the phosphides ($Ni_{12}P_5$, Ni_3P, and Ni_2P) and metallic Ni. The detection of phosphides coincides with the observation by XRD (Figure 4-3). The P 2p XPS spectra, as also shown in figures 4-7, exhibit a main peak at about 134 eV, regardless of the kind of the sample, which might be identified as the phosphate species such as PO_4^{3-} (133.75 eV) and metaphosphates (134.3 ± 0.3eV), and there is a weak peak at approximately 130.5 eV which may correspond to Ni_xP or Fe_xP (similar as indicated in this Figures for the XPS spectra of Ni 2p).

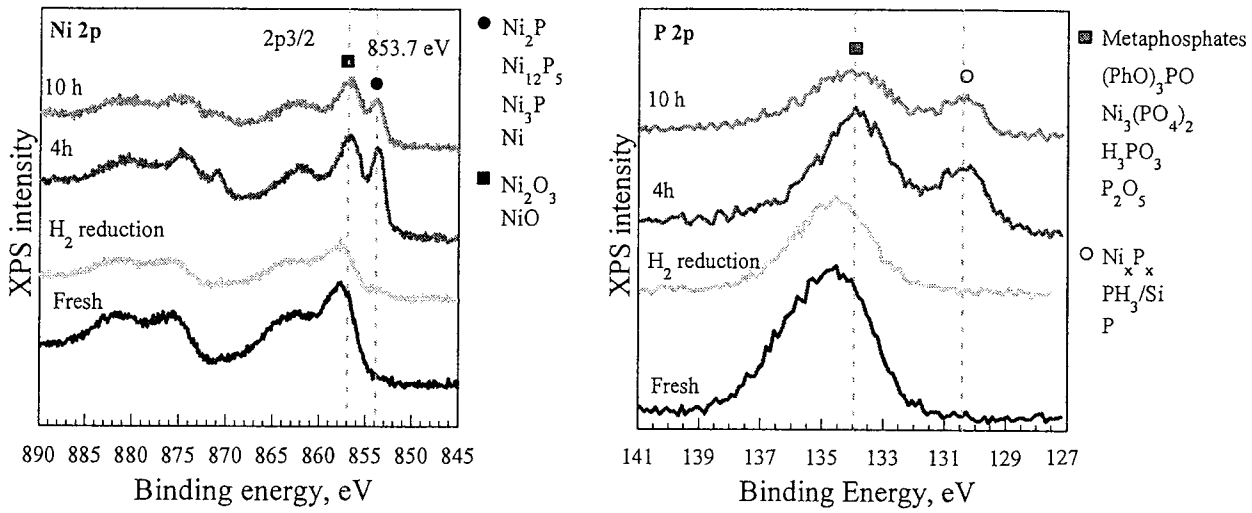

Figure 4-7 XPS spectra of Ni 2p and P 2p for the Ni/AC catalyst before and after H_2 reduction, and after the NH_3 decomposition for 4 and 10 hours.

The XPS spectra of Fe 2p and P 2p for the fresh and spent catalysts of Fe/AC are shown in Figure 4-8. According to the Fe 2p spectra for all samples (fresh and spent), Fe exists mainly in the forms of Fe^{x+} ($x = 2 \sim 3$) cations (Fe 2p3/2 peak at around 711.8 eV) due to the presence of Fe_2O_3, Fe_3O_4 and FeO formed by air oxidation of sample prior to or during the XPS measurements. Similar as that was shown in Figure 4-7 for the Ni/AC catalysts, a weak Fe 2p peak at around 707 eV can be observed in the spent catalysts after 4h and 10h on the stream of 2000 ppm NH_3/He at 750°C. This weak peak may be due to the phosphides (Fe_2P) and metallic α-Fe, as evidenced by the XRD observation discussed previously (Figure 4-4). The P 2p XPS spectra in Figure 4-8 also reveal the presence of Fe-phosphate species such as PO_4^{3-} (133.75 eV) and metaphosphates (134.3 ± 0.3eV), and the Fe_xP species (of weak signals) at approximately 130.5 eV. The presence of Fe_xP species may be evidenced by the XRD measurements (Figure 4-4) and the XPS spectra of Fe 2p in Figure 4-8.

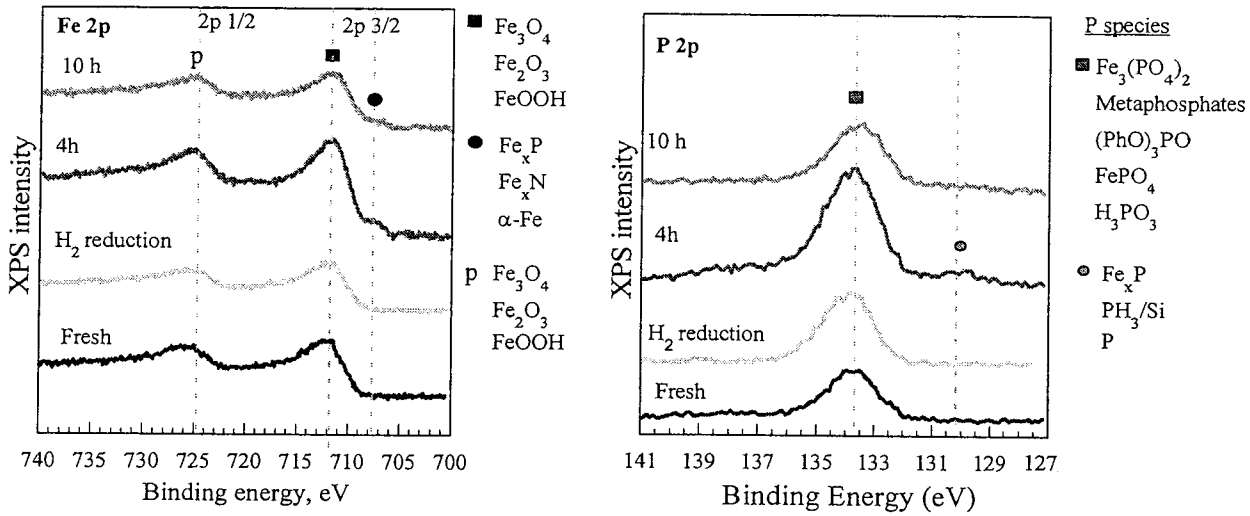

Figure 4-8 XPS spectra of Fe 2p and P 2p for the Fe/AC catalyst before and after H_2 reduction, and after the NH_3 decomposition for 4 and 10 hours.

Quantitative analysis of atomic ratios was accomplished by determining the elemental peak areas, using the Shirley background subtraction with the sensitivity factors supplied from the instrument maker. Table 4-4 shows the atomic ratios of many elements (O, P, N, Ni and Fe) in relation to carbon on the surfaces of the fresh and spent catalysts of Ni/AC and Fe/AC determined by XPS. Atomic ratios of P/C with the fresh Fe and Ni catalysts were 0.02 and 0.07, respectively, indicating the significant retention of the P sourced from H_3PO_4, used as the activation agent for preparation of the AC support from the raw peat. If plotting the atomic ratios of Fe/P and Ni/P against time on stream, as illustrated in Figure 4-9, it can be seen that the surface atomic ratios of Ni/P in the Ni catalyst were relatively stable at about 1.5 during the reactions. This value is just slightly smaller than the stoichiometric values (Ni/P = 2.0-3.0) in Ni_2P and Ni_3P, estimated by the XRD measurement (Figure 4-3). The surface atomic ratios of Fe/P in the Fe catalyst remained approximately constant at about 2.3, which is very close to the the stoichiometric value (Fe/P = 2.0) in Fe_2P, evidenced by the XRD measurement (Figure 4-4).

As also shown in Table 4-4, the surface O/C ratios for both catalysts decreased during the ammonia decomposition experiments, in particular after 10 hours on stream. This may be explained by the release of elemental oxygen from the AC support or the combined oxygen from residual P_2O_5 during the experiment under an elevated temperature (750°C), which can be evidenced by formation of CO and CO_2 in the effluent gases (Figure 4-6). To the contrary, the surface N/C ratios for both catalysts significantly increased during the ammonia decomposition experiments, compared with that of the respective fresh catalyst. The increase in N/C ratios on

the two catalysts during the ammonia decomposition implies the chemisorption of NH_3 to the catalysts or the formation of nitrogen-containing compounds (e.g., metallic nitrides), as will be discussed in the following section.

Table 4-4 Atomic ratios of the fresh and spent catalysts of Ni/AC and Fe/AC.

Sample	Atomic Ratios				
	O/C	P/C	N/C	Ni/C	Fe/C
Ni/AC, Fresh	0.44	0.07	0.03	0.10	-
Ni/AC, 4 h	0.29	0.05	0.06	0.07	-
Ni/AC, 10 h	0.20	0.03	0.05	0.04	-
Fe/AC, Fresh	0.26	0.02	0.02	-	0.05
Fe/AC, 4 h	0.26	0.02	0.05	-	0.05
Fe/AC, 10 h	0.19	0.02	0.04	-	0.04

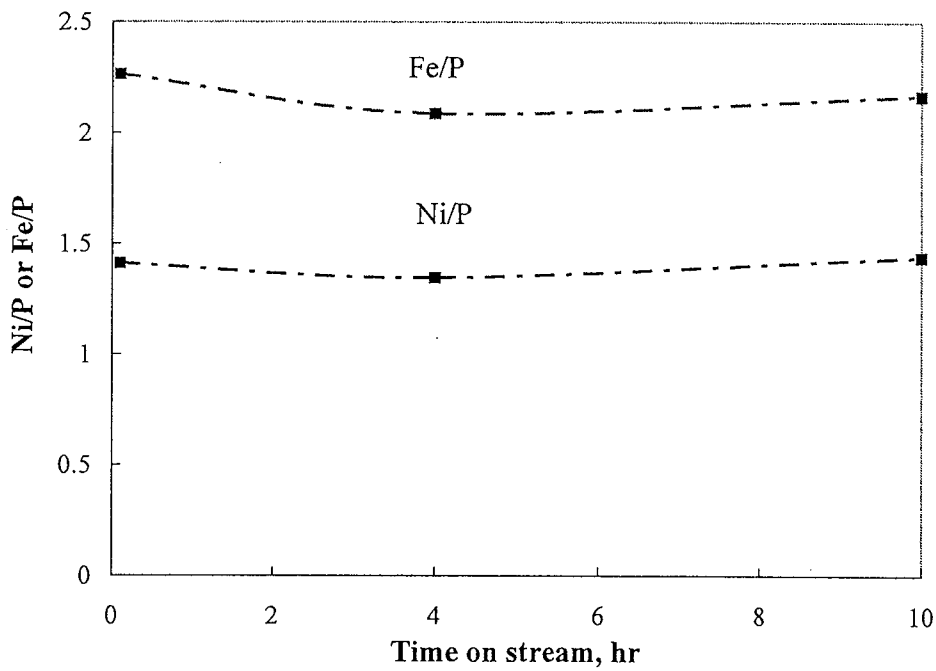

Figure 4-9. Changes in atomic Fe/P and Ni/P ratios determined by XPS during the NH_3 decomposition

Figure 4-10 illustrates the N 1s XPS spectra for the fresh and spent catalysts of Fe/AC. In the fresh catalyst, the widened peak at around 400 eV may be attributed to nitrogen present in an organic matrix, but this peak intensity was reduced after H_2 reduction, possibly due to the release nitrogen from the samples during reduction. After the NH_3 decomposition at 750°C over the catalyst, the intensity of this main peak increases with increasing time on stream. After 4 and 10

hour NH_3 decomposition, the XPS N 1s spectra revealed the presence of NH_3 (399.1 ± 0.1 eV) or cyanides (399±1.5) on the surface of the catalysts due to the physio-/chemi-sorption of the NH_3 reactant or the HCN by-product. A smaller peak was detected in the spectrum at the binding energy of 397.4±0.1 eV, which might be attributed to Fe nitrides (Fe_xN). Fe_xN were detected in some previous studies on ammonia decomposition using limonite Fe catalysts and brown coal chars supported Fe catalysts, and they were considered as the active intermediates involved in the catalytic mechanism for NH_3 decomposition [21, 23].

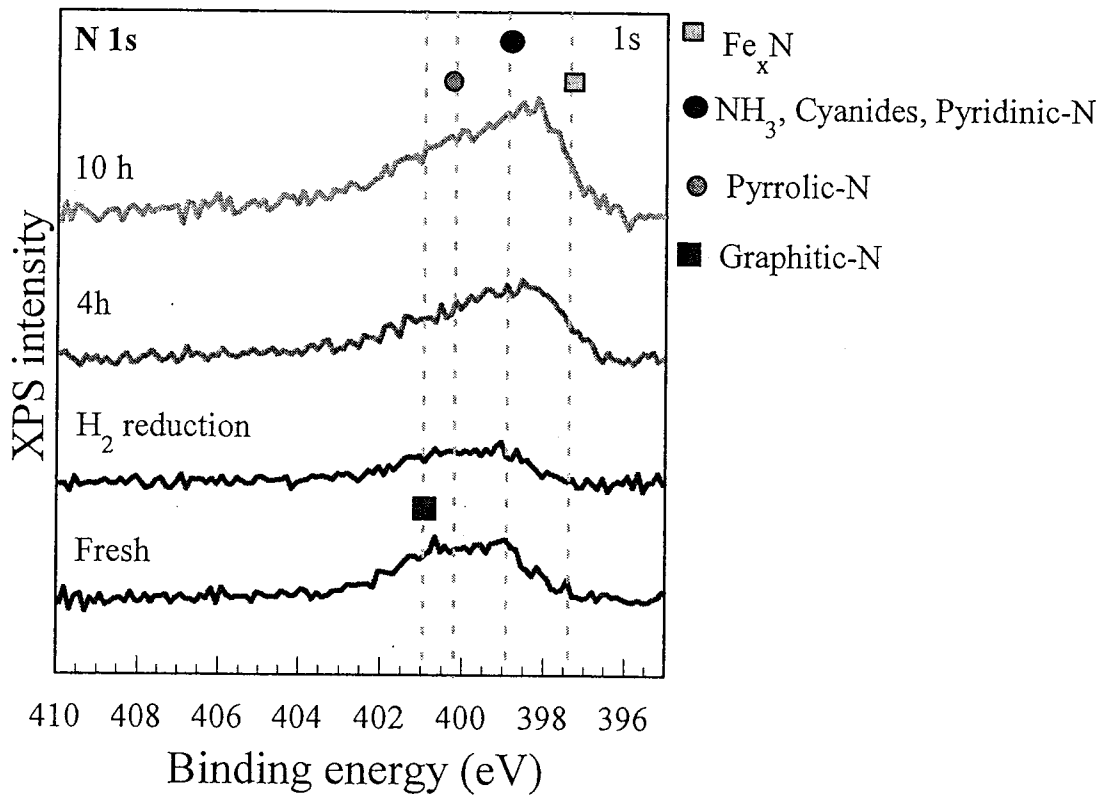

Figure 4-10 XPS spectra of N 1s for the Fe/AC catalyst before and after H_2 reduction, and after NH_3 decomposition for 4 and 10 hours.

4.4.3 Catalytic Mechanisms

The high activities of the Fe/AC and Ni/AC for the decomposition of 2000 ppm NH_3/He at 750°C were shown and discussed in Figure 4-1, where ammonia decomposition efficiencies (conversion of ammonia into N_2 and H_2) reached 90% with the Fe catalyst and 75% for the Ni catalyst, while it was only 15% with AC alone. Both catalysts showed superior stability or resistance to deactivation compared with other patented carbon-based Fe catalysts [18, 21]. As

shown in Figure 4-1, both catalysts remained active with even slightly climbing activities as the reaction time increased up to 10 hours, showing no sign of deactivation, while the activity of the previously patented carbon based Fe catalysts declined after about 3 hours on the stream [18, 21]. Possible mechanisms to explain the high activities of the new catalysts are thus discussed as follows.

In the spent catalysts, even after the ammonia decomposition for 10 hours, no metal nitrides (such as Ni_xN or Fe_xN) or metal carbides were detectable by XRD and XPS (Figures 4-3, 4-4, 4-7 and 4-8). In contrast, in some previous work with limonite Fe catalysts and coal chars supported Fe catalysts, Fe_xN species were detected by XRD after NH_3 decomposition, and these metal nitrides were considered as the active intermediates involved in the catalytic mechanism for NH_3 decomposition [18, 23]. Furthermore, it has been demonstrated in the previous work that Fe carbide was formed during the ammonia decomposition process at 750°C over coal char supported Fe catalysts, which led to of the deactivation of the Fe catalyst [18]. As such, the ammonia decomposition over the new catalysts may proceed with a different mechanism. The presence of P in both the AC-supported catalysts was evidenced by XPS analyses (Figures 4-7 and 4-8 and Table 4-4), and nickel/iron phosphides ($Ni_{12}P_5$, Ni_3P, and Ni_2P, Fe_2P) were observed by both XRD and XPS in these catalysts after the hydrogen reduction and the ammonia decomposition. This suggests that these metal phosphides ($Ni_{12}P_5$, Ni_3P, and Ni_2P, Fe_2P) might play an important role in the ammonia decomposition reactions. To investigate whether these metal phosphides were responsible for the conversion of NH_3 to N_2 and H_2, commercial compounds of Fe_2P and Ni_2P were mixed physically with the AC alone to make 25 wt % Fe_2P/AC and 25 wt % Ni_2P/AC respectively, and their catalytic effects were examined at 750°C under the same reaction conditions. The results are shown in Figure 4-11 in comparison to those from the Fe/AC and Ni/AC catalysts. Although these bulk compounds were much less active than the AC-supported Fe and Ni catalysts, the activities of Ni_2P and Fe_2P were still evident, in particular for Ni_2P. It is thus probable that the fine dispersion of these phosphides in-situ formed in the two new catalysts (Ni/AC and Fe/AC) during the ammonia decomposition process may be responsible for the high activities of these new catalysts as reported in this work.

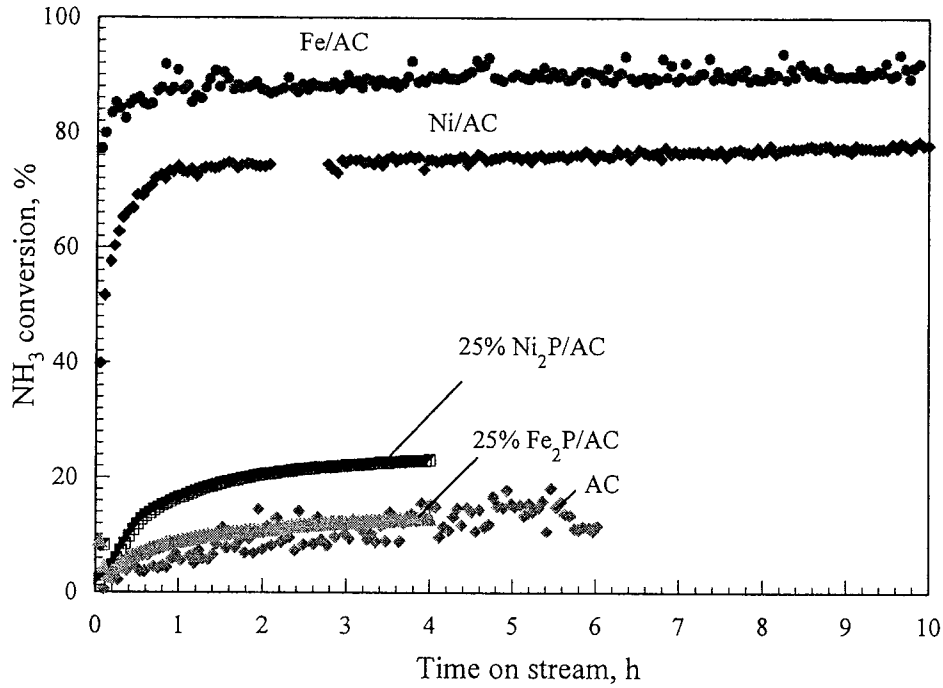

Figure 4-11 Effects of Fe_2P/AC and Ni_2P/AC on NH_3 decomposition (experimental conditions: 750°C, 2000 ppm NH_3/He and space velocity of 45000 h^{-1}).

The Fe/AC catalyst was subjected to TPD measurements, and the results are shown in Figure 4-12. For the curve (b) in the Figure, the catalyst was first reduced by H_2 at 500°C for 2 hours, and it was then treated with 2000 ppm/He NH_3 for 4 h at 500°C before being quenched to room temperature and subjected to the TPD measurement. The TPD measurements were carried out by heating the catalyst sample in high-purity helium up to 800°C or 900°C and held at this temperature for 30 minutes, when the desorbed N_2 was detected by a GC-TCD. As shown in the Figure, evolution of N_2 proceeded significantly at temperatures ≥600°C. At approximately 730°C a significant amount of N_2 was detected from the ammonia-treated sample (Figure 4-12b), and as the temperature was increased to 800°C there was further N_2 detected at an increased rate. The fresh Fe/AC catalyst after H_2 reduction was also subjected to TPD measurements, as shown in Figure 4-12a, so as to distinguish between the nitrogen present in the fresh Fe catalyst and the chemisorbed ammonia or the Fe-nitride complexes formed during the NH_3 treatment. As evidenced by the bulk CHN elemental analysis (Table 4-3) and the XPS measurement (Table 4-4), the fresh catalyst of Fe/AC or Ni/AC contained a significant amount of inherent nitrogen (bulk composition of N of 1.6 wt% (db) and an atomic ratio N/C of 0.02 or 0.03). As shown in Figure 4-12a, the inherent nitrogen evolved insignificantly at temperatures <800°C, and it peaked at 870°C in the Fe/AC catalyst without the ammonia treatment. This might imply that the

peaks formed in the Fe catalyst after NH_3 treatment at temperatures of 600-800°C were more likely a result of the decomposition of the chemisorbed NH_3 on the catalyst's surface or the decomposition of nitride species formed during the NH_3 treatment.

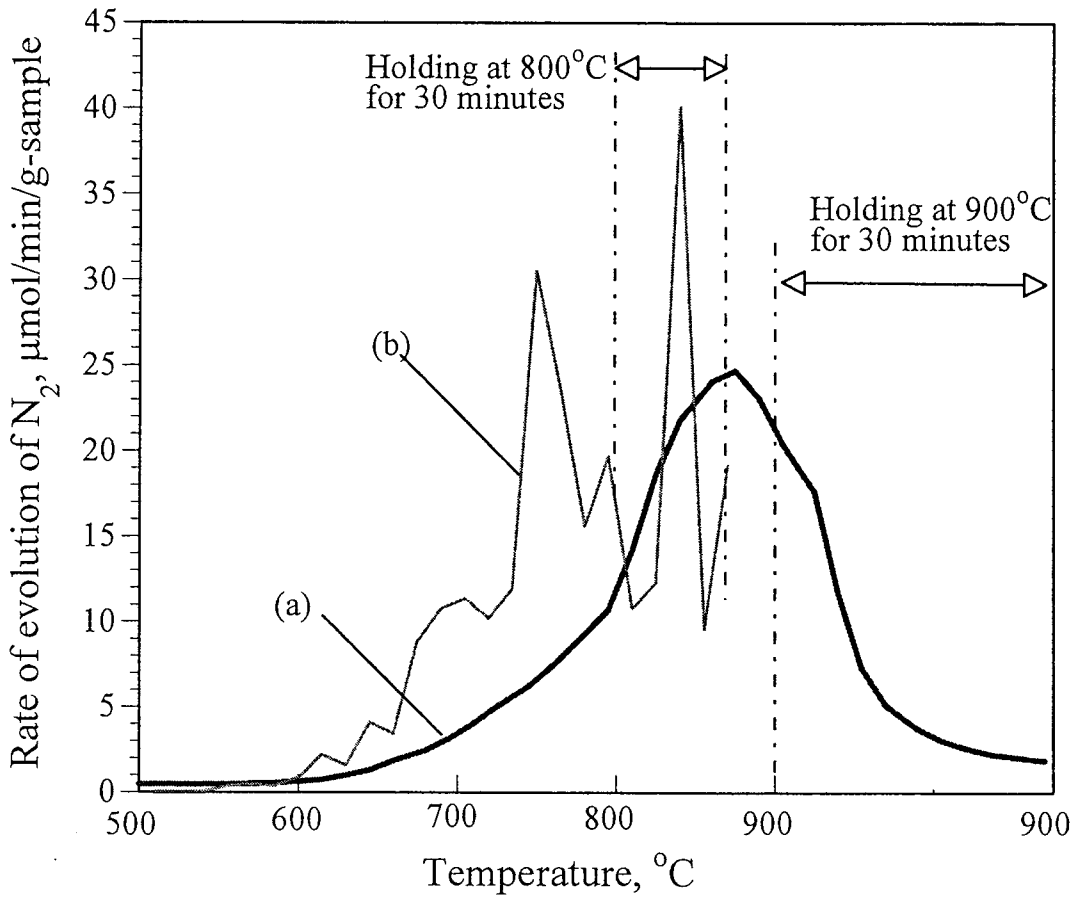

Figure 4-12 Evolution of N_2 during TPD of the fresh Fe/AC catalyst after H_2 reduction (a) and after NH_3 treatment at 500°C for 4 h (b).

By analogy with the cycle mechanism involving Fe metal and nitrides proposed in the Fe-catalyzed NH_3 decomposition studies [17, 18, 23], the following reaction schemes, involving intermediates of iron phosphide (Fe_2P) and iron nitride (Fe_4N), are proposed:

$$2Fe + P \rightarrow Fe_2P \quad (1)$$

$$6Fe + 3P + 2NH_3(g) \rightarrow 3Fe_2P + N_2(g) + 3H_2(g) \quad (2)$$

$$Fe_2P + 0.5NH_3(g) + 0.75H_2 \rightarrow 0.5Fe_4N + PH_3(g) \quad (3)$$

$$PH_3(g) + 2Fe \rightarrow Fe_2P + 1.5H_2(g) \quad (4)$$

$$Fe_4N \rightarrow 4Fe + 0.5N_2(g) \quad (5)$$

$$4Fe + NH_3\,(g) \rightarrow Fe_4N + 1.5H_2\,(g) \qquad (6)$$

The dependencies of standard Gibbs free energies ($\Delta G°$) with temperature for these reactions are given in Figure 4-13. As seen in this Figure, all of these reactions listed above are thermodynamically favourable at 750°C. Because the presence of Fe_2P was identified and suggested by the XRD (Figure 4-4) and XPS (Figure 4-8), this species could be formed via reactions (1) and (2) between α-Fe and the P in the AC support at elevated temperatures. The Fe_2P might react with NH_3 fed and the active H_2 or H atom on the catalyst surface to form Fe_4N and PH_3 through reaction (3) (PH_3 was actually detected by using a PH_3 detection tube at the initial period of the reactions). The Fe_2P could be regenerated by the reaction of PH_3 and α-Fe (reaction 4). The iron nitride species is very unstable and/or in a highly dispersed state in the catalyst (implied by the analyses of XRD and XPS), so that it would readily decompose to α-Fe and N_2 at low temperatures of ≥ 400 °C according to equation (5) [17, 18, 23], Reaction of α-Fe and NH_3 would regenerate Fe_4N and produce H_2 (reaction 6). It is thus possible that the NH_3 decomposition over the new AC-supported Fe/Ni catalyst may proceed through a cycle mechanism involving metal phosphides and nitrides.

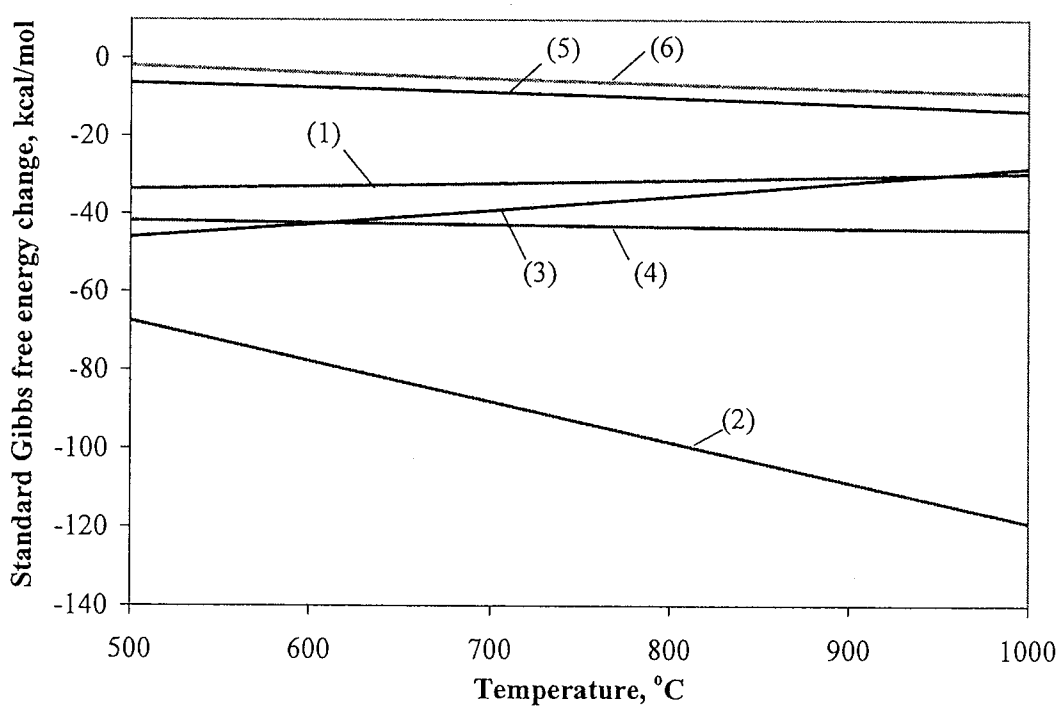

Figure 4-13, Dependencies of standard Gibbs free energies (ΔG°) with temperature for reactions (1), (2), (3), (4), (5) and (6).

4.5 Conclusions

(1) Novel Ni/Fe catalysts were prepared using a mesoporous activated carbon (AC) support derived from a Canadian peat by H_3PO_4 activation. The newly developed catalysts proved to be highly active for ammonia decomposition, Fe/AC having a higher activity compared to the Ni/AC. The conversion of 2000 ppm NH_3 diluted in helium over the Fe catalyst reached as high as 90% at 750°C and at the space velocity of 45000 h^{-1}, compared with only about 15% with the AC alone. The new catalyst of Fe/AC was also much more active than the Fe catalyst supported on a commercial AC reported previously.

(2) The newly developed Fe/Ni catalysts showed superior performance for hot gas ammonia decomposition with respect to their resistance to catalyst deactivation. Both catalysts remained active as the reaction time increased up to 10 hours without showing a sign of deactivation. The remarkable increases in mesoporous surface area and pore volume in the Ni/AC and Fe/AC catalysts during the ammonia decomposition might contribute to the high activities and stability of these catalysts in ammonia decomposition.

(3) Highly dispersed nanoparticles of metallic Ni or Fe were present in the fresh catalysts of Ni/AC and Fe/AC, evidenced by XRD. The XRD and XPS measurements of the spent catalysts showed the presence of nickel/iron phosphides ($Ni_{12}P_5$, Ni_3P, and Ni_2P, Fe_2P) and nitride (Fe_xN). It was proposed that the fine dispersion of the metal phosphides and nitrides in-situ formed in these catalysts (Ni/AC and Fe/AC) during the ammonia decomposition process were responsible for the high activities of these catalysts through a cycle mechanism.

References

[1] J. Zhou, S.M. Masutani, D.M. Ishimura, S.Q. Turn, C.M. Kinoshita, Release of fuel-bound nitrogen during biomass gasification. Ind. Eng. Chem. Res. 39 (2000): 626–634

[2] J. A.Miller, M. D. Smooke, R. M Green, R. J. Kee. Kinetic Modelling of the Oxidation of Ammonia in Flames. *Combustion Science Technology* 1983; 34:149–176.

[3] X.-K. Li, W.-J. Ji, J. Zhao, S.-J. Wang, C.-T. Au. Ammonia decomposition over Ru and Ni catalysts supported on fumed SiO_2, MCM-41, and SBA-15. *Journal of Catalysis* 2005; 236: 181

[4] W. Zheng, J. Zhang, Q. Ge, H. Xu, W. Li. Effects of CeO_2 addition on Ni/Al_2O_3 catalysts for the reaction of ammonia decomposition to hydrogen. *Applied Catalysis B: Environmental* 2008; 80:98.

[5] S.F. Yin, Q.H. Zhang, B.Q. Xu, W.X. Zhu, C.F. Ng, C.T. Au, Investigation on the catalysis of CO*x*-free hydrogen generation from ammonia. *Journal of Catalysis* 2004; 224:384-396.

[6] M.E.E. Abashar, Y.S. Al-Sughair, I.S. Al-Mutaz. Investigation of low temperature decomposition of ammonia using spatially patterned catalytic membrane reactors. *Applied Catalysis A: General.* 2002; 236:35-53.

[7] W. Arabczyk, J. Zamłynny, Study of the ammonia decomposition over iron catalysts. *Catalysis Letters* 1999; 60: 167-171.

[8] M.C.J. Bradford, P.E. Fanning, M.A. Vannice. Kinetics Of NH3 Decomposition Over Well Dispersed Ru. *J. Catal.* 1997;172:479-484

[9] K. Hashimoto, N. Toukai, J. Mol. Decomposition of ammonia over a catalyst consisting of ruthenium metal and cerium oxides supported on Y-form zeolite. *Catal. A: Chem.* 2000;161:171-178

[10] A. Chellappa, S. Fischer, W. Thomson. Ammonia decomposition kinetics over Ni-Pt/Al2O3 for PEM fuel cell applications. *Applied Catalysis A: General* 2002;227:231–240

[11] K. Kordesch, V. Hacker, R. Fankhauset, G. Faleschini, WO Patent 0 208 117 (2002).

[12] T.V. Choudhary,C. Sivadinarayana, D. W. Goodman. Production of CO_x-free hydrogen for fuel cells via step-wise hydrocarbon reforming and catalytic dehydrogenation of ammonia. *Chemical Engineering Journal,* 2003;93: 69-80

[13] J.-G. Choi, H.-G. Oh, Y.-S. Baek, Tantalum carbide hydrodenitrogenation catalysts. *J. Ind. Eng. Chem.* 1998;14:94-98.

[14] C.-H. Liang,W.-Z. Li, Z.-B.Wei, Q. Xin, C. Li, Catalytic Decomposition of Ammonia over Nitrided MoNx/α-Al_2O_3 and NiMoNy/α-Al_2O_3 Catalysts. *Ind. Eng. Chem. Res.* 2000;39:3694-3697.

[15] S.F. Yin, B.Q. Xu, C.F. Ng, C.T. Au, Nano Ru/CNTs: a highly active and stable catalyst for the generation of CO_x-free hydrogen in ammonia decomposition. *Appl. Catal. B: Environ.* 2004;48:237-241.

[16] S.F. Yin, B.Q. Xu, S.J.Wang, C.F. Ng, C.T. Au, Magnesia–Carbon Nanotubes (MgO–

CNTs) Nanocomposite: Novel Support of Ru Catalyst for the Generation of CO_x-Free Hydrogen from Ammonia. *Catal. Letters* 2004; 96:113

[17] C. Xu, N. Tsubouchi, H. Hashimoto, Y. Ohtsuka. Catalytic decomposition of ammonia gas with metal cations present naturally in low rank coals. *Fuel* 2005;84:1957-1967.

[18] Y. Ohtsuka, C. Xu, D. Kong, N. Tsubouchi. Decomposition of ammonia with iron and calcium catalysts supported on coal chars. *Fuel* 2004;83:685-692.

[19] C. Xu, J. Donald. Upgrading peat to gas and liquid fuels in supercritical water with catalysts *Fuel* (in press), 2008: doi:10.1016/j.fuel.2008.04.042

[20] Strack M. (ed.) *Peatlands and Climate Change*, International Peat Society, Saarijärven Offset Oy, Saarijärvi, Finland, 223 pp

[21] Y. Ohtsuka, U.S. Patent 6,555,084 B2 (April 23, 2003).

[22] K. S. W. Sing. REPORTING PHYSISORPTION DATA FOR GAS/SOLID SYSTEMS with Special Reference to the Determination of Surface Area and Porosity. *Pure & Appl.Chem.* 1982;54:2201—2218

[23] N. Tsubouchi, H. Hashimoto, Y. Ohtsuka. High catalytic performance of fine particles of metallic iron formed from limonite in the decomposition of a low concentration of ammonia. *Catalysis Letters* 2005;105:203-208.

CHAPTER 5

Hot Gas Decomposition of NH_3 in Simulated Gas over Carbon-based Ni/Fe Catalysts and Natural Limonite Ores

ABSTRACT

The catalytic performance of the peat-derived activated carbon supported Fe/Ni catalysts as well as three natural limonite ores (from Australia, Brazil and Canada) towards hot gas NH_3 decomposition in a simulated gas (14.9% CO, 2.9% CH_4, 11.2% H_2, 11.2% CO_2) with and without 5-15% H_2O, was investigated at 750°C. The Fe/AC and Ni/AC catalysts and all natural limonite ores were very active for ammonia decomposition in the inert atmosphere. However, both AC-supported catalysts could be severely deactivated by the simulated gas, and the Fe/AC catalyst was also deactivated by the presence of H_2O in the gas. In the presence of the simulated gas and H_2O, the activities of these two catalysts dropped drastically to as low as <10%. The three limonite ores showed high activities towards ammonia conversion to N_2 (>90% at 750°C) in both inert atmosphere or in a simulated gas with 0-15% H_2O. The deactivation of the Ni/AC and Fe/AC by the simulated gas and H_2O vapor may be caused by the carbon deposition resulting from Boudouard reaction of CO or decomposition of CH_4, by the oxidation of metal phosphides and metallic metals into less or inactive phosphates in the presence of the simulated gas species CO and H_2O, or by the competing adsorption of CO_2 and H_2O with NH_3 on the catalyst surface.

Keywords: Ammonia decomposition, Hot gas cleanup, Simulated gas, Biomass gasification, Carbon-based catalysts, Limonite.

5.1 Introduction

Gasification is a promising technology for bio-refining biomass into value added fuel and chemical products through the syngas platform. In biomass gasification, the biomass feedstock is partially oxidized/gasified in an oxidizing atmosphere of air, oxygen and/or steam to form a low to medium-BTU product gas containing primarily CO, H_2, CO_2, CH_4 and (C_2+C_3), which can be used for heat and electricity generation, or for synthesis of liquid fuels and methanol [1-4]. Gasification of biomass also generates some contaminants in the product gas, such as tars, NH_3, H_2S and SO_2, etc. [1-4]. These contaminants must be removed before the syngas is used for internal combustion, gas engines, and in particular for fuel cells and methanol synthesis, in order to achieve better efficiencies of the syngas applications.

Depending on the type of biomass used, as well as the gasifier parameters and operating conditions, the content of NH_3 in the product gas, is typically of 1000-5000 ppm [5]. The ammonia in the producer gas can be reduced by hot gas cleanup through catalytic decomposition into N_2 and H_2. The most common catalysts used in the NH_3 decomposition studies are supported metals of Ni [6-9] and Ru [6, 7, 9-11]. For instance, the Ru/Al_2O_3 catalyst obtained ammonia conversions of 95.3%, compared with 90.4% for the Ni catalysts at 850°C [9]. Al_2O_3 supported Ru or Ru-Ni catalysts (6-9 wt% total metal loading) obtained~90% ammonia conversion at 900°C for decomposition of 1000 ppm ammonia in a simulated coal-derived syngas (10 vol% H_2, 28 vol% CO, 54 vol% N_2, 3.6 vol% CO2 and 3 vol% H_2O) at a gas hourly space velocity (GHSV) of 20000 h^{-1} [11]. However, the major problem for these Al_2O_3-supported Ni or Ru catalysts for hot gas removal of ammonia is associated with the deactivation by fouling of the catalyst due to the carbon deposition, and catalyst poisoning by H_2S [12,13]. The problem would be serious for tarry fuel gases from gasification and pyrolysis of coal or biomass solid fuels, containing significant amounts of tar, CO, CH_4 and H_2S.

There were some successful studies reported recently on using natural Fe-based minerals as catalysts for hot gas ammonia decomposition. High conversions of NH_3 to N_2 were achieved using an Australian limonite with a high content of α-FeOOH in a study by Tsubouchi et al [14]. In an NH_3 gas stream diluted with high purity helium, almost complete conversion of ammonia (≥99%) was obtained at a temperature of 500°C and a space velocity of 45,000 h^{-1} with the

Australian limonite. The efficiency of the Australian limonite was tested for ammonia decomposition in an inert gas and a simulated gas typical of an air-blown gasification process, containing CO, H_2, CO_2, and H_2O. In the presence of fuel gas (20%CO/10%H_2) the ammonia conversion was found to decrease significantly at lower temperatures, accompanied with a higher conversion to HCN. At higher temperatures (>750°C), however, there was no deactivation of the limonite by the presence of CO and H_2. Also, it was found that the addition of 10%CO_2 or 3% H_2O, helped to restore the ammonia conversion to approximately 90% at 750°C, and by increasing the temperature further the conversion could approach to 100% [15].

Carbon-based catalysts have gained a lot of interest due to their advantages with respect to a lower cost, a high surface area and elaborate pore structure. In a study by Xu et al [16], pyrolysis chars from low rank coals containing inherently present Fe and Ca were tested as effective catalysts for the conversion of NH_3 to N_2. Studies using simulated gases containing CO, CO_2 and H_2 were also conducted [16], and the chars initially showed reduced activities initially, but after an induction period on stream, they attained high NH_3 conversions (~80% at 750°C) as in the inert atmosphere experiments. In another study by the same group [17], decomposition of ammonia with Fe and Ca catalysts supported on coal chars was investigated using 2000 ppm NH_3 diluted in helium in a fixed bed. The coal-char-supported Fe and Ca catalysts were found to be very effective for ammonia decomposition. An iron content of 6 wt% on an Australian brown coal char attained a conversion of nearly 100% at 750°C and a GHSV of 45000 h^{-1}.

Commercial ACs have been found to be much less active towards NH_3 decomposition compared to other catalysts such as iron-based and Ni-based catalysts, as well as chars derived from coals [16,17]. Although AC and AC supported metal catalysts are less active for ammonia and tar decomposition than those supported on other materials such as Al_2O_3, SiO_2, TiO_2, MgO, CNTs, etc., more research into the development of effective AC supported catalysts should be carried out because activated carbon materials have high surface areas and relatively low costs. The present work (Discussed in Chapter 4 of this thesis) has resulted in development of novel, less expensive activated carbon-supported (Fe, Ni) catalysts derived from peat for hot gas decomposition of ammonia (under patenting). The proprietary AC-supported catalysts obtained > 90% ammonia conversion at 750°C with 2000 ppm/helium and at a GHSV of 45000

h^{-1}.

The main objective of this study is to examine the catalytic performance of the peat-derived activated carbon supported Fe/Ni catalysts as well as three natural limonite ores (from Australia, Brazil and Canada) towards hot gas NH_3 decomposition in a simulated gas containing CO, H_2, CO_2, CH_4 and H_2O, typical of air-blown biomass gasification. The fresh and spent catalysts were characterized by XRD and XPS, and possible roles of the catalysts and simulated gas species in ammonia decomposition reactions were discussed.

5.2 Experimental

5.2.1 Materials

The activated carbon (AC) used as the catalyst support for two carbon based Fe/Ni catalysts was prepared from raw peat by a chemical activation method using H_3PO_4, discussed previously in detail in Chapters 3 and 4. The Fe and Ni loaded catalysts were prepared using the peat-derived AC by the wet impregnation method using $Fe(NO_3)_3 \cdot 9H_2O$ or $Ni(NO_3)_2 \cdot 6H_2O$ as the metal sources to a metal loading amount of 13 wt% Fe or Ni. The Fe(III) and Ni(II) impregnated ACs were calcined in N_2 at 500°C for 4 hrs, while the details of the AC-supported metal catalysts were given previously in Chapter 4. The as-prepared AC-supported Fe or Ni catalysts in this study were denoted as Fe/AC and Ni/AC for short. In addition, three natural limonite ore samples from Canada (CL), Brazil (BL) and Australia (AL) were used as catalysts in this study. Before use, the limonite ore samples were crushed and sieved into particles of 0.15-0.25 mm (CL), 0.25-0.5 (BL) and 0.15-0.25 mm (AL). The compositions of inorganic matter of the limonite samples were determined using ICP-AES (Inductively Coupled Plasma - Atomic Emission Spectrometer), and the analytical results are shown in Table 5-1 below.

Table 5-1 Limonite samples ultimate analysis

Limonite Sample	Major elements determined by ICP-AES (wt.%)											
	Al	Ba	Ca	Mg	**Fe**	Mn	Na	K	P	S	Ni	Si
CL	**0.4**	<0.1	<0.1	<0.1	**42.1**	<0.1	<0.1	<0.1	<0.1	0.2	<0.1	**3.1**
BL	**3.1**	<0.1	<0.1	**0.4**	**57.1**	<0.1	<0.1	<0.1	<0.1	<0.1	**0.7**	**1.9**
AL	**4.5**	<0.1	<0.1	**0.2**	**45.6**	<0.1	<0.1	<0.1	<0.1	<0.1	<0.1	**11.5**

5.2.2 NH_3 Decomposition Apparatus and Methods

NH_3 decomposition experiments were carried out with a flow-type, vertical quartz reactor placed in an electric furnace, as schematically illustrated in Figure 5-1. The catalyst bed within the reactor measured approximately 8 mm in height, and was held in place with fine grade quartz wool. Prior to NH_3 decomposition, the samples were heated to 500°C at a heating rate of 15°C/min in a helium flow of 180 ml/min, and then subjected to reduction using 200 ml/min of H_2 for 2 h. After H_2 reduction, the reactor was heated to 750°C with a heating rate of 15°C/min in a He flow of 180 ml/min. As the temperature reached 750°C, the helium flow was replaced with the reactant gas stream, either 2000 ppm NH_3 diluted in helium or the simulated gas containing 2000 ppm NH_3, 11.2% H_2, 14.9% CO, 11.17% CO_2, 2.92% CH_4, 5-15% H_2O and helium balance, at the space velocity of 45000 h^{-1}. The moisture content of the gas was controlled by increasing/decreasing the temperature of the water vaporizer between 60-85°C, as well as controlling the He flow through the vaporizer. Here, the composition of the simulated gas is typical product gas from air-blown biomass gasification [18, 19]. A high speed micro GC-TCD and a photo acoustic multi-gas monitor were used to determine N_2 formed and the un-reacted NH_3 as well as the formed HCN, respectively. Ammonia and moisture traps, located after the gas monitor consisting of distilled water, and calcium carbonate, respectively, were used to prevent NH_3 and H_2O from entering the GC.

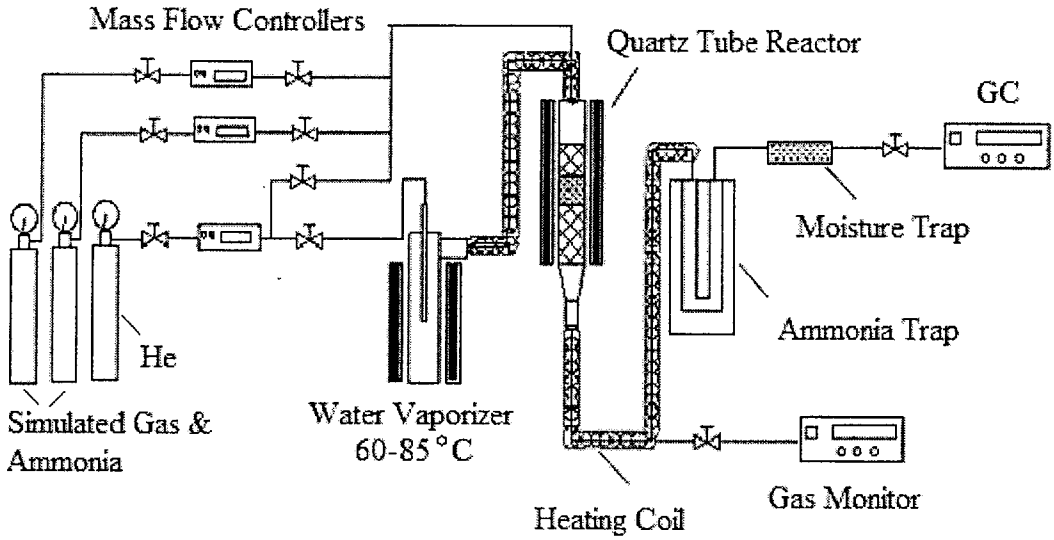

Figure 5-1 Experimental Apparatus

5.2.3 Characterization of the Catalysts

The as-prepared AC-supported Ni/Fe catalysts and the limonite catalyst samples (CL, BL and AL) were analyzed by N_2 isothermal adsorption (77K) for its surface area and textural structures, using NOVA 1200e/TO (Quantachrome Instruments). X-ray diffraction (XRD) with Cu Kα and Fe Kα radiation (Shimadzu XRD-6000, 30 mA and 40 kV) was used to characterize the crystalline structures of all the catalysts before and after the ammonia decomposition tests. The average crystalline size of the particles (L_c) was calculated using the Debye-Scherrer equation. X-ray photoelectron spectroscopy (XPS) was employed to characterize the chemical composition on the surfaces of the catalysts before and after ammonia decomposition experiments. The XPS experiments were performed on a ULVAC PHI 5600 spectrometer with an Al anode for K_α X-ray source operating at 200W. Charging effects were corrected by adjusting the binding energy of C_{1s} peak of carbon contamination to 284.6 eV.

5.3 Results

5.3.1 Characterization of the Fresh Catalysts

The fresh as-prepared Fe/AC and Ni/AC catalysts and the AC support (for comparison) were analyzed using N_2 isothermal adsorption (77K) for their surface areas and textural structures, and the results are summarized in Table 5-2. The as-synthesized AC has a BET surface area of 675 m^2/g, much greater than either the fresh Fe/AC (205 m^2/g) or the fresh Ni/AC (393 m^2/g), owing to the deposition of the metal ions (Fe or Ni) in the pores. The total pore (< 163 nm) volume is 0.25 cm^3/g for Ni/AC and 0.14 cm^3/g for Fe/AC, both lower than that of the AC support (0.50 cm^3/g). The average pore diameters from the metal catalysts are both 2.7 nm, slightly lowered than the support (3 nm). The AC support has a larger mesopore development (with a mesopore area of 375 m^2/g, mesopore volume of 0.42 cm^3/g and mesopore diameter of 4.4 nm), and as expected the Ni/AC and Fe/AC catalysts have greatly decreased mesopore areas (of 11 and 41 m^2/g, respectively), mesopore volumes (of 0.02 and 0.06 cm^3/g, respectively) and mesopore diameters (of both 3.7 nm). In addition, the crystalline structures in the Fresh Fe/AC and Ni/AC samples were analyzed using XRD, and the results have been reported previously in Chapter 4, where no Fe-related XRD signals were detectable in the fresh Fe/AC sample, and relatively weak signals from ultra-fine crystalline particles (L_c = 14 nm) were detected in the fresh Ni/AC catalyst. These results suggest a very high dispersion of as prepared AC-supported Fe/Ni catalysts.

Table 5-2 Surface areas and textural properties of the as-synthesized the AC-supported Fe and Ni catalysts, in comparison with the peat-derived AC support.

Catalyst and support	Multi-point BET (m^2/g)	Total pore volume (< 163 nm) (cm^3/g)	Average pore diameter (nm)	Mesopore surface area (m^2/g)	Mesopore volume (cm^3/g)	BJH desorption average pore diameter (nm)
AC support	675	0.50	3.0	375	0.42	4.4
Fe/AC	205	0.14	2.7	11	0.02	3.7
Ni/AC-fresh	393	0.25	2.7	41	0.06	3.7

The fresh limonite ores were also tested by N_2 isothermal adsorption (77K) to determine the BET surface areas, and the crystalline structures of the fresh limonite samples were analyzed using XRD. The physical and chemical properties of the fresh limonite samples are summarized in Table 5-3 below, and the XRD spectra of these samples are illustrated in Figure 5-2. As shown in the Table, the Brazilian limonite (BL) has the largest BET surface area of 90 m^2/g and the highest Fe content (57 wt%), while the Canadian limonite (CL) has the smallest BET surface area of only 11 m^2/g and the lowest Fe content (42 wt%). The major crystalline species detected by XRD in all fresh limonite samples were goethite (α-FeOOH), as shown in Figure 5-2. The crystalline size of the α-FeOOH, estimated by the Debye-Scherrer equation (5-1), was the largest for the CL sample (> 100 nm), followed by AL (25 nm) and BL (16 nm). Besides the goethite (α-FeOOH), α-Fe_2O_3 peaks of a medium intensity, and quartz (SiO_2) signals (of low-to-medium intensity) were detected in all the fresh limonite samples.

Table 5-3 Physical and chemical properties of the fresh limonite ores

Limonite ore	**AL**	**BL**	**CL**
Total Fe content (wt%)	46	**57**	42
Crystalline species [a]	α-FeOOH(s) α-Fe_2O_3 (m) SiO_2 (s)	α-FeOOH(s) α-Fe_2O_3 (m) SiO_2 (w)	α-FeOOH (s) α-Fe_2O_3 (m) SiO_2 (m)
Size of α-FeOOH (nm) [b]	25	**16**	>100
Surface Area (m^2/g) [c]	40	**90**	11

[a]Identified by XRD: w (weak); m (medium); s (strong) in intensity;

[b] Average crystalline size estimated by Debye-Scherrer method;

[c] Determined by BET method using N_2 isothermal adsorption (77K).

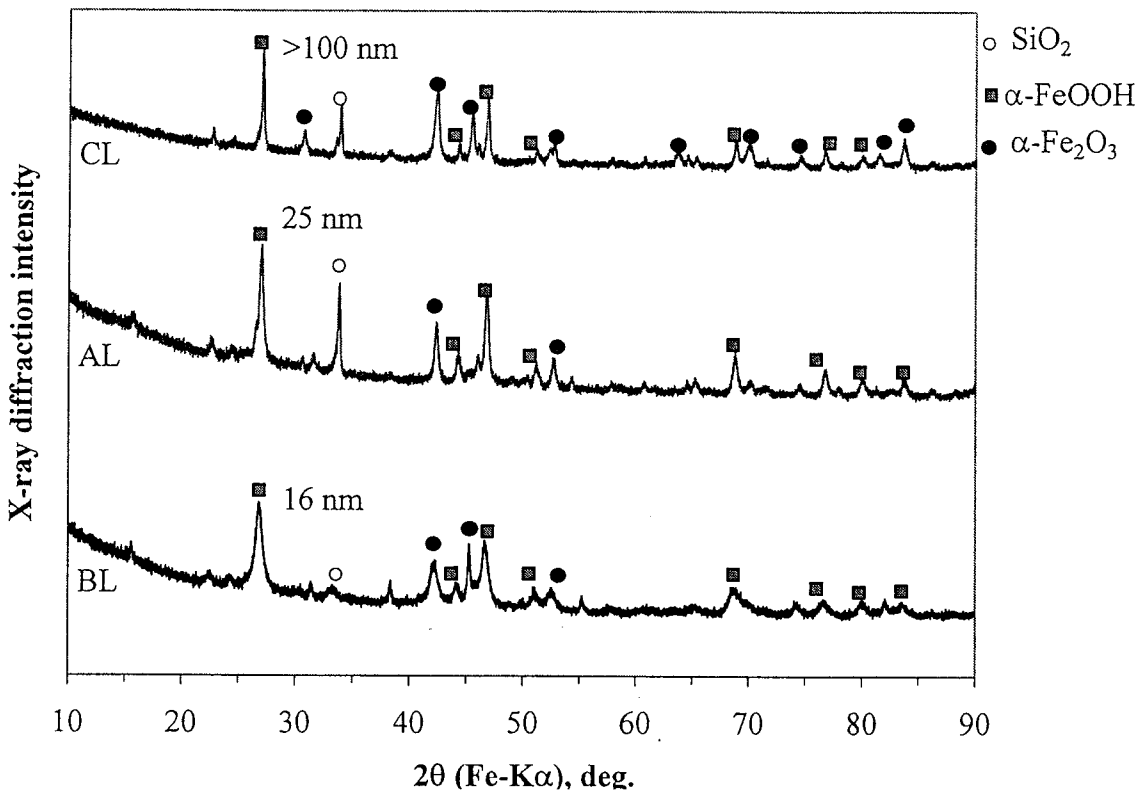

Figure 5-2 XRD spectra of fresh limonite samples

As described in the experimental section, each catalyst sample was pre-reduced in H_2 at 500°C for 2 hours before being subjected to the ammonia decomposition reaction. The reduction procedure to convert the α-FeOOH species into metallic Fe species (more reactive for NH_3 decomposition) has proved to be favorable for the NH_3 decomposition reactions [15]. To confirm the presence of the Fe metallic species in the limonite samples after the H_2 reduction, the pre-reduced samples (at 500°C for 2 hours) were cooled down to room temperature in helium and passivated using 2% O_2 in He before exposing the samples to air, to prevent the formation of oxides on the surface of the samples. The samples were analyzed by XRD and the results are illustrated in Figure 5-3. It is clearly shown in the Figure that metallic iron species (α-Fe) are dominant in all the limonite samples after H_2 reduction. In the H_2-reduced samples, the AL had the smallest particles of α-Fe (22 nm), followed by BL (24 nm) and CL (33 nm). In the reduced AL catalyst, very weak signals of α-FeOOH and Fe_3O_4 were detected, most likely due to partial oxidation by the passivation oxygen or air.

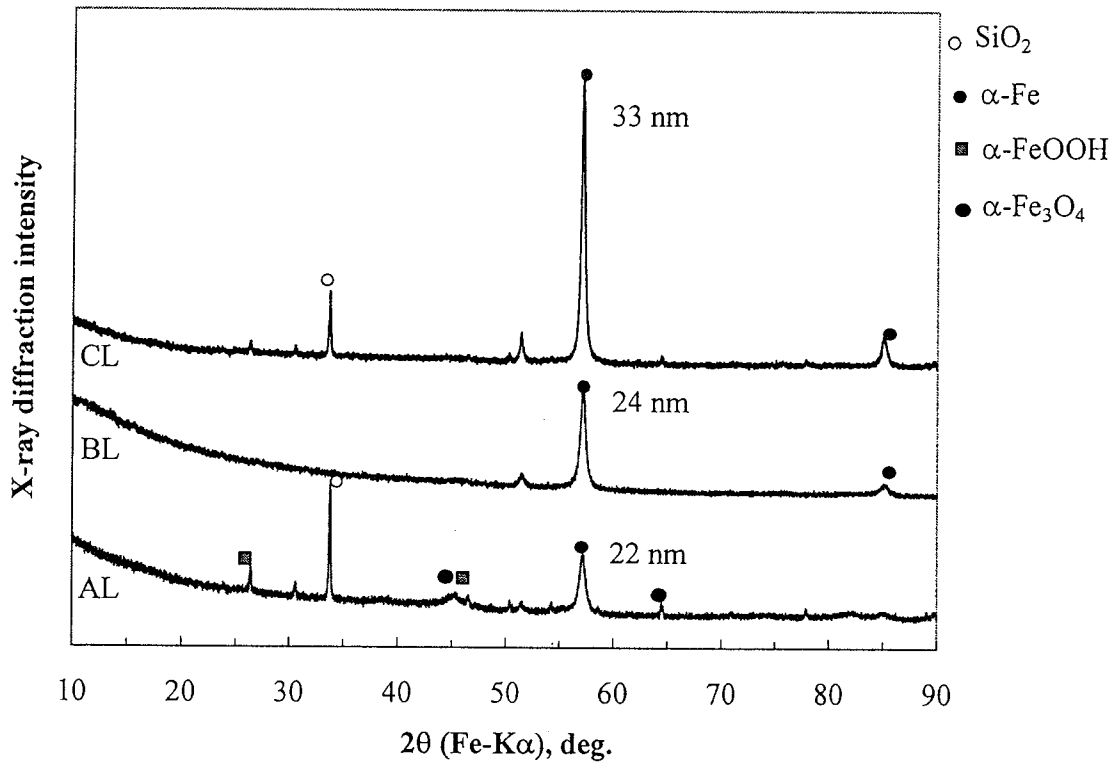

Figure 5-3 XRD profiles of raw limonite samples after H_2 reduction at 500°C for 2h.

5.3.2 Performance of the Fe/AC and Ni/AC Catalysts in NH_3 Decomposition in Simulated Gas

Figures 5-4 and 5-5 below show the effects of simulated gas and steam on the conversion of NH_3 using the Fe/AC and Ni/AC catalyst, respectively. The experiments were initially carried out with 2000 ppm NH_3 in an inert He atmosphere until a stable conversion of NH_3 to N_2 was reached in approximately 2 hours. After that, the reactor inlet gas stream was replaced by the simulated gas (2000 ppm NH_3, 11.2% H_2, 14.9% CO, 11.17% CO_2, 2.92% CH_4) with 0, 5, 10 and 15% H_2O. As shown in the Figures, the NH_3 conversions decreased drastically when switching the gas stream from inert helium to the simulated gas with/without H_2O for both Fe/AC and Ni/AC catalysts. For Fe/AC (Figure 5-4), the introduction of the simulated gas with 0% H_2O, the NH_3 conversion decreased from 86% (in helium) to approximately 26%, and as the H_2O content of the simulated

gas increased, the conversion dropped further from 26% (0% H_2O) to as low as 10% (15% H_2O). With Ni/AC (Figure 5-5), the decrease in NH_3 conversion was even more dramatic when the simulated gas was introduced into the gas stream. The NH_3 conversion decreased sharply from about 76% (in helium) to only 5% (in simulated gas with 0-15% H_2O), while differing from that observed with the Fe/AC, the NH_3 conversion over Ni/AC was independent of the H_2O content in the simulated gas. The above results strongly suggest that both Fe/AC and Ni/AC are severely deactivated by the simulated gas (H_2, CO, CO_2, CH_4) and the Fe/AC catalyst is further deactivated by the presence of H_2O in the gas. Some possible reasons will be discussed later in the section of Discussion.

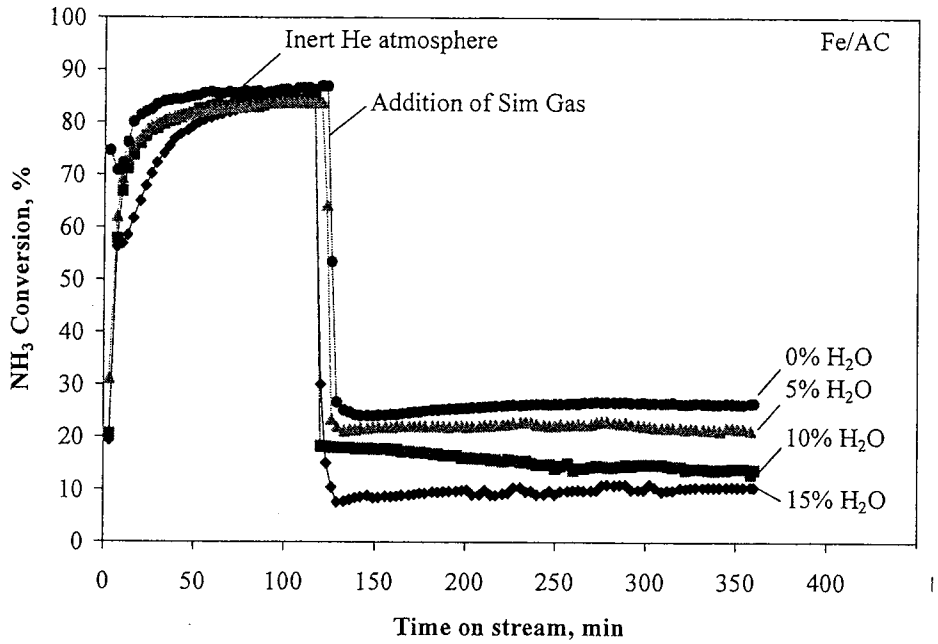

Figure 5-4 NH_3 conversion using the Fe/AC catalyst in the simulated gas with 0% H_2O, 5% H_2O, 10% H_2O and 15% H_2O.

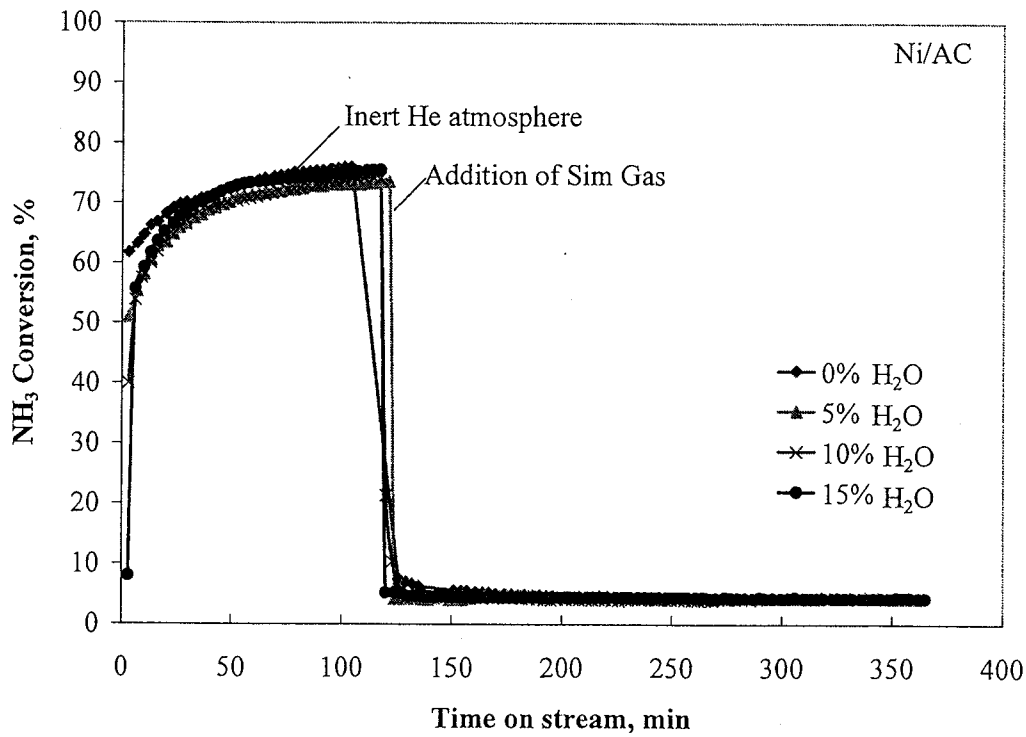

Figure 5-5 NH_3 conversion using the Ni/AC catalyst in the simulated gas with 0% H_2O, 5% H_2O, 10% H_2O and 15% H_2O.

5.3.3 Performance of the Limonite Ores in NH_3 Decomposition in Simulated Gas

The activity of a Canadian limonite (CL) as a catalyst for ammonia decomposition was also examined in inert helium and in the simulated gas with 0% and 15% H_2O under the same conditions (750°C and GHSV of 45000 h^{-1}). The results are shown in Figure 5-6 below. In the inert atmosphere, the CL was able to obtain 93% NH_3 conversion, as shown in Figure 5-6 (a). The presence of the simulated gas (14.9% CO, 2.9% CH_4, 11.2% H_2, 11.2% CO_2) without H_2O slightly decreased the conversion to around 90% (Figure 5-6b), suggesting the excellent performance of the limonite catalyst in hot gas decomposition of ammonia in both inert and simulated atmosphere. The addition of 15% H_2O to the simulated gas however led to a significant decrease in the NH_3 conversion, in particular at the initial period of reaction. In the presence of the simulated gas with 15% H_2O, the NH_3 conversion over the limonite catalyst was as low as about 65% for 1h on stream, while it climbed gradually with increasing time on stream, and approached to approximately 80% for 6 h on stream. From the increasing tendency of the conversion with time on stream for the CL in the simulated gas with 15% H_2O as shown in Figure 5-6c, it might be expected that the activity of the catalyst would eventually restore to the similar level of that in the H_2O-free simulated gas (i.e., 90% NH_3 conversion).

Australian and Brazilian limonite ore (AL and BL) were also tested in 2000 ppm NH_3 in the simulated gas with 15% H_2O, and the results are shown in Figure 5-7. Both AL and BL showed a very high activity for ammonia decomposition in the simulated gas with H_2O, leading to 95% conversion of NH_3. AL was slightly more active than BL although BL a larger Fe content, a greater surface area and smaller crystalline size of α-FeOOH in the fresh sample (Table 5-3). The better activity of AL over BL might be owing to the smaller α-Fe crystalline size after 2h H_2 reduction at 500°C prior to the ammonia decomposition reactions, as evidenced previously in Figure 5-3. After approximately 50 minutes on stream, both Australian and Brazilian limonite samples appeared to reach a stable conversion, whereas the activity of the Canadian limonite towards ammonia decomposition continued to increase with time, as discussed previously in Figure 5-6. Further testing for a longer period of time with the Canadian limonite may lead to conversion of ammonia

as high as that with the Australian and Brazilian limonite samples. The differences in the activities of the ferrous limonite samples might be related to the wt.% of Fe and crystalline size of α-FeOOH in the samples and the surface area of the samples. Among all the limonite samples, CL has the lowest Fe content (42.1 %), the largest size of α-FeOOH particles (>100 nm) and the smallest BET surface area (11 m^2/g), thus of the poorest dispersion, which may account for its lowest activity for ammonia decomposition, as revealed from Figure 5-7. The possible cause to the relatively lower activity for CL at the initial period of reaction could be that the Fe species (α-FeOOH and Fe_2O_3) of the Canadian limonite might require higher calcinations/reduction temperatures compared with the Australian and Brazilian limonite ores to obtain metallic Fe, which has proven to be the active species responsible for the decomposition of NH_3 [14-17].

In conclusion, all the limonite catalysts tested in this study showed stronger resistance to the simulated gas containing CO, CH_4, H_2, CO_2 and H_2O, which is superior to the AC-supported Fe/Ni catalysts, as discussed previously in Figures 5-4 and 5-5.

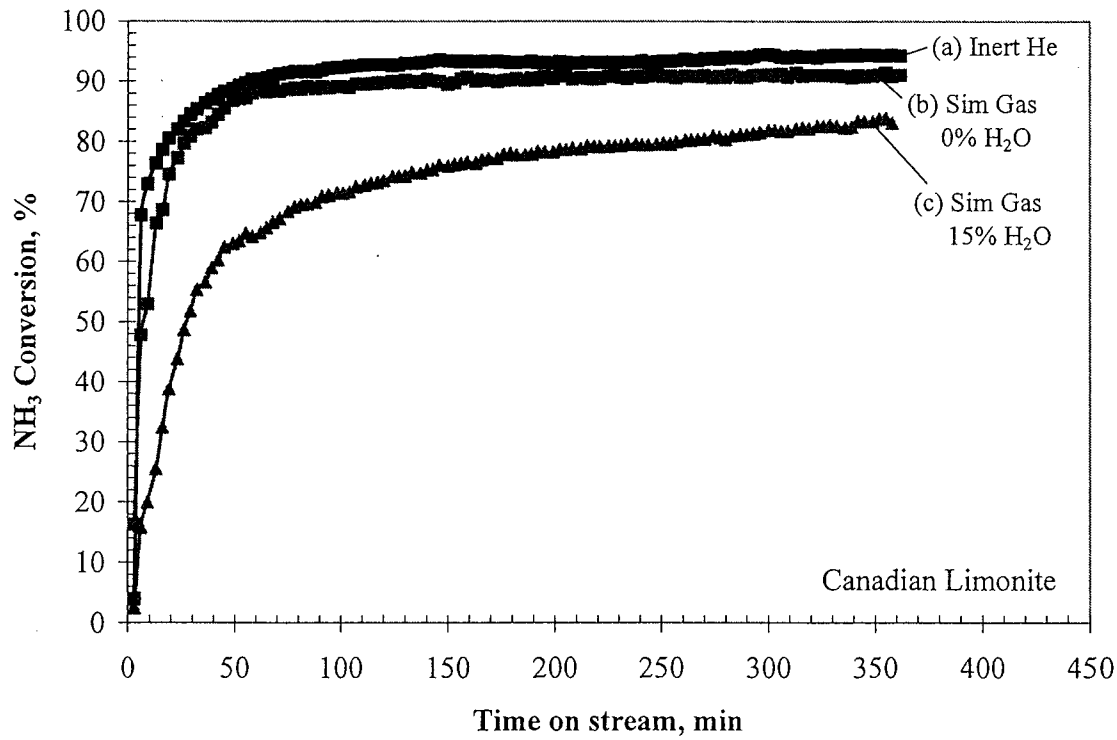

Figure 5-6 NH_3 conversion using Canadian Limonite in inert He (a), in the simulated gas with 0% H_2O (b), and in simulated gas with 15% H_2O (c).

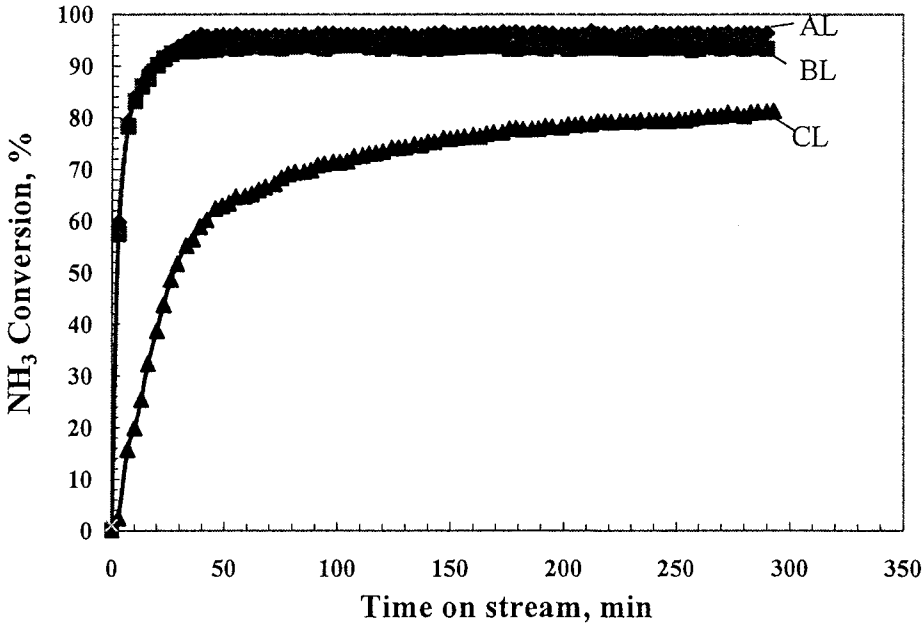

Figure 5-7 NH_3 conversion in the simulated gas with 15% H_2O using Canadian Limonite (AL), Brazilian limonite (BL) and Australian limonite (AL).

5.3.4 Characterizations of Spent Catalysts

5.3.4.1 Bulk Crystalline Structures of the Spent Catalysts

Figure 5-8 below shows the XRD (Cu K_α) profiles of the Ni/AC catalyst after NH_3 decomposition in the simulated gas (14.9% CO, 2.9% CH_4, 11.2% H_2, 11.2% CO_2) with 0% H_2O (d), 5% H_2O (c), 10% H_2O (b) and 15% H_2O (a). In spent catalyst from the test with the simulated gas without H_2O (Figure 5-8d), the diffraction lines of Ni_2P and $Ni_{12}P_5$ were the dominant signals detected in the XRD spectrum. With the introduction of H_2O in the simulated gas, the $Ni_{12}P_5$ peaks became more prominent than the Ni_2P, and the Ni_2P signals completely disappeared in the spent Ni/AC from the test with the simulated gas with 15% H_2O (Figure 5-8a).

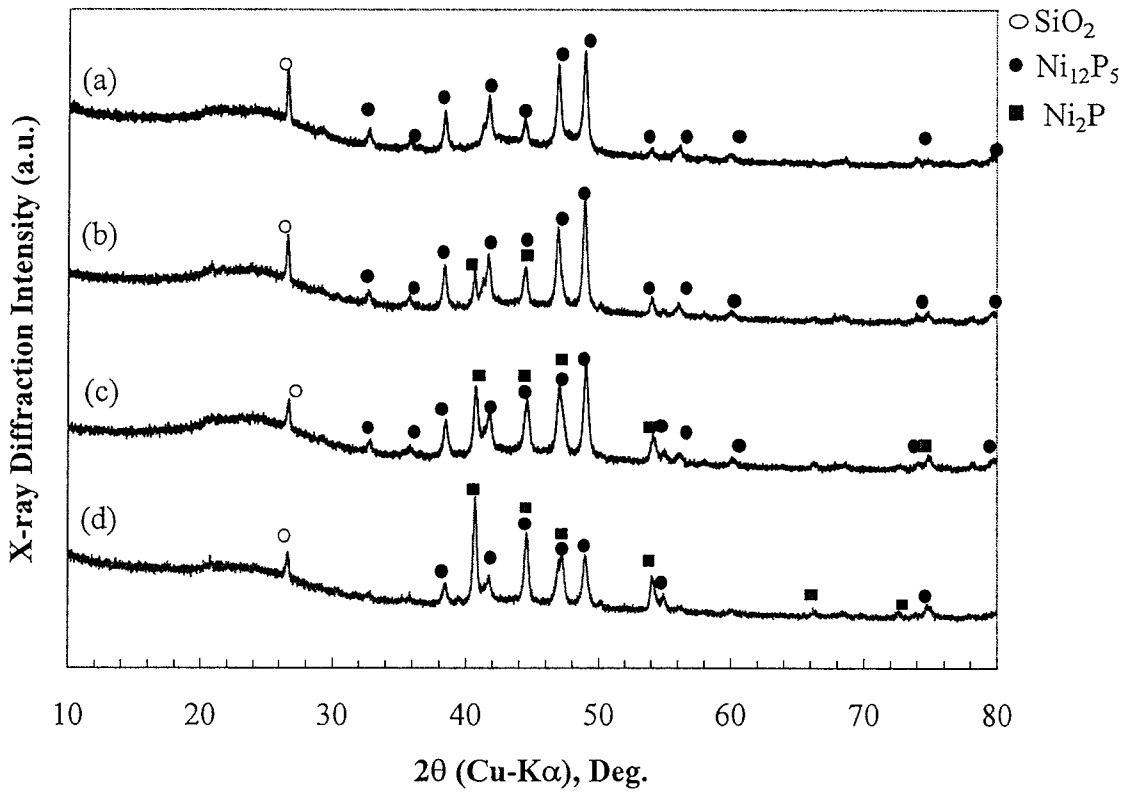

Figure 5-8 XRD profiles for the Ni/AC catalyst after H_2 reduction at 500°C for 2 hours and NH_3 decomposition at 750°C in the simulated gas with 15% H_2O (a), 10% H_2O (b), 5% H_2O (c) and 0% H_2O (d).

Figure 5-9 shows the XRD (Fe K_α) profiles of the Fe/ACcatalyst after NH_3 decomposition in the simulated gas (14.9% CO, 2.9% CH_4, 11.2% H_2, 11.2% CO_2) with 0% H_2O (d), 5% H_2O (c), 10% H_2O (b) and 15% H_2O (a). In spent catalyst from the test with the simulated gas without H_2O (Figure 5-9d), the diffraction lines of both Fe_2P and $Fe_3(PO_4)_2$ were detected by XRD, while the species of $Fe_3(PO_4)_2$ was not observed in the spent Fe/AC catalyst after ammonia decomposition in the inert helium gas (as discussed previous in Chapter 4). In the spent catalyst samples from the experiment in the simulated gas with H_2O, the signals of Fe_2P decreased considerably or became almost undetectable in the samples from the tests in the simulated gas with 10 and 15% H_2O (Figures 5-9a and 5-9b). It is thus clear that the presence of the simulated gas (CO, CH_4, H_2 and CO_2) as well as H_2O led to the conversion of metal phosphide (Fe_2P) into phosphate ($Fe_3(PO_4)_2$) during the experiment, which might deactivate the Fe/AC catalyst for ammonia decomposition, as revealed previously in Figure 5-4.

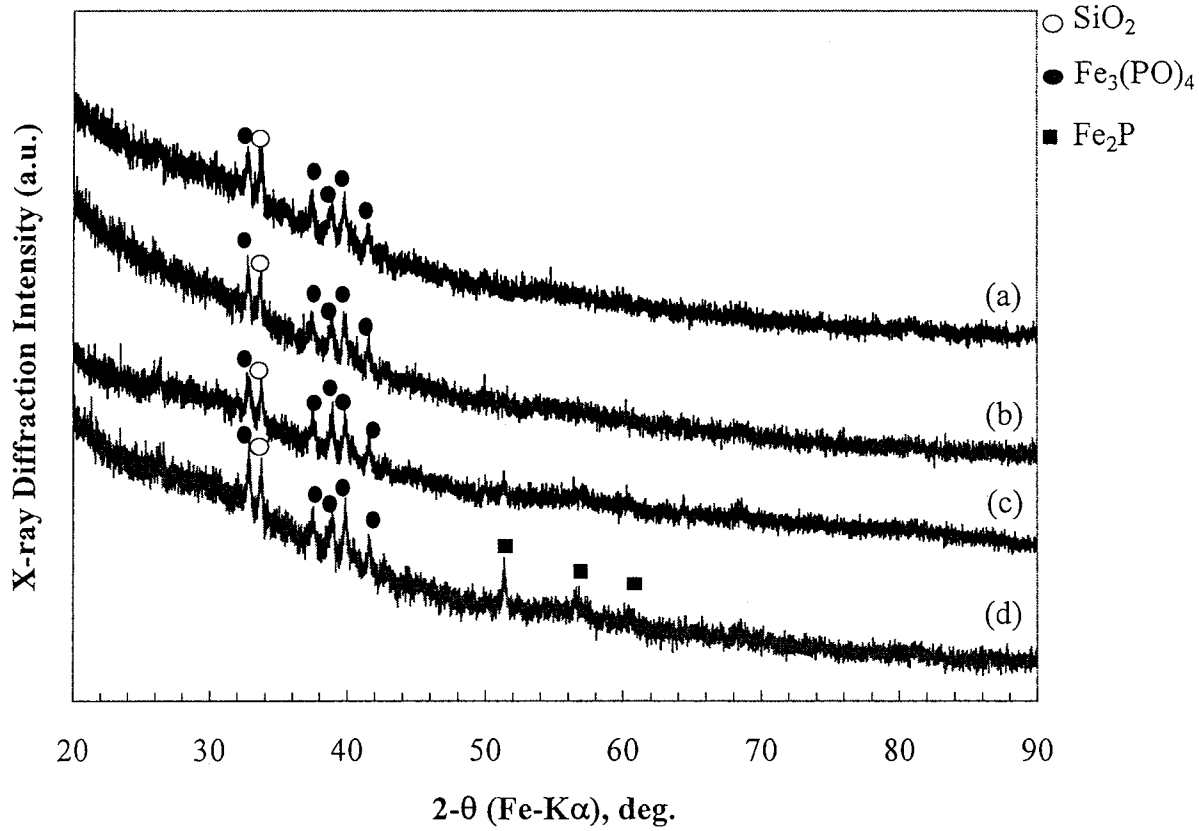

Figure 5-9 XRD profiles for the Fe/AC catalyst after H_2 reduction at 500°C for 2 h and NH_3 decomposition at 750°C in the simulated gas with 15% H_2O (a), 10% H_2O (b), 5% H_2O (c) and 0%H_2O (d).

Figure 5-10 shows the XRD (Fe K_α) profiles for the spent Canadian Limonite catalyst after the ammonia decomposition tests at 750°C in inert atmosphere (c), in the simulated gas with 0% H_2O (b) and in the simulated gas with 15% H_2O (a). There were no Fe-oxide or Fe-carbide diffraction peaks observed in all the samples, but very strong XRD signals of α-Fe species were present in the spent CL samples after the ammonia decomposition tests in either inert atmosphere or the simulating gas with/without H_2O. The crystalline size of the α-Fe was found to increase slightly from 59 nm in inert atmosphere to 62 nm in a simulated gas atmosphere. The addition of 15% H_2O increased the particle size further to 93 nm. This increase in crystalline size of α-Fe may be caused by agglomeration of the Fe particles, promoted by the presence of the simulated gas and H_2O, which might partially account for the lower activity of the catalyst in the simulated gas with H_2O,

as shown earlier in Figure 5-6. Figure 5-11 shows the XRD (Fe K_α) profiles of the spent AL, BL and CL after NH_3 decomposition in the simulated gas with 15% H_2O. Similarly, strong XRD signals from α-Fe species were detected in all the limonite samples. The spent CL sample had the largest α-Fe crystalline size (93 nm), compared with about 78-80 nm for the spent BL and AL catalysts, which may also partially explain why the activity of CL was slightly lower than those of BL and AL (Figure 5-7).

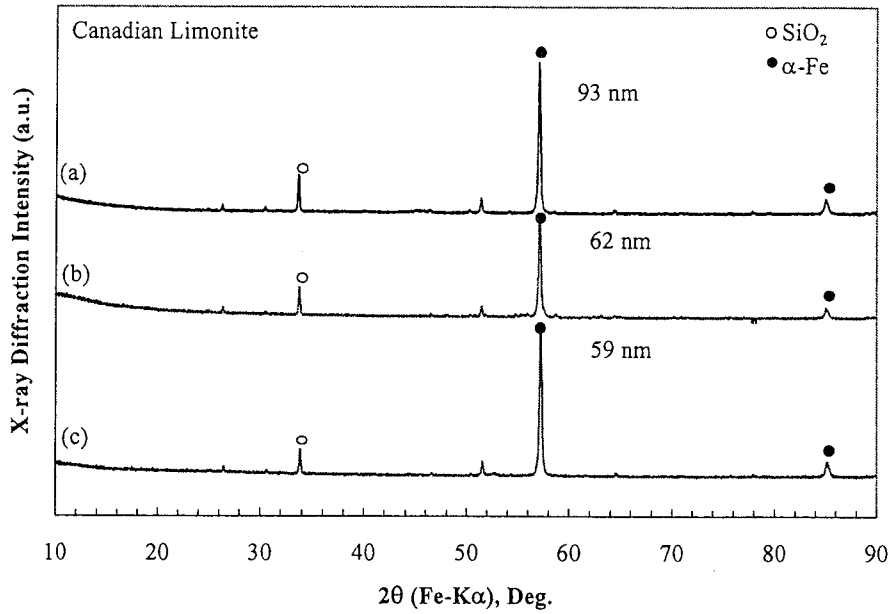

Figure 5-10 XRD Profiles for Canadian limonite after H_2 reduction at 500°C for 2 h and NH_3 decomposition at 750°C in the simulated gas with 15% H_2O (a), in the simulated gas with 0% H_2O (b), and in inert He (c).

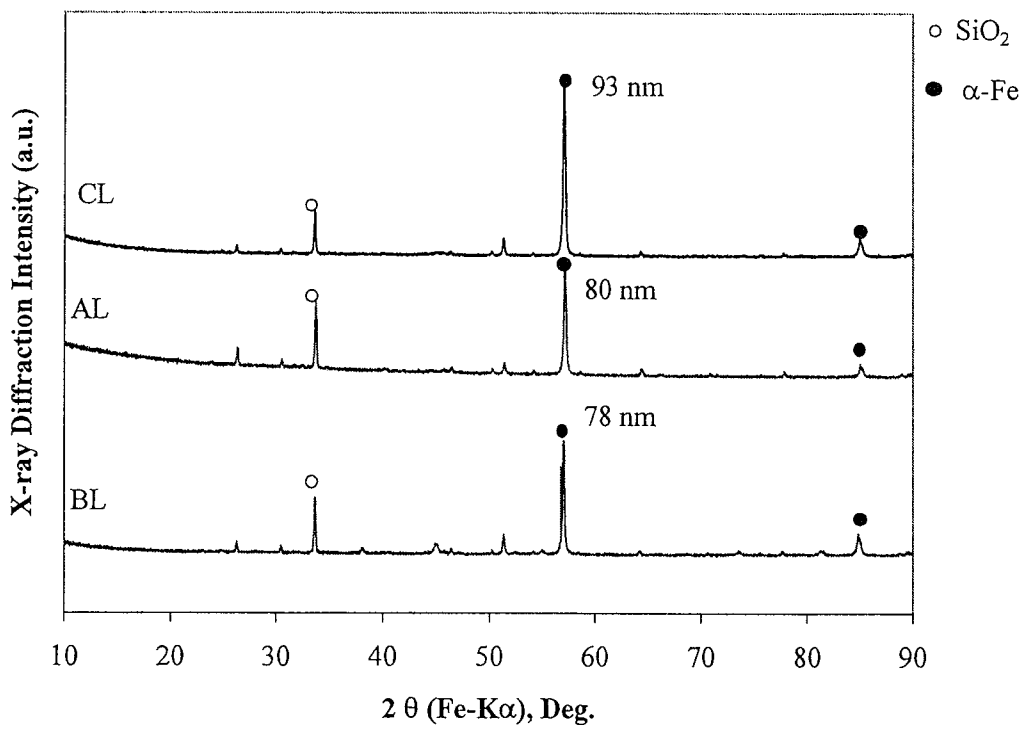

Figure 5-11 XRD Profiles for the CL, AL and BL after H_2 reduction at 500°C for 2 h and NH_3 decomposition at 750°C in the simulated gas with 15% H_2O.

5.3.4.2 Surface Chemical States of the Spent Catalysts

The chemical states on the catalyst surfaces of the spent Ni/AC and Fe/AC catalysts as well as the limonite ores (after the ammonia decomposition at 750°C in the simulated gas with/without H_2O) were analyzed by XPS.

Figure 5-12 illustrates the XPS spectra of Ni 2p and P 2p for the spent catalysts of Ni/AC. The major peak in the Ni 2p spectra occurs at around 853-854 eV which was also observed in the spent Ni/AC after NH_3 decomposition in inert atmospheres (Chapter 4), and this main peak corresponds to nickel phosphide ($Ni_{12}P_5$, Ni_3P, Ni_2P) and metallic Ni, which were also evidenced in the P 2p XPS spectra. The formation of Ni_2P and $Ni_{12}P_5$ in the Ni/AC samples during the ammonia decomposition was also evidenced by XRD, as discussed before (Figure 5-8). Interestingly, new Ni-related species (Ni_2O_3 and NiO and $Ni_3(PO_4)_2$ were observed in the Ni 2p and P 2p XPS spectra from the spent Ni/AC samples after NH_3 decomposition in the simulated gas with 5-15% H_2O. It may suggest that during the experiment the presence of the simulated gas and H_2O could oxidize the surface nickel species to oxidative ones (nickel oxides and phosphate).

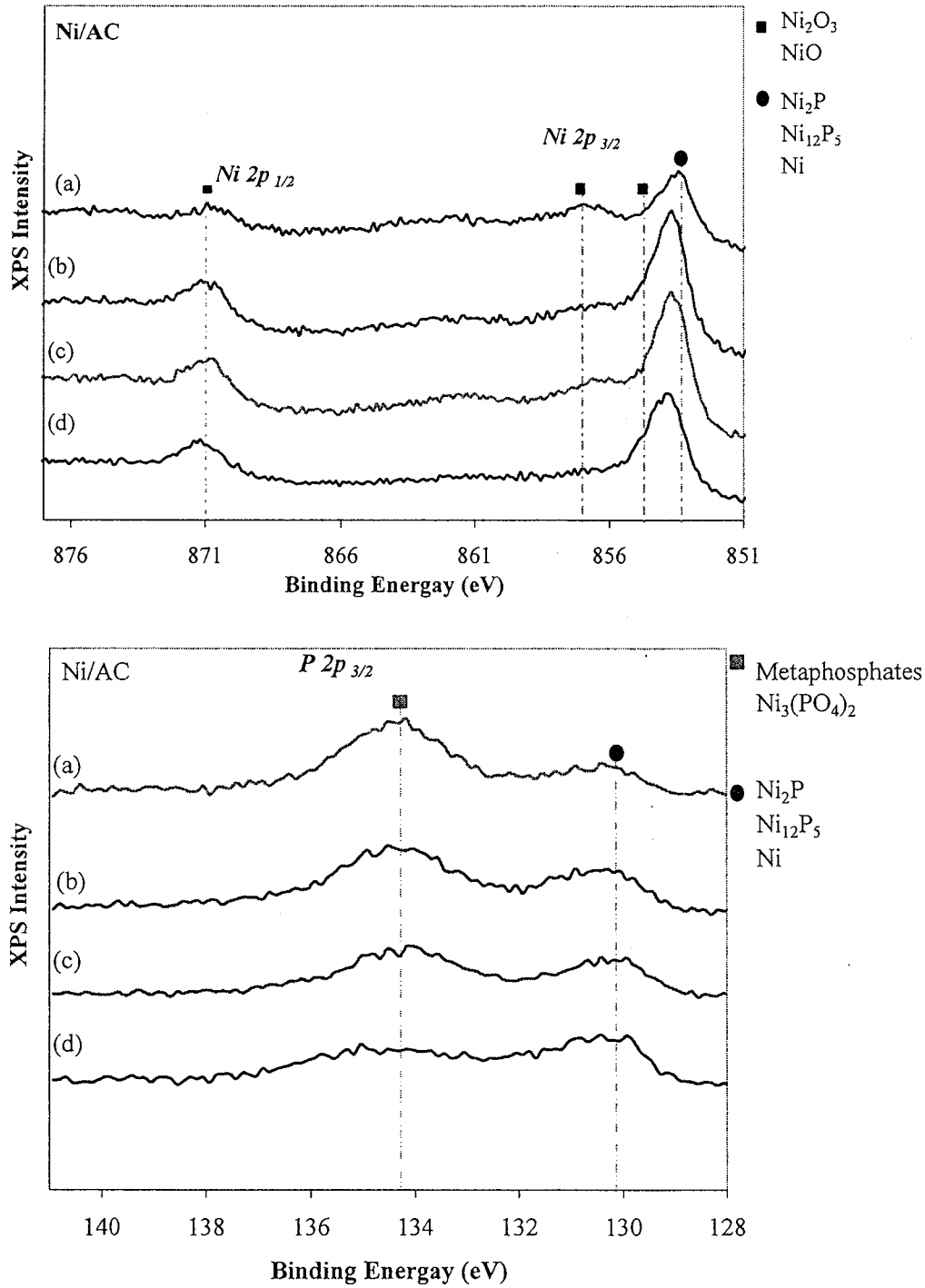

Figure 5-12 Ni 2p and P 2p XPS spectra for Ni/AC catalyst after NH_3 decomposition at 750°C in the simulated gas with 15% H_2O (a), 10% H_2O (b), 5% H_2O (c) and 0% H_2O (d).

Figure 5-13 shows the XPS Fe 2p and P 2p spectra of the spent Fe/AC catalyst after NH_3 decomposition in the simulated gas atmospheres with 0-15% H_2O. The most prominent component of the Fe 2p3/2 peak in each sample at binding energies of approximately 711-712 eV are associated with Fe^{2+} and Fe^{3+}. These peaks may be attributed to a combination of iron oxides species (Fe_2O_3, Fe_3O_4, FeOOH) which have binding energies of around 711 eV, and various Fe phosphate species, such as $FePO_4$, Fe_3PO_7 or $Fe_3(PO_4)_2$, which have binding energies of around 712 eV. The 2p1/2 peak is characteristic of iron oxides, such as Fe_3O_4 and Fe_2O_3. Compared with those for the Fe/AC sample after the experiment with 0% H_2O (Figure 5-13d), all spectra from the catalyst after the experiment with 5-15% H_2O showed increased intensities of the Fe oxides and phosphates species, suggesting oxidation of the Fe species on the surface of the catalysts by the H_2O in the gas stream. The formation of the iron phosphate species, such as $FePO_4$, Metaphosphates and $Fe_3(PO_4)_2$, was also evidenced in the P 2p 3/2 spectra for the spent Fe/AC catalysts after ammonia decomposition in the simulated gas with H_2O, as shown in Figure 5-13. No iron phosphide species (Fe_xP) or nitrides (Fe_xN) were able to be detected by XPS in all the spent Fe/AC samples after the experiments with or without H_2O.

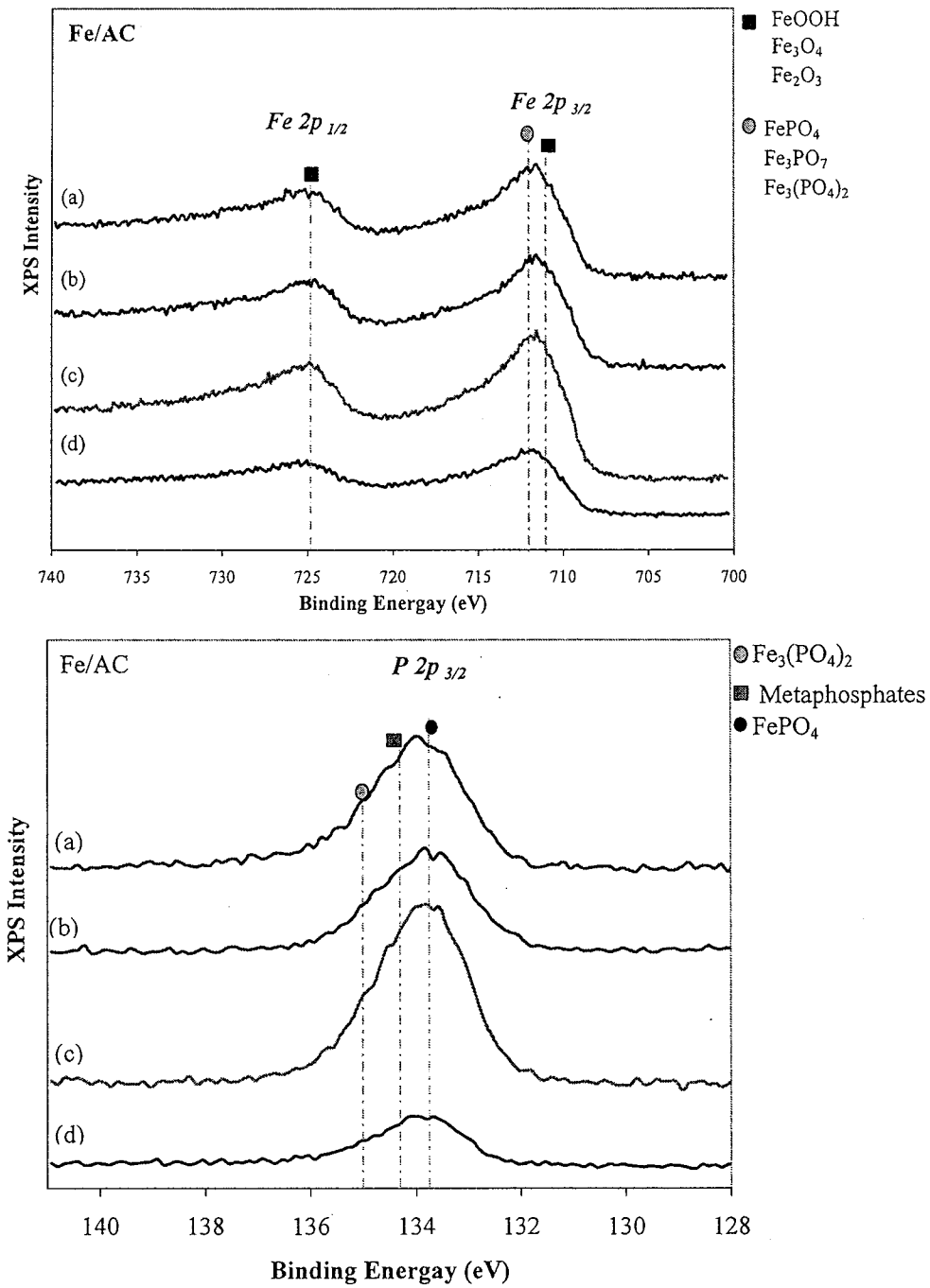

Figure 5-13 Fe 2p and P 2p XPS spectra for Fe/AC catalyst after NH_3 decomposition at 750°C in the simulated gas with 15% H_2O (a), 10% H_2O (b), 5% H_2O (c) and 0% H_2O (d).

Figure 5-14 shows the Fe 2p spectra for the CL, AL and BL catalysts before (labeled as fresh) and after NH_3 decomposition in the simulated gas atmospheres with 15% H_2O (labeled as

spent). The fresh CL, AL and BL ores all have major peaks at approximately 711 eV due to the natural presence of FeOOH, Fe_2O_3 or Fe_3O_4. The minor peak at approximately 719 eV in the fresh catalysts is also attributed to FeOOH. As clearly shown in the figure, compared with those in the fresh catalysts, the peaks at both 719 eV and 711 eV in the spent samples are diminished or weakened in XPS intensities, suggesting reduced Fe-oxides contents on the surface of these limonite samples, which might result from the migration of surface Fe into the bulk sample or from the deposition of carbon on the catalyst surface due to the Boudouard reaction of CO or the decomposition reaction of CH_4. Interestingly, however, no metallic Fe or iron nitrides species (Fe_xN) were able to be detected by XPS in all the spent limonite samples after the ammonia experiments in the simulated gas with or without H_2O.

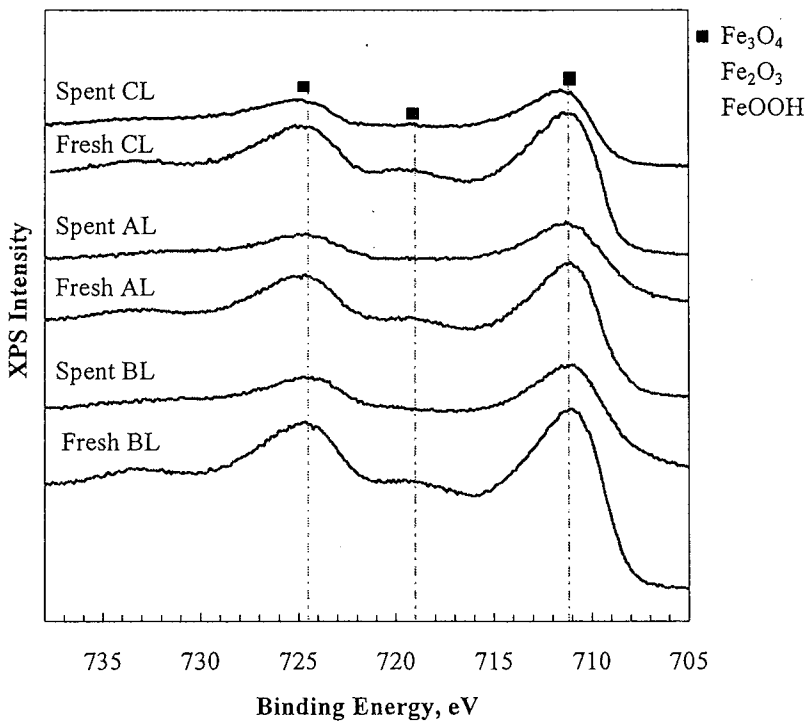

Figure 5-14 Fe 2p XPS spectra for the fresh and spent CL, AL and BL ore samples (spent: after NH_3 decomposition at 750°C in the simulated gas with 15% H_2O).

5.4 Discussion

5.4.1 Catalytic Mechanisms of Ammonia Decomposition over the AC-supported Fe/Ni and Limonite Catalysts

The XRD and XPS for the spent Ni/AC catalysts showed the formation of Ni-phosphides (Ni2P, Ni12P5) during the ammonia decomposition in the simulated gas with or without H_2O (Figures 5-8 and 5-12). These metal phosphides have also been found in the spent Ni/AC catalyst from the NH3 decomposition experiment in inert helium (Chapter 4). This implies that these metal phosphides ($Ni_{12}P_5$ and Ni_2P) might play an important role in the ammonia decomposition reactions over the Ni/AC catalyst. In Chapter 4, it has also been confirmed that commercial compounds of Ni_2P and Fe_2P were active as catalysts for ammonia decomposition in inert atmosphere. In addition, metallic Ni was also likely present on the surface of Ni/AC during the ammonia decomposition reaction as shown by the XPS measurement (Figure 5-12).

As shown and discussed previously in Chapter 4, iron phosphide species (Fe_xP) were detected by XPS on the Fe/AC surface after the ammonia decomposition in the inert gas. The presence of Fe_2P was also revealed by XRD measurement of the spent Fe/AC from the experiment in the simulated gas with 0% H_2O (Figure 5-9d), although iron phosphide species (Fe_xP) were not detected by XPS in all the spent Fe/AC samples after the experiments with or without H_2O (Figure 5-13). Fe_xP species such as Fe_2P was believed to be the critical species responsible for the activity of Fe/AC towards NH_3 decomposition [14-17], in accordance with the mechanism proposed previously in Chapter 4.

Therefore, metal phosphides (such as Ni_2P and Fe_2P) and metallic Ni/Fe might play an important role as the active species in ammonia decomposition, and the following cycle mechanism was proposed. Wherein, the "Me" denotes either "Ni" or "Fe", and the presence of P element was owing to the residual P in the AC support prepared from peat activated by H_3PO_4.

$$2Me + P \rightarrow Me_2P \qquad (1)$$

$$6Me + 3P + 2NH_3(g) \rightarrow 3Me_2P + N_2(g) + 3H_2(g) \quad (2)$$

$$Me_2P + 0.5NH_3(g) + 0.75H_2 \rightarrow 0.5Me_4N + PH_3(g) \quad (3) \text{ or}$$

$$Me_2P + 0.5H_2(g) + 2/3NH_3(g) \rightarrow 2/3Me_3N + PH_3(g) \quad (3)'$$

$$PH_3(g) + 2Me \rightarrow Me_2P + 1.5H_2(g) \quad (4)$$

$$Me_4N \rightarrow 4Me + 0.5N_2(g) \quad (5) \text{ or}$$

$$Me_3N \rightarrow 3Me + 0.5N_2(g) \quad (5)'$$

$$4Me + NH_3(g) \rightarrow Me_4N + 1.5H_2(g) \quad (6) \text{ or}$$

$$3Me + NH_3(g) \rightarrow Me_3N + 1.5H_2(g) \quad (6)'$$

Iron phosphide species (Fe_xP) were not detected by XPS in all the spent Fe/AC samples after the experiments with or without H_2O (Figure 5-13). As such, the presence of the simulated gas and H_2O could enhance oxidization of the surface Fe species to less active iron oxides and phosphates species, and prevent formation of active iron phosphide species (Fe_xP), which were evidenced by both XRD and XPS analyses as discussed in Figures 5-9 and 5-13. This would account for the drastic deactivation of the Fe/AC towards ammonia decomposition by the presence of the simulated gas and H_2O (Figure 5-4), according to the above mechanism. The above mechanism clearly shows that the metal nitrides (Me_4N or Me_3N) were the active intermediate compound responsible for the catalytic decomposition of NH_3 over the Ni/Fe catalysts, as suggested by many previous studies [14-17]. These metal nitride species were however undetectable in all the spent catalysts (Ni/AC, Fe/AC and limonite) by either XRD or XPS techniques. The authors postulate that these metal nitride species might have formed during the reactions, while they were unable to be detected by XRD or XPS, likely due to their low concentrations in the sample, the unstable nature as an intermediate during the reaction, the air oxidation of the surface nitride species prior to the XPS measurements, or because of the shielding effect of the deposited carbon on the surface of the spent catalysts.

5.4.2 Roles of Simulated Gas Species in Ammonia Decomposition over the AC-supported Fe/Ni and Limonite Catalysts

As discussed before in Figures 5-6 and 5-7, all the limonite catalysts tested in this study showed stronger resistance to the simulated gas containing CO, CH_4, H_2, CO_2 and H_2O, which is superior to the AC-supported Fe/Ni catalysts. It has been reported by Tsubouchi et al [15] that the efficiency of an Australian limonite was found to decrease significantly at lower temperatures <700°C in the presence of fuel gas (20%CO/10%H_2), but there was no deactivation of the limonite by the presence of CO and H_2 at higher temperatures (>750°C), which is in a good agreement with the above findings of the current study. For the AC-supported Fe/Ni catalysts, however, there was a drastic decrease in activities of these carbon supported catalysts for the decomposition of NH_3 in the simulated gas (14.9% CO, 2.9% CH_4, 11.2% H_2, 11.2% CO_2) with and without H_2O, as shown in Figures 5-4 and 5-5. The decreased activities may be caused by the carbon deposition resulting from Boudouard reaction of CO or decomposition of CH_4, by some chemical reactions of the simulated gas species and H_2O with the active metal species (e.g., Fe_xP), or by the competing adsorption of CO_2 and H_2O with NH_3 on the catalyst surface, as discussed below in more details.

The results as discussed previously in Figures 5-4 and 5-5 strongly suggest that both Fe/AC and Ni/AC were severely deactivated by the simulated gas (H_2, CO, CO_2, CH_4) and the Fe/AC catalyst could also be deactivated by the presence of H_2O in the gas. Similar observations were reported in the previous study by Xu et al [16], where it was found that the pyrolysis chars from low rank coals, containing inherently present Fe and Ca, could be deactivated by simulated gases containing CO, CO_2 and H_2 due to the formation of carbon and less active metal carbides [16]. Although there are no distinct XRD diffraction lines ascribable to iron carbides or carbon in the spent catalysts of AC supported Fe/Ni catalysts and all the limonite samples as shown previously in Figures 5-8 through 5-11 it is possible these carbon-related species formed were finely dispersed on the catalyst, with crystalline sizes below the detection limit of the XRD (< 5nm). The formation of carbon over the Ni/AC or Fe/AC catalysts in the presence of the simulated gas (H_2, CO, CO_2, CH_4) may proceed via the Boudouard reaction of CO or the decomposition reaction of CH_4, as

shown below.

$$2CO \rightarrow C + CO_2 \quad (7)$$

$$CH_4 \rightarrow C + 2H_2 \quad (8)$$

The carbon deposition via the above two equations might be retarded if there are high concentrations of H_2O, CO_2 and H_2 in the simulated gas, which was the case in present study (with the simulated gas consisting of 1.2% H_2, 11.2% CO_2 and 5-15% H_2O). As a matter of fact, in the experiments with either Ni/AC or Fe/AC in the simulated gas with 0% H_2O, carbon deposition was observed on the walls of the reactor but in the experiments involving H_2O vapor the carbon deposition was not observed, suggesting that the presence of H_2O in the gas could effectively limit the carbon deposition likely via the following C gasification reaction, water gas shift reaction and the steam methane reforming reactions:

$$C + H_2O \rightarrow H_2 + CO \quad (9)$$

$$CO + H_2O \rightarrow CO_2 + 2H_2 \quad (10)$$

$$CH_4 + H_2O \rightarrow CO + 3H_2 \quad (11)$$

The above is consistent with the findings reported by Tsubouchi et al [15], where the addition of 10%CO_2 or 3% H_2O helped to restore the ammonia conversion activity of the Australia limonite at high temperatures. The results in the current study, as discussed previously in Figures 5-4 and 5-5, however suggest that the Fe/AC catalyst could also deactivated by the presence of H_2O in the gas, although the presence of H_2O vapor could prevent the carbon deposition, in accordance to the above reactions (9) through (11). For the Fe-based catalysts (Fe/AC and limonite), the catalyst deactivation by the simulated gas species and H_2O may be related to the oxidization of the active metal species (e.g., Fe_xP) into less or in-active iron species, such as $FePO_4$, Metaphosphates and $Fe_3(PO_4)_2$, as evidenced by both XRD and XPS analysis results discussed before in Figures 5-9 and 5-13. Compared with those for the Fe/AC sample after the experiment with 0% H_2O (Figure 5-13d), all spectra from the catalyst after the experiment with 5-15% H_2O showed increased intensities of the Fe oxides and phosphates species ($FePO_4$, Metaphosphates and $Fe_3(PO_4)_2$), suggesting oxidation of the Fe species on the surface of the catalysts by the H_2O in the gas stream.

The formation of the iron phosphate species might occur through the following reactions, taking $FePO_4$ as an example.

$$4CO(g) + Fe + P = FePO_4 + 4C \quad (12)$$

$$\Delta G = -6.9 \text{ kcal at } 750°C$$

$$Fe_2P + 4H_2O = FePO_4 + Fe + 4H_2\,(g) \quad (13)$$

$$\Delta G = -32.0 \text{ kcal at } 750°C$$

$$5.2Fe + 7.4P + CO(g) + 7.8H_2O = Fe_3C + 2.2FePO_4 + 5.2PH_3\,(g) \quad (14)$$

$$\Delta G = -67.2 \text{ kcal at } 750°C$$

$$Fe_2P + 8H_2O + P = 2FePO_4 + 8H_2\,(g) \quad (15)$$

$$\Delta G = -95.8 \text{ kcal at } 750°C$$

The presence of the simulated gas species CO and H_2O could lead to the conversion of metal phosphide (Fe_2P) as well as metallic Fe into phosphate ($Fe_3(PO_4)_2$) during the experiment, which might deactivate the Fe/AC catalyst for ammonia decomposition, as shown previously in Figure 5-4.

5.5 Conclusions

(1) Fe/AC and Ni/AC catalysts were very active for ammonia decomposition in the inert atmosphere at 750°C, but both AC-supported catalysts were severely deactivated by the simulated gas (14.9% CO, 2.9% CH_4, 11.2% H_2, 11.2% CO_2), and the Fe/AC catalyst was also deactivated by the presence of H_2O in the gas. In the presence of the simulated gas and H_2O, the activities of these two catalysts dropped drastically to as low as <10%.

(2) The three limonite ores, i.e., Canadian limonite (CL) with 42 wt% Fe, Brazilian

limonite (BL) with 57 wt% Fe and Australian limonite (AL) containing 46 wt% Fe, showed high activities towards ammonia conversion to N_2 (>90% at 750°C) in both inert atmosphere or in a simulated gas with 0-15% H_2O.

(3) The metal phosphides (such as Ni_2P and Fe_2P) and metallic Ni/Fe might play an important role as the active species in ammonia decomposition over the Fe- and Ni-based catalysts, and the ammonia decomposition reactions seemed to proceed through a cycle mechanism involving metal nitrides as the intermediates.

(4) The deactivation of the Ni/AC and Fe/AC by the simulated gas and H_2O vapor may be caused by the carbon deposition resulting from Boudouard reaction of CO or decomposition of CH_4, by the oxidation of metal phosphides and metallic metals into less or inactive phosphates in the presence of the simulated gas species CO and H_2O, or by the competing adsorption of CO_2 and H_2O with NH_3 on the catalyst surface.

References

[1] P.L. Spath, D.C. Dayton. Preliminary Screening—Technical and Economic Assessment of Synthesis Gas to Fuels and Chemicals with Emphasis on the Potential for Biomass-Derived Syngas; National Renewable Energy Laboratory: Golden, CO., 2003. http://www.nrel.gov/docs/fy04osti/34929.pdf.

[2] M.P. Aznar, M.A. Caballero, J. Corella, G. Molina, and J.M. Toledo. Hydrogen production by biomass gasification with steam-O_2 mixtures followed by a catalytic steam reformer and a CO-shift system. *Energ. Fuel* 2006; 20: 1305–1309.

[3] T. Bui, R. Loofand, S.C. Bhattacharya, Multi-stage reactor for thermal gasification of wood. *Energy* 1994; 19:397–404.

[4] L.K. Mudge, E.G. Baker, D.H. Mitchell, M.D. Brown. Catalytic steam gasification of biomass for methanol and methane production. *J. Solar Energ. Eng.*, 1985;107 (1): 88–92.

[5]. J. Zhou, S.M. Masutani, D.M. Ishimura, S.Q. Turn, C.M. Kinoshita, Release of fuel-bound nitrogen during biomass gasification. Ind. Eng. Chem. Res. 39 (2000): 626–634.

[6] S.F. Yin, Q.H. Zhang, B.Q. Xu, W.X. Zhu, C.F. Ng, C.T. Au, Investigation on catalysis of COx-free hydrogen generation from ammonia. J. Catal. 224 (2004) 384-396.

[7] X.-K. Li, W.-J. Ji, J. Zhao, S.-J. Wang, C.-T. Au. Ammonia decomposition over Ru and Ni catalysts supported on fumed SiO_2, MCM-41, and SBA-15. *Journal of Catalysis* 2005; 236: 181.

[8] W. Zheng, J. Zhang, Q. Ge, H. Xu, W. Li. Effects of CeO_2 addition on Ni/Al_2O_3 catalysts for the reaction of ammonia decomposition to hydrogen. *Applied Catalysis B: Environmental* 2008; 80:98.

[9] W Mojtahedi, J. Abbasian. Catalytic decomposition of ammonia in a fuel gas at high temperature and pressure. *Fuel* 1995; 74:1698-1703

[10] M.C.J. Bradford, P.E. Fanning, M.A. Vannice. Kinetics of NH_3 Decomposition Over Well Dispersed Ru. J. Catal. 172 (1997) 479-484.

[11] Y. Ozawa et al. Catalytic decomposition of ammonia in simulated coal-derived gas. Chemical

Engineering Science 62 (2007) 5364 – 5367

[12] G.N. Krishnan, W.J. Wood, G.T. Tong, J.G. McCarty, Study of Ammonia Removal in Coal Gasification Processes; Report DOE/MC/23087-2667; SRI International: Menlo Park, CA, 1988.

[13] H. Depner, A. Jess, Kinetics of nickel-catalyzed purification of tarry fuel gases from gasification and pyrolysis of solid fuels. Fuel, 78 (1999) 1369-1377.

[14] N. Tsubouchi, H. Hashimoto, Y. Ohtsuka, High catalytic performance of fine particles of metallic iron formed from limonite in the decomposition of a low concentration of ammonia. *Catalysis Letters* 2005; 105: 203-208.

[15] N. Tsubouchi, H. Hashimoto, Y. Ohtsuka. Catalytic Performance of Limonite in the Decomposition of Ammonia in the Coexistence of Typical Fuel Gas Components Produced in an Air-Blown Coal Gasification Process. *Energy & Fuels* 2007;*21*: 3063–3069

[16] C. Xu, N. Tsubouchi, H. Hashimoto, Y. Ohtsuka Catalytic decomposition of ammonia gas with metal cations present naturally in low rank coals. *Fuel* 2005:84:1957–1967

[17] Y. Ohtsuka, C. Xu, D. Kong, N. Tsubouchi. Decomposition of ammonia with iron and calcium catalysts supported on coal chars. *Fuel* 2004; 83: 685–692

[18] J. Gil, J. Corella, M. P. Aznar, M. A. Caballero. Biomass Gasification in Atmospheric and Bubbling Fluidized Bed: Effect of the Type of Gasifying Agent on the Product Distribution. *Biomass and Bioenergy* 1999; 17: 389-403.

[19] J. Leppalahti, E. Kurkela. Behaviour of nitrogen compounds and tars in fluidized bed air gasification of peat. *Fuel* 1991; 70: 491-497

CHAPTER 6

Catalytic Decomposition of Model Tar Compound using Natural Limonite Ores for Hot Gas Cleanup of Biomass Gasification Gas

ABSTRACT

In this study, three types of natural limonite iron ores from Canada (CL), Brazil (BL), and Australia (AL) were tested as inexpensive catalysts for tar reforming/cracking experiments at 500-900°C using benzene as the model compound (1000-1400 ppm) in the co-existence of H_2O/helium a simulated gas mixture containing $H_2/CH_4/CO/CO_2$ with and without H_2O. The activities of these limonite catalysts of benzene decomposition follow the order of priority of BL > AL > CL. Canadian Limonite (CL) was inactive for steam reforming of benzene, probably resulting from the chemical deactivation of catalyst by the H_2O vapor to prevent formation of the active α-Fe species on the catalyst surface. However, in the presence of the simulated gas consisting without H_2O, the CL showed improved higher activity, of about 65% at 900°C, while its performance was deactivated slightly by the presence of H_2O in the gas. The Brazilian limonite (BL) showed the highest activities in benzene decomposition in the presence of the simulated gas with and without H_2O, owing to its high Fe content with smaller crystalline sizes of active Fe-species in the fresh sample or during the benzene decomposition tests. The use of BL catalyst obtained almost complete conversion of benzene (>95%) at above 650°C in the simulated gas irrespective of whether or not 15 vol% H_2O was present in the reactant gas. The activity of the BL catalyst was unaffected by the addition of H_2O and the presence of H_2O was found to be beneficial to maintain the high activity of BL by preventing formation of carbon deposition. The activation energies were determined as E_a =130 kJ/mol and 120 kJ/mol for benzene decomposition over CL at 750-900°C in the simulated gas with and without 15vol.% H_2O, respectively. The obtained E_a

values are much lower than the literature values for benzene decomposition reactions under similar conditions with other catalysts such as CaO.MgO and Ni/MgO, suggesting the limonite material can be a promising less expensive catalyst for hot gas cleaning of tar in the biomass gasification syngas.

Keywords: Limonite, catalyst, hot gas cleanup, tar, benzene, reforming, cracking

6.1 Introduction

Compared with coal gasification, biomass gasification produces a raw gas that contains a large amount of tar due to the cellulose-based structure. In an air-blown or steam fluidized bed gasifier for biomass gasification, typical tar yield have been reported in the range of 4-62 g/kg and 60-95 g/kg, respectively [1]. The tar in the gas can condense in the downstream pipes and equipment such as heat exchangers causing equipment to corrode and possibly fouling and blocking the lines. This will result in increased costs of the gasification process, and also a decreased efficiency of the gas, therefore removal of the tar is vital for utilizing the biomass gas efficiently. Moreover, tar is highly undesirable because of the detrimental problems associated with end use applications such as engines and turbines. As reported by Milne and Evans [2] less than 50-500 mg/ Nm^3, 50-100 mg/Nm^3 and 5 mg/Nm^3 of tar is recommended for compressors, internal combustion systems, and direct-fired industrial gas turbines, respectively. For methanol synthesis, the content of tar is required to be <0.1 mg/Nm^3 [3].

Tar reduction can be achieved within the gasifier itself or downstream from the gasifier. Tar conversion or prevention within the gasifier is known as a primary method, and may involve reactor design, parameter optimization, or catalyst beds [4]. In secondary methods, which take place downstream, the tar can be either removed physically or converted chemically through hot gas cleanup. Physical processes include wet scrubbing and filtration. Wet scrubbing is an effective gas conditioning method that condenses tars out of the product gas, but requires that the gas be

cooled. If the end applications are high temperature processes, extra energy will be required to cool and reheat the syngas stream, thus decreasing the overall energy efficiency [5]. Another disadvantage of this method is that the tar is only transferred from a gas phase to a condensed phase, producing a secondary waste stream that needs to be treated. By converting the tar to gas via hot gas cleanup, the gas does not need to be cooled and reheated for its final use, and by converting the tar to desired gas components, the chemical energy of the gas product is retained and treatment of the secondary waste streams is avoided [6].

The most common secondary methods used for tar reduction are thermal or catalytic cracking [7]. Thermal cracking requires high temperatures (>1100°C) in order to obtain a high conversion, this can be achieved by adding oxygen to the process, but these high temperatures can lead to soot formation in the product stream [8]. Catalysts can be used to lower the required reaction temperatures and increase the conversion of tar to gas (CO and H_2). Catalytic tar cracking/reforming is achieved by passing the raw gas produced from the biomass gasification process, over a solid catalyst in a fixed bed reactor, having the same or similar temperature and pressure as the gasifier [8]. The biomass-derived tars consist of a wide range of condensable hydrocarbon and oxygen containing hydrocarbons compounds, which are mostly aromatics and complex poly-aromatic hydrocarbons (PAHs) [9]. The complex composition of biomass tars makes it difficult to understand the reaction mechanisms. In the fluidized-bed air-blown gasification biomass, the major components could be benzene, toluene, phenol, naphthalene and their derivatives [10], and benzene and derivatives were found to be the dominant components in the tar derived from steam/O_2 gasification of sawdust [11], Therefore, model tar compounds such as benzene, toluene, phenol, and naphthalene were often used in the research [9-12], and the thermal reactivity was found to follow the order of toluene > naphthalene > benzene [2]. Tars can be catalytically reformed/cracked at a high temperature via steam/dry reforming or cracking/hydro-cracking to form gas products of carbon monoxide and hydrogen and methane, as presented in the following equations:

Steam reforming: $C_nH_m + nH_2O \leftrightarrow nCO + (n + \frac{m}{2})H_2$

Dry reforming: $C_nH_m + nCO_2 \leftrightarrow 2nCO + (\frac{m}{2})H_2$

Cracking: $C_nH_m \leftrightarrow nC + (\frac{m}{2})H_2$

Hydro-cracking: $C_nH_m + (\frac{4n-m}{2})H_2 \leftrightarrow nCH_4$

The most common catalysts tested for tar cracking/reforming are calcined dolomite, CaO or MgO [13-16], Supported transition and nobel metals (primarily Ni and Ni/Mo) [17-19], carbon-based catalysts (such as biuomass chars) [20]. Inexpensive Fe-containing materials (olivine and iron oxide) have all been used in studies for steam reforming/cracking of benzene and toluene model tar compounds [21, 22]. Except for being used as the ammonia decomposition catalysts [23], natural limonite iron ores, mainly composed of goethite (α-FeOOH), have not been investigated so far for hot gas tar reduction.

The main objective of this study is to test limonite ores, the inexpensive and readily available locally natural materials, for tar reforming/cracking experiments using benzene as the model compound. In this study, three types of limonite iron ores originated from Canada (CL), Brazil (BL), and Australia (AL) were tested for reforming/cracking of benzene in the co-existence of a simulated gas mixture containing $H_2/CH_4/CO/CO_2$ or an inner gas (helium) with and without H_2O.

6.2 Experimental

6.2.1 Materials

Three natural limonite ore samples from Canada (CL), Brazil (BL) and Australia (AL) were used as catalysts in this study. The as received ores were crushed and sieved into particles of 0.15-0.25 mm (CL), 0.25-0.5 (BL) and 0.15-0.25 mm (AL) and 0.5-1.0 mm (AL). The compositions of the inorganic matter (e.g., Fe content) of the limonite samples were determined using ICP-AES (Inductively Coupled Plasma – Atomic Emission Spectrometer). The fresh limonite ores were also tested by N_2 isothermal adsorption (77K) to determine the BET surface

areas. The crystalline structures of the fresh limonite samples were analyzed using XRD. The physical and chemical properties of the fresh limonite samples are summarized in Table 6-1 below. As shown in the Table, the Brazilian limonite (BL) has the largest BET surface area of 90 m^2/g and the highest Fe content (57 wt%), while the Canadian limonite (CL) has the smallest BET surface area of only 11 m^2/g and the lowest Fe content (42 wt%). The major crystalline species detected by XRD in all fresh limonite samples were goethite (α-FeOOH), as shown in Figure 5-2. The crystalline size of the α-FeOOH, estimated by the Debye-Scherrer equation, was the largest for the CL sample (> 100 nm), followed by AL (25 nm) and BL (16 nm). Besides the goethite (α-FeOOH), α-Fe_2O_3 peaks of a medium intensity, and quartz (SiO_2) signals (of low-to-medium intensity) were detected in all the fresh limonite samples.

Prior to the tar decomposition studies, all catalyst samples were reduced using 200 ml/min of H_2 for 2 h at 500°C, and the XRD analytical results are also presented in Table 6-1. As clearly shown in the Table, metallic iron species (α-Fe) were the dominant Fe-species in all the limonite samples after H_2 reduction. In the H_2-reduced samples, the AL had the smallest particles of α-Fe (22 nm), followed by BL (24 nm) and CL (33 nm). In the reduced AL catalyst, very weak signals of α-FeOOH were detected.

Table 6-1 Physical and chemical properties of the fresh limonite ores and the limonite samples after H_2 reduction at 500°C for 2 h

Limonite ore	Fresh sample			Sample after H_2 reduction		
	AL	BL	CL	AL	BL	CL
Total Fe content (wt%)	46	57	42	n.a.[d]	n.a.	n.a.
Crystalline species [a]	α-FeOOH(s) α-Fe_2O_3 (m) SiO_2 (s)	α-FeOOH(s) α-Fe_2O_3 (m) SiO_2 (w)	A-FeOOH (s) α-Fe_2O_3 (m) SiO_2 (m)	α-Fe (s) α-FeOOH(w) SiO_2 (s)	α-Fe (s) SiO_2 (w)	α-Fe (s) SiO_2 (m)
Size of α-FeOOH or α-Fe (nm) [b]	25	**16**	>100	22	24	33
Surface Area (m^2/g) [c]	40	**90**	11	n.a.[d]	n.a.	n.a.

[a]Identified by XRD: w (weak); m (medium); s (strong) in intensity;
[b] Average crystalline size estimated by Debye-Scherrer method;
[c] Determined by BET method using N_2 isothermal adsorption (77K);
[d] Not analyzed.

6.2.2 Experimental Apparatus and Methods

The benzene or toluene reforming/cracking experiments were carried out with a flow-type, vertical tubular quartz reactor (8 mm ID) placed in an electric furnace, as schematically illustrated in Figure 6-1. The catalyst bed within the reactor was 8 or 16 mm in height for all the tests with benzene and was held in place with fine grade quartz wool. Prior to the decomposition studies, the samples were reduced using 200 ml/min of H_2 for 2 h at 500°C. After H_2 reduction, the reactor was heated to the desired temperature with a He flow of 180 ml/min at 15°C/min. As the temperature reached the desired reaction temperature, the helium flow was replaced with the following two types of reactant gas stream:

(a) 300 ml/min of 1000ppm benzene diluted in helium (balance) with 15 vol% H_2O, corresponding to a GHSV of 45000 h^{-1};

(b) 110 ml/min of 1360ppm benzene diluted in a simulated gas (9.6 vol%H_2, 13 vol%CO, 9.5 vol%CO_2, 2.5 vol%CH_4) and helium (balance) with or without 15 vol% H_2O, corresponding to a GHSV of 8200 h^{-1}.

The H_2O vapor content of the gas was controlled by the temperature of the water vaporizer and the helium flow through the vaporizer, which was kept at a set temperature of 85 °C for the studies using 15% H_2O. A high speed micro GC-TCD was used to determine the CO and CH_4 formed and the un-reacted benzene (C_6H_6) and toluene (C_7H_8). A moisture trap, located after the reactor, consisting of calcium carbonate, was used to prevent H_2O from entering the GC.

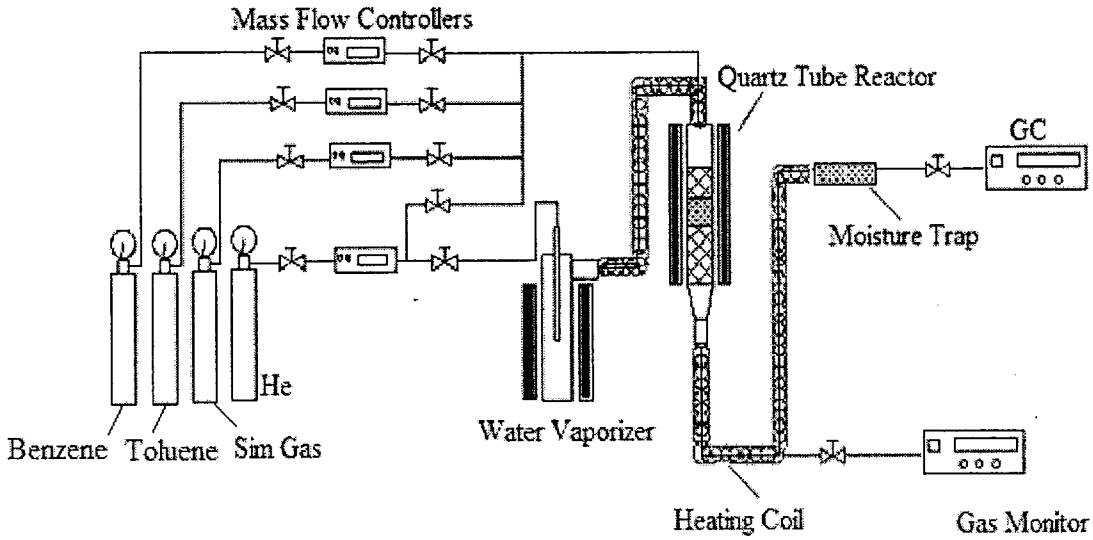

Figure 6-1 Experimental Apparatus for tar reforming/cracking

6.2.3 Characterization of the Catalysts

X-ray diffraction (XRD) with Fe Kα radiation (Shimadzu XRD-6000, 30 mA and 40 kV) was used to characterize the crystalline structures of all the catalysts before (fresh catalysts) and after (spent catalysts) the ammonia decomposition tests. The average crystalline size of the particles (L_c) was calculated using the Debye-Scherrer equation. X-ray photoelectron spectroscopy (XPS) was employed to characterize the chemical composition on the surfaces of the catalysts before and decomposition experiments (for benzene decompositions). The XPS experiments were performed on a ULVAC PHI 5600 spectrometer with an Al anode for K_α X-ray source operating at 200W. Charging effects were corrected by adjusting the binding energy of C_{1s} peak of carbon contamination to 284.6 eV.

6.3 Results and Discussion

6.3.1 Steam Reforming of Benzene using Canadian Limonite

Catalytic steam reforming of 1000ppm benzene was carried out using CL in a 15%H_2O/He atmosphere at reaction temperatures of 650°C, 750°C, and 850°C and a space velocity of 45000 h^{-1}. The results are shown in Figure 6-2. Very low conversion of benzene at approximately 10% was observed for all the temperatures. Very low formation of CO at a rate of < 3μmol/min/g-catalyst was observed during the experiments, and no CH_4 formation was observed during the tests for all temperatures, suggesting the following steam reforming reaction of benzene over the CL catalyst:

$$C_6H_6 + 6H_2O \rightarrow 6CO + 9H_2 \qquad \Delta H°_{298} = 704.9 \text{ kJ/mol} \qquad (6\text{-}1)$$

$$C_6H_6 + 12H_2O \rightarrow 6CO_2 + 15H_2 \qquad \Delta H°_{298} = 457.7 \text{ kJ/mol} \qquad (6\text{-}2)$$

$$C_6H_6 + 7H_2O \rightarrow CO_2 + 10H_2 + 5CO \qquad \Delta H°_{298} = 663.7 \text{ kJ/mol} \qquad (6\text{-}3)$$

The standard Gibbs free energy changes for the above reactions were calculated as negative values at temperatures >400°C.

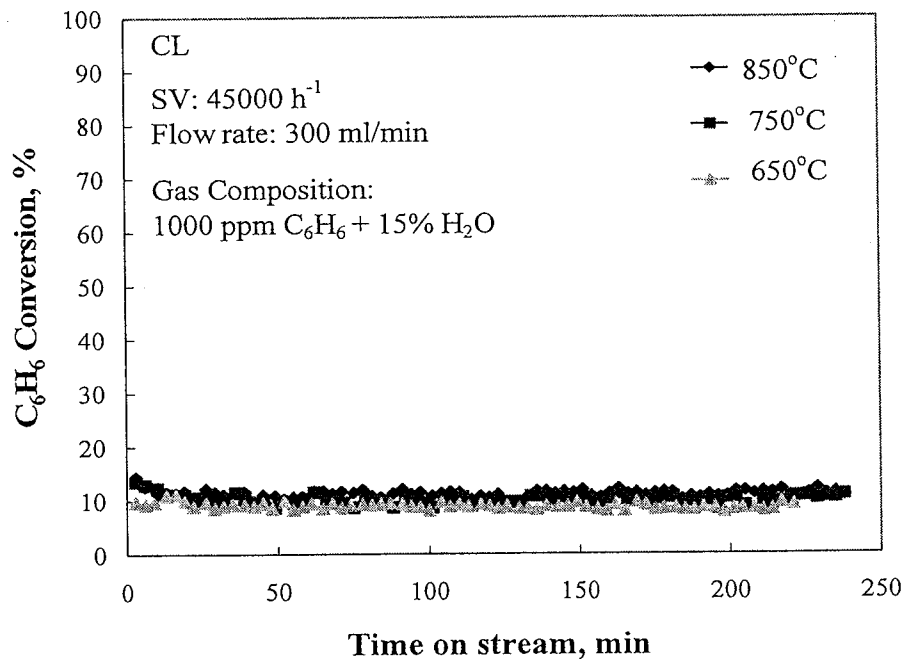

Figure 6-2 Benzene conversion over Canadian limonite (CL) in steam reforming. (1000ppm benzene in a 15%H_2O/He atmosphere at 650°C, 750°C, and 850°C and an SV of 45000 h^{-1})

The low activity of the Canadian Limonite (CL) for steam reforming of benzene might result from the competing adsorption of the H_2O vapor and benzene vapor, or the chemical deactivation of catalyst by the H_2O vapor. To determine why the Canadian Limonite was inactive in the steam reforming of benzene, XRD analysis of the spent catalyst samples was carried out. Figure 6-3 below shows the XRD (Fe K_α) profiles for the spent Canadian limonite catalyst after reforming experiments of 1000ppm benzene in a 15% H_2O/He atmosphere at temperatures of 650, 750 and 850°C. The spent catalysts showed strong diffraction peaks for Fe_3O_4, all having crystalline sizes greater than >100 nm, and in the sample that was tested at 750°C there were weak diffraction peaks attributed to FeO. There were no signals of α-Fe species, commonly regarded as the active species for a Fe-based catalyst [21-23]. The low activity of the CL sample towards steam reforming of benzene was thus likely due to the oxidation of the active α-Fe species to form inactive Fe_3O_4 and FeO species.

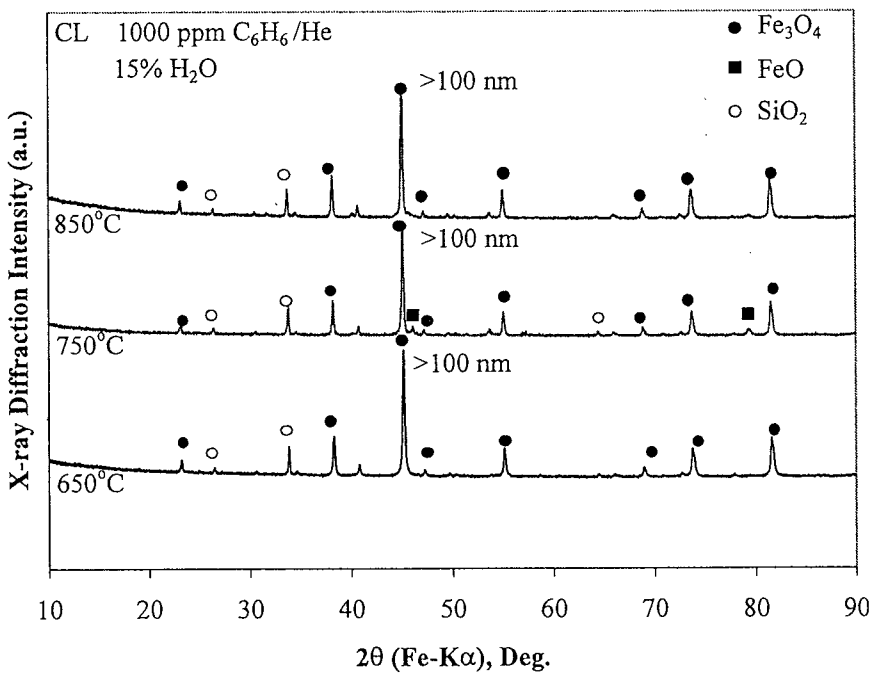

Figure 6-3 XRD profiles of Canadian limonite samples after steam reforming of benzene at 650, 750 and 850°C, in a 15%H_2O/He atmosphere.

6.3.2 Decomposition of Benzene using Canadian Limonite in Simulated Gas with and without H_2O

As discussed above, the CL was inactive in steam reforming of benzene, or benzene was highly resistant to steam reforming even at a high temperature (850°C) with the presence of an iron-based catalyst. In fact, this low conversion is no surprise since the thermal reactivity of benzene was found to be the lowest compared with other tar model compounds (toluene, naphthalene) [2]. The Canadian limonite (CL) was further tested for decomposition of benzene in a stream of simulated gas consisting of 1360 ppm benzene, 9.6 vol%H_2, 13 vol%CO, 9.5 vol%CO_2, 2.5 vol%CH_4 and helium (balance) with or without 15 vol% H_2O. In these tests, the reactant gas flow rate was reduced to from 300 ml/min to 110 ml/min and the catalyst bed height was increased to 16 mm, hence decreasing the GHSV to 8200 h^{-1}. The results from these tests are presented in Figure 6-4.

Figure 6-4a shows the performance of the Canadian limonite in conversion of benzene, at steady state, in the simulated gas with and without 15 vol% H_2O at a temperature ranging from 750 to 900°C. A blank run was carried out at 900°C using quartz wool as the bed material to determine the possibility of thermal cracking reactions of benzene in the simulated gas with 0% H_2O, and approximately 0% benzene conversion was obtained for 4h on the stream, suggesting the extremely low thermal reactivity of benzene as discussed in the previous section. As clearly shown in the figure, in the presence of the simulated gas, CL was fairly active for decomposition of benzene and its activity increased with increasing temperature irrespective of whether the H_2O was present or not. For example, in the simulated gas without H_2O, the benzene conversion increased significantly from about 15% at 750°C to approximately 65% at 900 °C. In the simulated gas with 15 vol% H_2O, benzene conversion increased from 10% at 750 °C to approximately 50% at 900°C. As demonstrated before in the previous section, the CL was inactive for steam reforming reaction of benzene (reactions 6-1 through 6-3). Therefore, the activity of CL for benzene decomposition in the simulated gas was mainly due to dry reforming of benzene by CO_2.

Decomposition of benzene in the simulated gas (containing H_2, CO, CO_2 and CH_4) and H_2O may involve the following reactions:

Steam reforming:

$$C_6H_6 + 6H_2O \rightarrow 6CO + 9H_2 \quad \Delta H°_{298} = 704.9 \text{ kJ/mol} \qquad (6\text{-}1)$$

Dry reforming:

$$C_6H_6 + 6CO_2 \rightarrow 12CO + 3H_2 \quad \Delta H°_{298} = 952.1 \text{ kJ/mol} \qquad (6\text{-}4)$$

Hydro-cracking:

$$C_6H_6 + 9H_2 \rightarrow 6CH_4 \quad \Delta H°_{298} = -529.9 \text{ kJ/mol} \qquad (6\text{-}5)$$

In addition to the decomposition reactions of benzene, the following reactions might also occur in the simulated gas atmospheres at a high temperature:

Steam methane reforming:

$$CH_4 + H_2O \leftrightarrow CO + 3H_2 \quad \Delta H°_{298} = 205.8 \text{ kJ/mol} \qquad (6\text{-}6)$$

Dry reforming of methane:

$$CH_4 + CO_2 \leftrightarrow 2CO + 2H_2 \quad \Delta H°_{298} = 247 \text{ kJ/mol} \qquad (6\text{-}7)$$

Water-gas shift:

$$CO + H_2O \leftrightarrow CO_2 + H_2 \quad \Delta H°_{298} = -41.2 \text{ kJ/mol} \qquad (6\text{-}8)$$

From the above reaction schemes, CO is a main reforming product from benzene and CH_4 (through reactions 6-1, 6-4, 6-6 and 6-7). The net formation rate of CO during the experiments using CL was determined by the difference of the outlet CO concentration to that of the inlet concentration, and is shown in Figure 6-4b. Since the above listed reforming/cracking reactions are endothermic, the formation of CO increased with increasing temperature as expected irrespective of whether the H_2O is present or not. In the presence of H_2O, however, CO can also be consumed by a reactant (via the water gas shift reaction 6-8). At a low temperature when the endothermic reforming/cracking reactions are less favorable and slow, the CO in the simulated gas may be consumed via the waster gas shift reaction (exothermic reaction favorable at lower temperatures), leading to net consumption of CO. This was actually evidenced by the negative value of the net CO formation (–20 μmol/min/g-cat) at 700°C in the simulated gas with 15 vol% H_2O, as shown in Figure 6-4b. During the experiments, the concentration of methane was found to decrease,

suggesting net consumption of CH_4 mainly via steam/dry reforming of methane (reactions 6-6 and 6-7), both endothermic and thermodynamically favorable at a higher temperature. As shown in Figure 6-4c, there is a general trend showing that CH_4 consumption rate increases with increasing temperature. At temperature <800°C, however, the consumption of methane decreased as the temperature increased, probably due to the generation of CH_4 via the exothermic hydro-cracking reaction (reaction 6-5).

As discussed above, the activity of CL for benzene decomposition in the simulated gas was mainly due to dry reforming of benzene. The results shown in Figure 6-4 also clearly indicate that the addition of 15% H_2O to the simulated gas caused a significant decrease in benzene conversion, as well as appreciable reduction in both CO net formation and CH_4 consumption. These results strongly suggest that the presence of H_2O deactivated the catalyst towards dry reforming of benzene (via reaction 6-4). The XRD profiles of the spent CL samples after the benzene decomposition tests at 750-900°C in the simulated gas without and with 15 vol% H_2O are illustrated in Figure 6-5. In the spent CL samples after the reactions in the simulated gas without or with H_2O, strong diffraction peaks of α-Fe species were observed. In the simulated gas without H_2O, as shown in Figure 6-5a, the average crystalline size of α-Fe increased from 89 nm at 750°C to >100 nm at temperatures greater than 850°C. The addition of H_2O was found to increase the crystalline sizes of α-Fe to >100nm at all the temperatures even at 750°C. The increased crystalline sizes of the α-Fe particles with the addition of H_2O may have caused a decrease in the activity of the CL samples, as revealed from Figure 6-4.

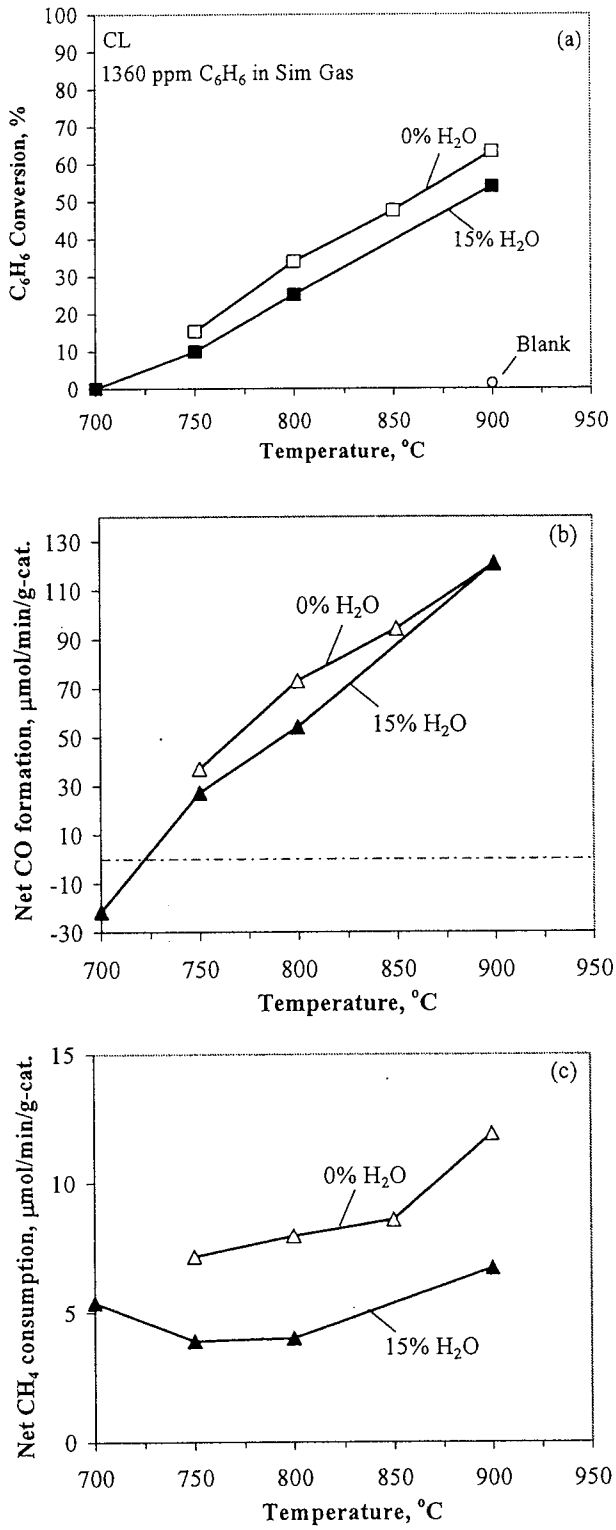

Figure 6-4 Benzene conversion (a), net CO formation (b) and net CH_4 consumption (c) with Canadian limonite in the simulated gas with and without H_2O at temperatures from 750 to 900°C (GHSV = 8200 h^{-1}).

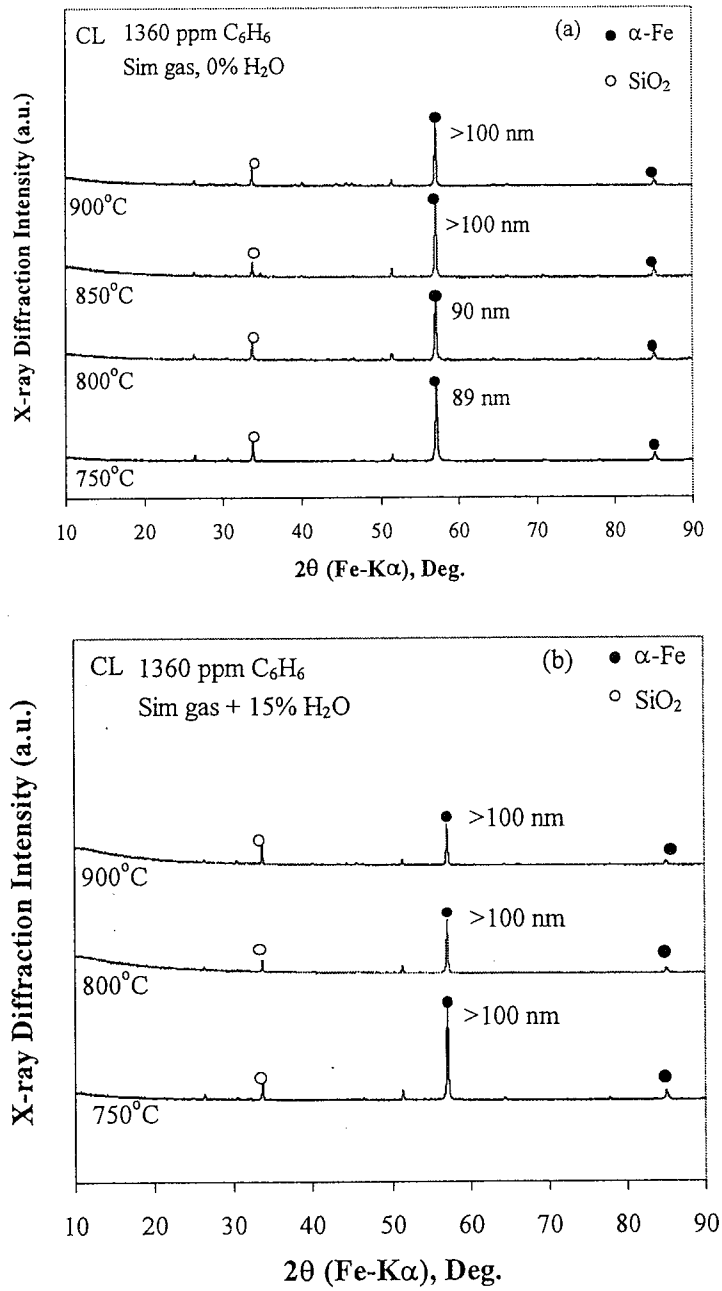

Figure 6-5 XRD profiles of the spent CL samples after the benzene decomposition tests at 750-900°C in the simulated gas without (a) and with 15 vol% H_2O (b).

6.3.3 Performance of Australian and Brazilian Limonites in Benzene Decomposition in Simulated Gas with H_2O

As shown earlier in Figure 6-4, the CL showed no activity for benzene decomposition in the simulated gas with the presence of 15 vol% H_2O at 700°C. The physical and chemical properties of the fresh limonite samples, as summarized in Table 6-1, indicate that the other two types of limonite ores might be more active for benzene decomposition as they both have a larger BET surface area, a higher Fe content and a smaller crystalline size of the α-FeOOH than CL. The activities of AL, BL and CL ores for benzene decomposition were comparatively examined in the simulated gas (containing 9.6%H_2, 13%CO, 9.5%CO_2 and 2.5% CH_4) with 15% H_2O at 700°C. Figure 6-6 shows benzene conversion (a), net CO formation (b) and net CH_4 consumption (c) vs. time on stream over AL, BL and CL in the simulated gas with 15 vol% H_2O at 700°C at a GHSV of 8200 h^{-1}. Compared with 0% benzene conversion with CL, and about 10% conversion with AL, the benzene conversion over the BL catalyst was strikingly high, approaching 100% conversion initially although with a slight decrease in activity with increasing time on stream. The high benzene conversion for BL was also accompanied by the large net CO formation rate and CH_4 consumption rate, as shown in Figures 6-6b and 6-6c, suggesting that the dry reforming reactions of benzene and methane (reactions 6-4 and 6-7) were dominant in the reaction system, as discussed before. For the Australian limonite, two different particle sizes were tested, (0.5-1.0mm) and (0.15-0.25mm). There was not a significant difference between these particle sizes with respect to benzene conversion or net CO formation or CH_4 consumption, which means that the reaction is not pore diffusion controlled.

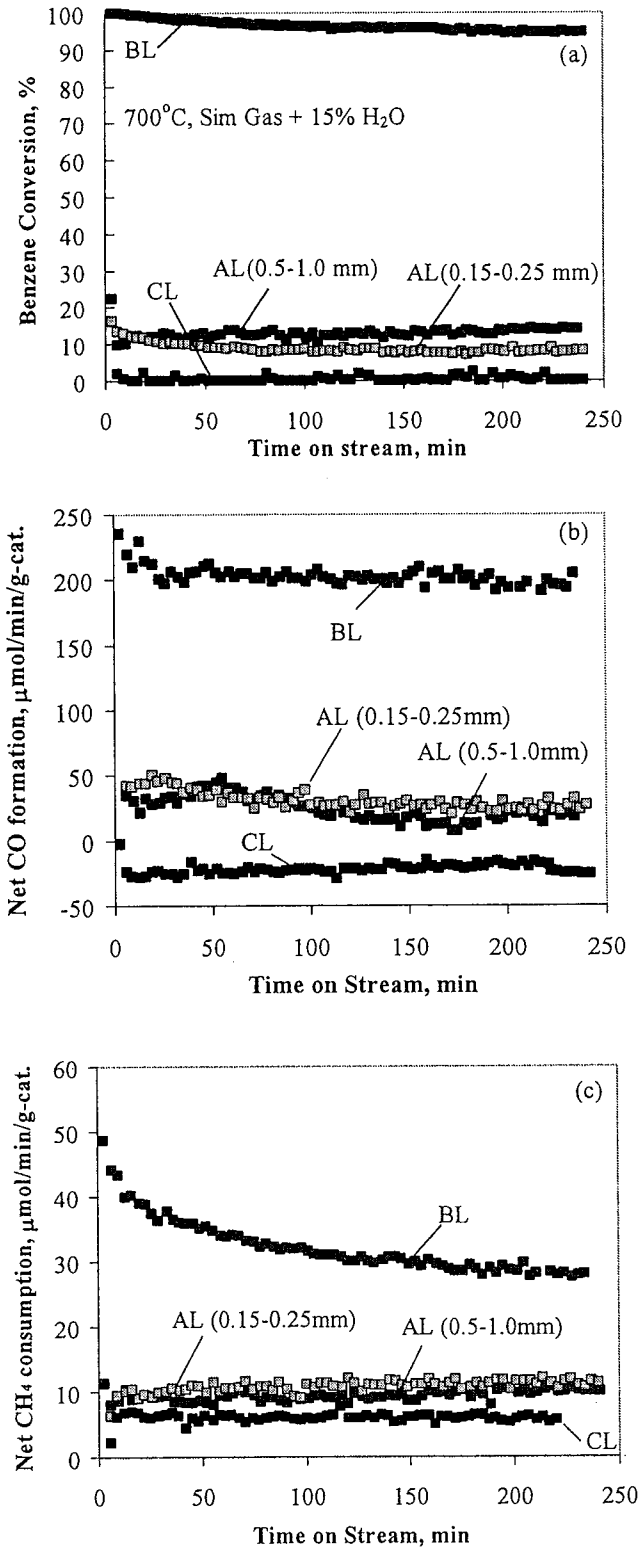

Figure 6-6 Benzene conversion (a), net CO formation (b) and net CH_4 consumption (c) vs. time on stream over AL, BL and CL catalyst in the simulated gas with 15 vol% H_2O at 700°C (GHSV = 8200 h^{-1})

Figure 6-7 shows the XRD (Fe-Kα) profiles for the spent limonite ore catalysts after decomposition of 1360 ppm benzene in the simulated gas with 15% H_2O. In all samples, strong α-Fe diffraction peaks were detected. The spent BL (the most active sample) had the smallest α-Fe crystalline size of 41nm, whereas the CL, the least active sample, had the largest α-Fe crystalline size of >100nm. Very similar crystalline size of α-Fe species (42 and 45 nm) were observed in the spent samples of AL in two different sizes.

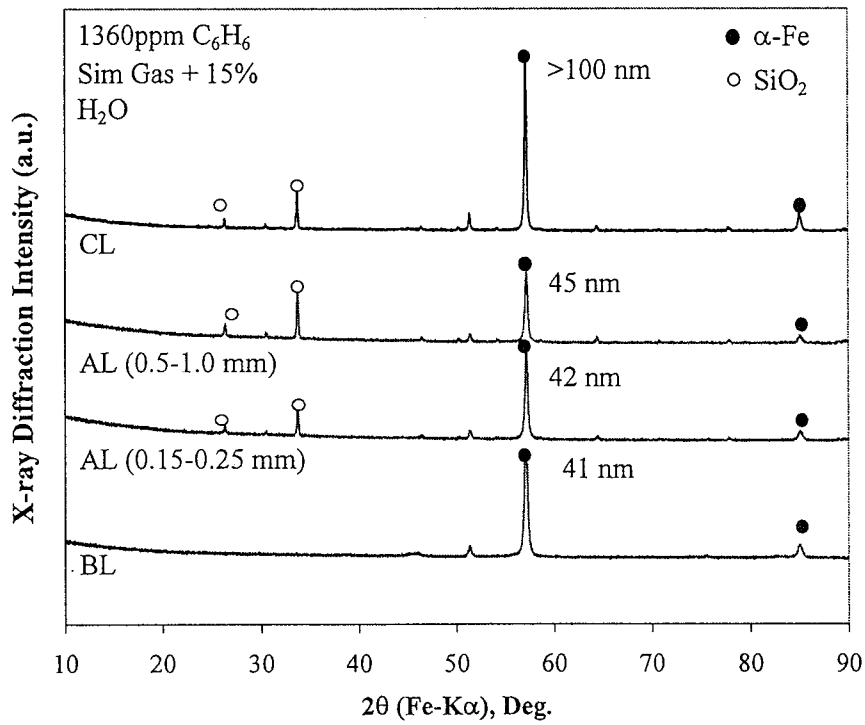

Figure 6-7 XRD profiles of the spent CL, AL and BL samples after decomposition of 1360 ppm benzene at 700°C in the simulated gas with 15% H_2O

Figure 6-8 shows the Fe 2p spectra for the CL and BL catalysts before (labeled as fresh) and after benzene decomposition in the simulated gas atmospheres with 15% H_2O (labeled as spent). The fresh CL and BL ores all have major peaks at approximately 711 eV due to the presence of FeOOH, Fe_2O_3 or Fe_3O_4. The minor peak at approximately 719 eV in the fresh catalysts is also attributed to FeOOH. In the spent catalyst of CL these peak intensities at 711 and 719 eV are

remarkably weakened possibly due to the deposition of carbon on the surface of the catalysts from CO (through the reverse Boudouard reaction) or cracking of CH_4. Moreover, on the surface of the spent CL, metallic α-Fe species were not detected likely due to the oxidation by CO_2 and H_2O. These might account for its low activity of CL for benzene decomposition (Figure 6-6a). The spent BL sample had broader peaks compared with the fresh samples, which may be due to the formation of α-Fe species which has a binding energy approximately 708.6±2.1 eV. In the spent BL catalyst, a small peak at around 707 eV may be attributed to metallic α-Fe, which was not observed in the other two spent limonite catalysts. The presence of metallic Fe species on the BL's surface might explain the much higher activities of the BL for benzene decomposition in the simulated gas.

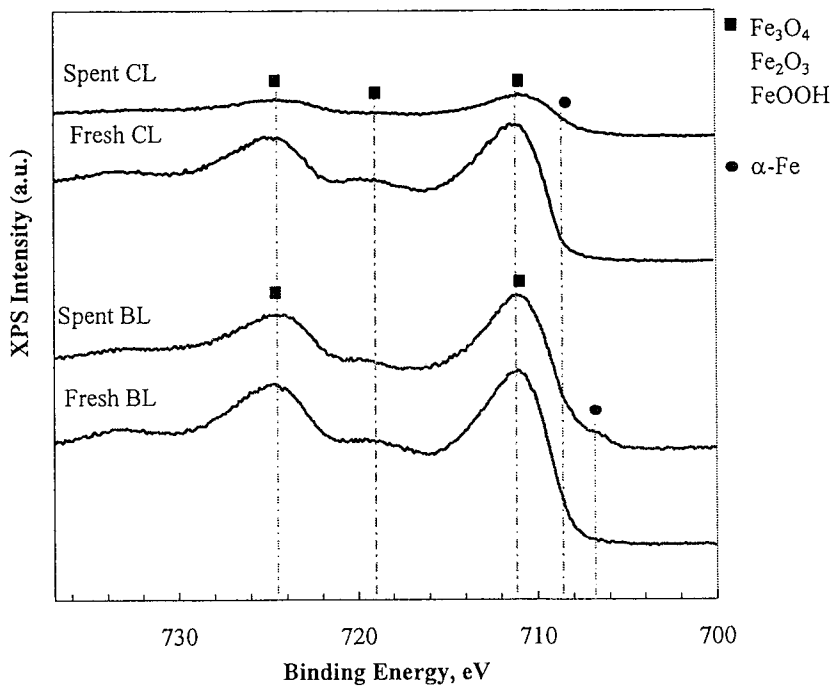

Figure 6-8 Fe 2p XPS spectra for the fresh and spent BL and CL catalysts after benzene decomposition at 700°C in the simulated gas with 15% H_2O .

Because the Brazilian limonite showed a very high activity for the decomposition of 1360ppm benzene in the simulating gas containing 15% H_2O (Figure 6-6), the BL sample was subjected to further testing at different temperatures from 500-900°C, with and without H_2O, and the steady state results are summarized in Table 6-2. At all temperatures ≥ 650°C, the BL was

highly active for benzene decomposition, leading to almost complete conversion of benzene (>95%) in the simulated gas irrespective of whether or not 15 vol% H_2O was present in the inlet gas. The high benzene conversions were accompanied with high net formation rates of CO and large CH_4 consumption, as given in Table 6-2. The BL catalyzed the benzene decomposition reaction even at 500°C with the presence of 15 vol% H_2O, while the conversion dropped rapidly from its highest value (~61%) after about 3h on stream, probably due to the significant carbon deposition on the catalyst surface. As temperature increased to 650 or 700°C, the activity of BL climbed drastically to as high as 95%. Carbon deposition was found to be severe during the reactions of benzene in the simulated gas with or without H_2O at a low reaction temperature < 700°C, likely resulting from the following reactions:

Carbon formation: $C_6H_6 \rightarrow 6C + 3H_2$ (6-9)

Reverse boudouard: $2CO \leftrightarrow CO_2 + C$ (6-10)

Table 6-2 Benzene conversion and net formation rates of CO and CH_4 in decomposition of benzene catalyzed by BL in the simulated gas with and without H_2O at varying temperatures (at steady state).

Temperature (°C)	H_2O (vol%)	Benzene Conv. (%)	Net formation rate[a] (μmol/min/g-catalyst)	
			CO	CH_4
500	15	61[b]	–302.9	67.6
650	15	95	156.5	-15.8
700	15	95	206.6	-29.1
900	15	96	366.3	-91.3
700	0	94	220.9	-29.4
900	0	96	380.9	-76.8

[a] Negative value means consumption of CO or CH_4;

[b] The conversion dropped rapidly after about 3 h on stream;

Unlike in the benzene decomposition experiments with CL and AL where the presence of H_2O could deactivate the catalyst (Figures 6-2, 6-4 and 6-6), the addition of H_2O was found to be

beneficial to maintain the high activity of BL by preventing formation of carbon deposition likely through the steam gasification reactions of carbon as shown below:

Steam gasification: $H_2O + C \leftrightarrow CO + H_2$ (6-11)

$2H_2O + C \leftrightarrow CO_2 + 2H_2$ (6-12)

The prevention of carbon deposition by the addition of steam may be evidenced by the reduced carbon deposition in the reactor after the benzene decomposition reactions at 700°C in the simulated as with 15 vol% H_2O, as illustrated in Figure 6-9.

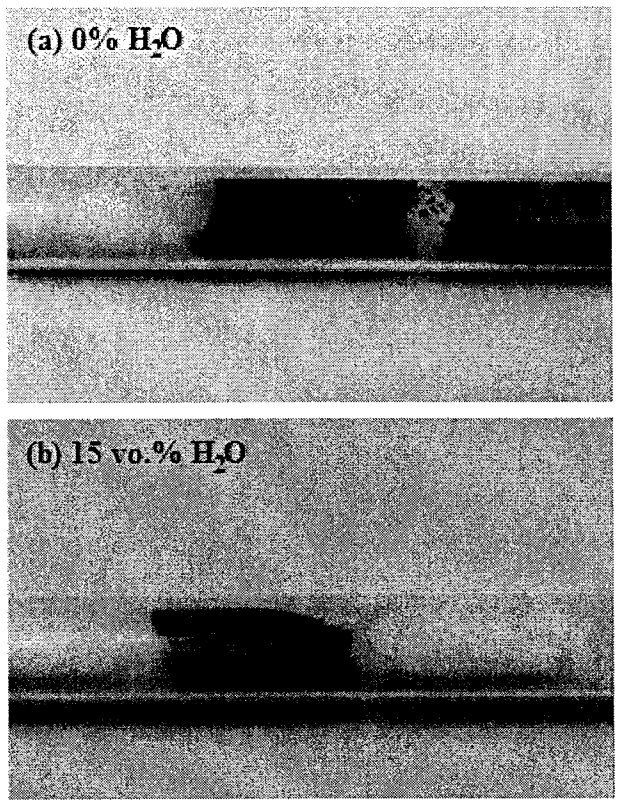

Figure 6-9 Carbon deposition in the reactor with BL catalyst after decomposition of benzene at 700°C in the simulated gas without (a) and with 15 vol.% H_2O (b).

The catalyst states of the BL after benzene decompositions under different conditions were observed and analyzed by XRD, and the results are summarized in Table 6-3. For the BL after the low-temperature tests at 500°C and 650°C, weak signals of iron oxides such as Fe_3O_4 and FeO

were observed. After the decomposition tests in the simulated gas at above 700°C with or without H_2O, α-Fe was the dominant species on the spent BL samples, which may account for its high activity towards benzene decomposition as evidenced in Table 6-2. Cementite (Fe_3C) was observed on the spent BL sample for the tests where severe carbon deposition was observed, as reported previously in the limonite-catalyzed ammonia decomposition in syngas [23]. As expected, the average crystalline size of α-Fe increased with increasing temperature, and the results in Table 6-3 also reveals that the presence of H_2O (although being beneficial for reducing carbon deposition) slightly increased the crystalline size of α-Fe on the limonite sample. For example, it increased from 30 nm without H_2O to 46 nm with 15 vol.% H_2O under the same operating conditions (e.g., 1360 ppm benzene in the simulated gas at 700°C).

Table 6-3 Catalyst states of the BL after benzene decomposition under different conditions

Temperature	500	650	700	900	700	900
H_2O (vol.%)	15	15	15	15	0	0
Carbon deposition	heavy	slight	none	none	Heavy	No
Crystalline Fe species[a]	α-Fe? (w)	α-Fe (s)	α-Fe (s)	α-Fe (s)	α-Fe (s)	α-Fe (s)
	Fe_3O_4 (w)	FeO (w)			Fe_3C (w)	
	Fe_3C (w)	Fe_3O_4 (w)				
Size of α-Fe[b] (nm)	-	27	46	92	30	89

[a] Identified by XRD; w, weak; m, medium; s, strong in intensity;

[b] Average crystalline size estimated by the Debye-Scherrer method.

To summarize, the above results show that the Brazilian limonite, as a less expensive Fe-based catalyst, provided excellent performance in tar decomposition for hot gas cleaning of syngas from biomass gasification, compared with the literature results using other low cost Fe-based materials [7, 24].

6.3.4 Benzene Decomposition Kinetics with Limonite Catalysts in Simulated Gas

Dry and steam reforming of benzene involves a number of primary and secondary reactions, as discussed before. To simplify the kinetic studies, a lumped reaction for dry and steam reforming reaction may be used below:

$$C_6H_6 + CO_2 (+ H_2O) \rightarrow CO + H_2 + CH_4 + C + \ldots \quad (6\text{-}13)$$

As the inlet concentrations of CO_2 (9.5 vol%) and/or H_2O (15 vol%) were in a great excess compared with that of benzene (1360 ppm), the reaction rate of benzene decomposition can be modeled as the following equation assuming the above reaction is an irreversible and first-order reaction with respect to all the reactants:

$$-r_B = kC_B \quad (6\text{-}14)$$

where $-r_B$ is the consumption rate of benzene, k is the lumped specific reaction rate constant and C_B is the initial concentration of benzene in the reactor. Assuming constant volumetric flow rate for the process, the conversion (X) of benzene was defined as:

$$X = \frac{(C_{B,in} - C_{B,out})}{C_{B,in}} \quad (6\text{-}15)$$

where $C_{B,in}$ is the inlet concentration of the model tar c and $C_{B,out}$ is the outlet model tar compound concentration. The residence time (τ) in the catalyst bed was defined as:

$$\tau = \frac{V_{cat}}{Q_{in}} \quad (6\text{-}16)$$

where V_{cat} is the volume of the catalyst bed, mL, and Q_{in} is the inlet volumetric flow rate of the reactant gas, mL/s.

For the first-order constant volumetric flow rate PFR reactor, the rate constant can thsu be estimated from the following equation:

$$k = \frac{-\ln(1 - X)}{\tau} \quad (6\text{-}17)$$

Here, τ =0.44 s in the present experiments (GHSV = 8200 h^{-1}). From the Arrhenius' Law, the temperature dependency of k can be represented as

$$\ln k = \frac{-E_a}{RT} + \ln C \quad (6\text{-}18)$$

Plotting ln$k$ and 1/T would yield a linear relationship, and the activation energy of the catalytic benzene decomposition reaction (E_a) can be obtained from the slope of the curve. The benzene conversion results using Canadian limonite at various temperatures of 750-900°C in the simulated gas containing 1360 ppm C_6H_6, 9.5 vol% CO_2, 13 vol% CO, 9.6 vol% H_2, 2.5 vol% CH_4 and He balance with or without 15 vol.% H_2O, as presented in Figure 6-4, were used to estimate the activation energy. Figure 6-10 shows the Arrehnius plot for the CL in benzene decomposition studies in the simulated gas with and without steam. From this plot, the activation energies were determined as E_a =130 kJ/mol and 120 kJ/mol for benzene decomposition over CL in the simulated gas with and without 15vol.% H_2O, respectively. The obtained Ea values are much lower than the literature values, e.g., E_a = 197 kJ/mol for stream reforming benzene with CaO.MgO catalysts at 750-900°C [25] and E_a = 177 kJ/mol for decomposition of benzene in a simulated gas consisting of H_2, CO, CO_2 and H_2S with Ni/MgO catalysts at 750-900°C [26]. The lower E_a values determined for CL suggests that the limonite material can be a more active catalyst for benzene decomposition. No data were available for the estimation of E_a for the AL catalyst, and the data for BL (as shown in Table 6-2) were not suitable for the calculation of E_a either due to the high benzene conversions at temperatures ≥ 650°C. Future work is needed to determine E_a for AL and BL.

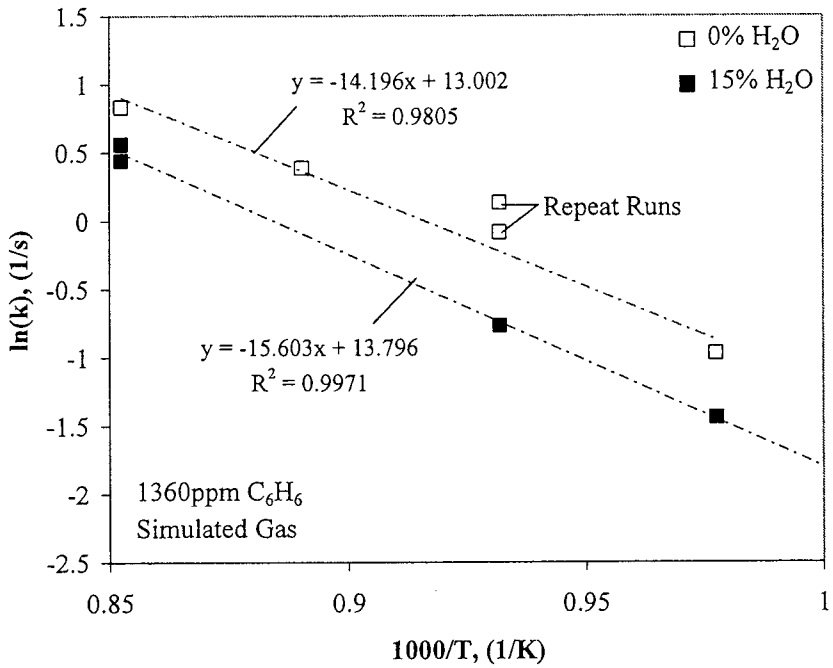

Figure 6-10 Arrhenius plot for calculation of activation energy for the benzene decomposition reaction over CL at temperatures of 750-900°C in the simulated gas with and without H_2O.

6.4 Conclusions

(1) Canadian Limonite (CL) showed very low activity for steam reforming of benzene, due to the competing adsorption of the H_2O vapor and benzene vapor, and the chemical deactivation of catalyst by the H_2O vapor to prevent formation of α-Fe species on the catalyst surface. However, in the presence of a simulated gas consisting of 1360 ppm C_6H_6, 9.5 vol% CO_2, 13 vol% CO, 9.6 vol% H_2, 2.5 vol% CH_4 without H_2O, the CL showed improved higher activity, of about 65% at 900°C, while its performance was deactivated slightly by the presence of 15 vol.% H_2O in the gas.

(2) The Brazilian limonite (BL) showed the highest activities in benzene decomposition in the presence of a simulated gas containing $H_2/CO/CO_2/CH_4$ with and without H_2O, owing to its high Fe content with smaller crystalline sizes of α-FeOOH in the fresh sample and α-Fe

species formed in the H_2-reduced sample or during the benzene decomposition tests. The use of BL catalyst obtained almost complete conversion of benzene (>95%) at above 650°C in the simulated gas irrespective of whether or not 15 vol% H_2O was present in the reactant gas.

(3) The activity of the BL catalyst was unaffected by the addition of H_2O and in fact the presence of H_2O was found to be beneficial to maintain the high activity of BL by preventing formation of carbon deposition through the steam gasification reactions of carbon.

(4) The activation energies were determined as E_a =130 kJ/mol and 120 kJ/mol for benzene decomposition over CL at 750-900°C in the simulated gas with and without 15vol.% H_2O, respectively. The obtained E_a values are much lower than the literature values for benzene decomposition reactions under similar conditions with other catalysts such as CaO.MgO and Ni/MgO, suggesting the limonite material can be an inexpensive but active catalyst for benzene decomposition and hot gas cleanup of biomass gasification gas.

References

[1]. J. Gil, J. Corella, M. P. Aznar, M. A. Caballero. Biomass Gasification in Atmospheric and Bubbling Fluidized Bed: Effect of the Type of Gasifying Agent on the Product Distribution. *Biomass and Bioenergy* 1999; 17: 389-403.

[2]. T.A. Milne, R.J. Evans. Biomass gasification "tars": their nature, formation and conversion. NREL, Golden, CO, USA, Report no. NREL/TP-570-25357, 1998.

[3]. L.K. Mudge, E.G. Baker, D.H. Mitchell, M.D. Brown. Catalytic steam gasification of biomass for methanol and methane production. *J. Solar Energ. Eng.*, 1985;107 (1): 88–92.

[4]. L. Devi, K. J. Ptasinski, F. J. J. G. Janssen. A review of the primary measures for tar elimination in biomass gasification processes. *Biomass and Bioenergy* 2003; 24: 125-140.

[5]. T. Wang, J. Chang, P. Lv. Novel Catalyst for Cracking of Biomass Tar. Energy & Fuels, 19 (2005) 22-27

[6]. D. Dayton.A Review of the Literature on Catalytic Biomass Tar Destruction. National Renewable Energy Laboratory. NREL/TP-510-32815 (2002)

[7]. T Nordgreen, T. Liliedahl, K. Sjostrom. Metallic iron as a tar breakdown catalyst related to atmospheric, fluidised bed gasification of biomass. *Fuel* 2006; 85: 689-694

[8]. E. Kurkela,. Air Gasification of Peat, Wood and Brown Coal in a Pressurized Fluidized-Bed Reactor. I. Carbon Conversion, Gas Yields and Tar Formation. *Fuel Processing Technology* 1992 31: 1-21.

[9]. L. Devi, K.J. Ptasinski, F. J. Janssen .Pretreated olivine as tar removal catalyst for biomass gasifiers: investigation using naphthalene as model biomass tar. *Fuel Processing Technology* 2005; 86: 6: 707-730

[10]. J. Leppalahti, E. Kurkela. Behaviour of nitrogen compounds and tars in fluidized bed air gasification of peat. *Fuel* 1991; 70: 491-497.

[11]. C.M. Kinoshita, Y. Wang, J. Zhou. Tar formation under different biomass gasification conditions. J. Anal. Appl. Pyrolysis 1994; 29: 169–181.

[12]. D. Swierczynski, S. Libs, C. Courson, A. Kiennemann. Steam reforming of tar from a biomass gasification process over Ni/olivine catalyst using toluene as a model compound. *Applied Catalysis B: Environmental* 2007;74: 211–222

[13]. J.Corella, M.P. Aznar, J. Gill, M.A. Caballero. Biomass Gasification in Fluidized Bed: Where To Locate the Dolomite To Improve Gasification. *Energy Fuels* 1999; 13: (6) 1122-1127.

[14]. P. Simell, E. Kurkela, P. Ståhlberg, J. Hepola. Catalytic hot gas cleaning of gasification gas. *Catalysis Today* 1996; 27:55-62.

[15]. S. Rapagnà, N. Jand, P. U. Foscolo. Catalytic gasification of biomass to produce hydrogen rich gas. *International Journal of Hydrogen Energy* 1998; 23 (7): 551-557

[16]. G. Hu, S. Xu, S. Li, C. Xiao, S. Liu. Steam gasification of apricot stones with olivine and dolomite as downstream catalysts. *Fuel Processing Technology* 2006; 87: 375-382.

[17]. B. Dou, J. Gao, X. Sha, S. Wook Baek. Catalytic cracking of tar component from high temperature fuel gas. *Applied Thermal Engineering* 2003; 23: 2229-2239

[18]. P. A. Simell, J.B.-son Bredenberg. Catalytic purification of tarry fuel gas. *Fuel*, 1990; 69:

1219-1225

[19]. D. Sutton, B. Kelleher, A. Doyle, J. R. H Ross. Investigastion of nickel supported catalysts for the upgrading of brown peat derived gasification products. *Bioresource Technology 2001*; 80: 111-116.

[20]. Z. Abu El-Rub,E.A. Bramer, G. Brem. Experimental comparison of biomass chars with other catalysts for tar reduction. *Fuel* 2008; 87: 2243–2252

[21]. D. Swierczynski, S. Libs, C. Courson, A. Kiennemann. Steam reforming of tar from a biomass gasification process over Ni/olivine catalyst using toluene as a model compound. *Applied Catalysis B: Environmental* 2007;74:211-222.

[22]. S. Tamhankar, K. Tsuchiya, J. Riggs. Catalytic cracking of benzene on iron oxide-silica: catalyst activity and reaction mechanism. Applied Catalysis 1995;16:103-121.

[23]. N. Tsubouchi, H. Hashimoto, Y. Ohtsuka. Catalytic Performance of Limonite in the Decomposition of Ammonia in the Coexistence of Typical Fuel Gas Components Produced in an Air-Blown Coal Gasification Process. *Energy & Fuels* 2007;*21*: 3063–3069.

[24]. P.A. Simell, J. Leppälahti, J.B. Bredenberg. Catalytic purification of tarry fuel gas with carbonate rocks and ferrous materials. Fuel 1992; 71: 211-218.

[25]. P.A. Simell, E.K. Hirvensalo, V.T. Smolander, A.O.I. Krause. Steam reforming of gasification gas tar over dolomite with benzene as a model compound. Ind. Eng. Chem. Res. 1999); 38: 1250–1257.

[26]. L. Ma, H.Verelst, G.V. Baron. Integrated high temperature gas cleaning: tar removal in biomass gasification with a catalytic filter. Catal.Today 2005; 105: 729–734.

CHAPTER 7

Conclusions and Recommended Future Work

7.1. Summary and Conclusions

The research presented in this thesis involves the catalytic hot gas cleanup of biomass gasification gas with the use of Canadian peat-derived activated carbon catalysts as well as natural limonite ore catalysts. Production of activated carbon for the support of Ni and Fe was carried out with a chemical activation method using H_3PO_4. The activated carbon supported Ni/Fe catalysts, and three natural limonite ores (from Australia, Brazil and Canada) were used in NH_3 decomposition studies in inert atmosphere and in a simulated gas containing CO, H_2, CO_2, CH_4 and H_2O, typical of air-blown biomass gasification. These experiments were carried out in a vertical quartz tube reactor at 750°C, and a space velocity of 45000h^{-1}. Catalytic tar cracking was carried out, using benzene as a model tar compound, with the Australian, Brazilian and Canadian limonite catalysts in simulated gas atmospheres with and without H_2O, at temperatures between 500-900°C with a space velocity of mainly 8200 h^{-1}. All fresh and spent catalysts were characterized to determine changes in physical and chemical states before and after decomposition studies to help determine why the catalysts may have been active or inactive and possible reaction mechanisms related to NH_3 and C_6H_6 decomposition. The detailed conclusions for each part of this work are summarized as follows.

Part-I: Production and Characterization of Activated Carbons from a Canadian Peat

(1) Activated carbons (ACs) with surface areas of 675-888 m^2/g and total pore volumes of 0.36-0.51 cm^3/g were produced from a Canadian peat by chemical activation using either H_3PO_4 or $ZnCl_2$ as the activation agent, followed by carbonization at 450°C.

(2) $ZnCl_2$ proved to be very effective for developing microporous structures in the ACs, leading

to greater surface areas, while H_3PO_4 is highly active in developing the mesopores, leading to much higher mesopore volumes and average pore size.

(3) Demineralization of the peat precursor before the chemical activation greatly improved the surface area and pore structure of the resulting ACs. The demineralization greatly promoted the development of the micropores during the activation process irrespective of which activation agent was used, and it could also significantly improve the mesoporous structure when $ZnCl_2$ was used.

(4) The AC derived from the demineralised peat activated by $ZnCl_2$ attained the highest BET surface area of 888 m^2/g.

Part-II: Novel Carbon-based Ni/Fe Catalysts Derived from Peat for Hot Gas Ammonia Decomposition.

(1) Novel Ni/Fe catalysts were prepared using a mesoporous activated carbon (AC) support derived from a Canadian peat by H_3PO_4 activation. The newly developed catalysts proved to be highly active for ammonia decomposition. The conversion of 2000 ppm NH_3 diluted in helium over the Fe catalyst reached as high as 90% at 750°C and at the space velocity of 45000 h^{-1}, compared with only about 15% with the AC alone. The new catalyst of Fe/AC was also much more active than the Fe catalyst supported on a commercial AC reported previously.

(2) The newly developed Fe/Ni catalysts showed superior performance for hot gas ammonia decomposition with respect to their resistance to catalyst deactivation. Both catalysts remained active as the reaction time increased up to 10 hours without showing a sign of deactivation. The remarkable increases in mesoporous surface area and pore volume in the Ni/AC and Fe/AC catalysts during the ammonia decomposition might contribute to the high activities and stability of these catalysts in ammonia decomposition.

(3) Highly dispersed nanoparticles of metallic Ni or Fe were present in the fresh catalysts of Ni/AC and Fe/AC, evidenced by XRD. The XRD and XPS measurements of the spent

catalysts showed the presence of nickel/iron phosphides ($Ni_{12}P_5$, Ni_3P, and Ni_2P, Fe_2P) and nitride (Fe_xN). It was proposed that the fine dispersion of the metal phosphides and nitrides in-situ formed in these catalysts (Ni/AC and Fe/AC) during the ammonia decomposition process were responsible for the high activities of these catalysts through a cycle mechanism.

Part-III: Hot Gas Decomposition of NH_3 in Simulated Gas over Carbon-based Ni/Fe Catalysts and Natural Limonite Ores

(1) Fe/AC and Ni/AC catalysts were very active for ammonia decomposition in the inert atmosphere at 750°C, but both AC-supported catalysts could be severely deactivated by the simulated gas (14.9% CO, 2.9% CH_4, 11.2% H_2, 11.2% CO_2), and the Fe/AC catalyst was also deactivated by the presence of H_2O in the gas. In the presence of the simulated gas and H_2O, the activities of these two catalysts dropped drastically to as low as <10%.

(2) The three limonite ores, i.e., Canadian limonite (CL) with 42 wt% Fe, Brazilian limonite (BL) with 57 wt% Fe and Australian limonite (AL) containing 46 wt% Fe, showed high activities towards ammonia conversion to N_2 (>90% at 750°C) in both inert atmosphere or in a simulated gas with 0-15% H_2O.

(3) The metal phosphides (such as Ni_2P and Fe_2P) and metallic Ni/Fe might play an important role as the active species in ammonia decomposition over the Fe- and Ni-based catalysts, and the ammonia decomposition reactions seemed to proceed through a cycle mechanism involving metal nitrides as the intermediates.

(4) The deactivation of the Ni/AC and Fe/AC by the simulated gas and H_2O vapor may be caused by the carbon deposition resulting from Boudouard reaction of CO or decomposition of CH_4, by the oxidation of metal phosphides and metallic metals into less or inactive phosphates in the presence of the simulated gas species CO and H_2O, or by the competing adsorption of CO_2 and H_2O with NH_3 on the catalyst surface.

Part-IV: Catalytic Decomposition of Model Tar Compound using Natural Limonite Ores for Hot Gas Cleanup of Biomass Gasification Gas

(1) Canadian Limonite (CL) showed very low activity towards steam reforming of benzene, due to the competing adsorption of the H_2O vapor and benzene vapor, and the chemical deactivation of catalyst by the H_2O vapor to prevent formation of α-Fe species on the catalyst surface. However, in the presence of a simulated gas consisting of 1360 ppm C_6H_6, 9.5 vol% CO_2, 13 vol% CO, 9.6 vol% H_2, 2.5 vol% CH_4 without H_2O, the CL showed improved higher activity, of about 65% at 900°C, while its performance was deactivated slightly by the presence of 15 vol.% H_2O in the gas.

(2) The Brazilian limonite (BL) showed the highest activities in benzene decomposition in the presence of a simulated gas containing $H_2/CO/CO_2/CH_4$ with and without H_2O, owing to its high Fe content with smaller crystalline sizes of α-FeOOH in the fresh sample and α-Fe species formed in the H_2-reduced sample or during the benzene decomposition tests. The use of BL catalyst obtained almost complete conversion of benzene (>95%) at above 650°C in the simulated gas irrespective of whether or not 15 vol% H_2O was present in the reactant gas.

(3) The activity of the BL catalyst was unaffected by the addition of H_2O and in fact the presence of H_2O was found to be beneficial to maintain the high activity of BL by preventing formation of carbon deposition through the steam gasification reactions of carbon.

(4) The activation energies were determined as E_a =130 kJ/mol and 120 kJ/mol for benzene decomposition over CL at 750-900°C in the simulated gas with and without 15vol.% H_2O, respectively. The obtained *E*a values are much lower than the literature values for benzene decomposition reactions under similar conditions with other catalysts such as CaO.MgO and Ni/MgO, suggesting the limonite material can be an inexpensive but active catalyst for benzene decomposition and hot gas cleanup of biomass gasification gas.

7.2. Recommendations for Future Work

This research involved the decomposition of ammonia and benzene for the purpose of hot gas cleanup of biomass gasification gas. The activated carbon supported Ni/Fe catalysts showed to be

highly effective for ammonia decomposition in inert helium atmospheres, but their activities decreased significantly in the presence of a simulated gas containing $CO/CO_2/CH_4/H_2/H_2O$. The natural limonite ores proved to be effective for ammonia decomposition in both inert and simulated gas atmospheres due to the high Fe-contents and finely dispersed Fe-species of these ores. In benzene cracking experiments, the Brazilian limonite showed the highest activity towards benzene decomposition compared to Canadian and Australian limonite. Although these results are very promising, further studies are required for the use of these catalysts in industrial applications. For hot gas cleaning of ammonia and tars with the use of the activated carbon supported Ni/Fe catalysts as well as the natural limonite ores, the following recommendations may be considered for future research:

- The use of Ni and Fe activated carbon catalysts showed high and stable catalytic activities towards NH_3 decomposition in inert atmosphere, though longer runs should be carried out to determine the catalytic life and durability of each catalyst
- In simulated gas atmosphere the Ni/AC catalysts showed to be inactive towards NH_3 decomposition, and the activity of the Fe/AC catalyst was reduced by the presence of moisture in the gas, therefore if the Fe/AC catalyst is to be used in syngas atmospheres, the removal of H_2O is required to keep the catalyst from being deactivated.
- Higher metal loadings of Ni and Fe to the surface of the catalysts may help increase the activities in atmospheres containing $CO/CO_2/CH_4/H_2/H_2O$. Higher reaction temperatures should also be examined.
- The Canadian, Brazilian and Australian limonite ores all showed high activities towards NH_3 decomposition in simulated gas atmospheres, but longer reaction times are still required to determine the catalytic life of each catalyst.
- In tar cracking experiments the Brazilian limonite catalyst showed the greatest activity, attaining conversions of nearly 100% at temperatures between 650-900°C, but again, longer runs are required to determine the catalytic life and durability.
- In biomass gasification gas contains not only CO, H_2, CO_2, CH_4 and (C_2+C_3), but also

contaminants such as tars, NH_3, H_2S and SO_2, etc., therefore further testing of the catalysts should be carried out in the presence of mixed NH_3 and tar atmosphere with and without H_2S and SO_2 which have shown to be poisoning agents with respect to catalytic activity.